An Experimental Investigation of Liquid Jet Impingement Heat Transfer Theories

by

James S. Lombara

Submitted to the Department of Mechanical Engineering in
partial fulfillment of the requirements for the degree of
Bachelor of Science in Mechanical Engineering
at the
Massachusetts Institute of Technology
May 1990

Signature of Author James S. Lombara
Department of Mechanical Engineering
May 11, 1990

Certified by
Professor John H. Lienhard V
Thesis Supervisor

Accepted by
Professor Peter Griffith
Chairman, Department Committee

An Experimental Investigation of Liquid Jet Impingement Heat Transfer Theories

by

James S. Lombara

Submitted to the Department of Mechanical Engineering in
partial fulfillment of the requirements for the degree of
Bachelor of Science in Mechanical Engineering
at the
Massachusetts Institute of Technology

ABSTRACT

Liquid jet impingement heat transfer is investigated. Experiments were performed in which a free liquid impinged upon a uniform heat flux surface, spread out in a thin radial film, and cooled the surface through convective heat transfer. Local Nu_d numbers were calculated. Experimental results were compared to Nu_d predictions from two recent theories, an integral method developed by Liu and Lienhard (1989) and a correlation based on experimental data developed by Stevens and Webb (1989).

Experiments were run with 1/8 inch, 1/4 inch. and 3/8 inch orifices, and a range of Reynolds numbers and heat fluxes, and compared to the theories. Despite the experimental uncertainty pf the data (at times greater than ±20%), Liu and Lienhard's theories show good agreement with the data. The correlation of Stevens and Webb underpredicts the data beyond a small r/d.

Table of Contents

INTRODUCTION

Impinging jets can provide high heat flux cooling, which is important in many modern technologies, such as cooling supercomputers or high power lasers, and it has applications in manufacturing. Jets can be classified as either free or submerged. Submerged jets are liquid jets passing through a liquid or a gas jet passing through a gas, while free jets are liquids jets passing through a gas.

When a liquid jet strikes normal to a smooth surface the liquid spreads out radially in a thin sheet. This flow starts as laminar and then has a clear transition boundary into turbulence. Further out in the flow, a hydraulic jump occurs when the velocity of the liquid slows down and the thickness of the liquid abruptly increases. If this surface is heated with a constant and uniform heat flux, the convective heat transfer that occurs is very high in the laminar and turbulent region, but drops significantly after the hydraulic jump. The region after the hydraulic jump is not dealt with in this paper.

Much is still unknown about the cooling characteristics of free liquid jets. Many theoretical studies have dealt with submerged jet heat transfer, however very few theoretical analyses have investigated the heat transfer from free liquid jets. This study will compared two recent predictions with experimental results. Liu and Lienhard (1989) have developed a theory to predict the Nusselt using an integral method and combining with previous theories of Watson (1964) and Sharan (1984). They found good agreement with a limited set of data. Stevens and Webb (1989) correlate their data, giving Nusselt number as a function of radial location, Reynolds number, Prandtl number, jet nozzle to plate spacing, and jet velocity. Their results, however, are confined to small distances from the point of jet impact.

The present experiment used water for the liquid jet The wall temperature distribution was measured up to 43 jet diameters away from the point of impingement using thermocouples. Local Nusselt numbers were calculated and compared to the theoretical models.

THEORETICAL ANALYSIS

Liu and Lienhard

Liu and Lienhard (1989) follow the model of Watson (1964) and divide the liquid flow into separate heat transfer regions. Watson divided the flow into four regions

1. *The stagnation zone.*

2. *The boundary later region.* In this region the viscous boundary layer, δ, is growing but has not reach the height of the liquid sheet, h.

3. *The fully viscous sheet.* Here the boundary layer has reached the surface of the liquid sheet, so $\delta = h$.

4. *The hydraulic jump.* In this region the thickness of the sheet increases suddenly and the radial flow velocity of the liquid slows down.

Watson's results have been experimentally verified by Azuma and Hoshino (1983).

Similarly, Liu and Lienhard divide the flow into 6 distinct heat transfer regions, shown in Figure 1. For this model they assume the $Pr > 1$, as is the case for most liquids. The six regions are:

1. *The stagnation zone.* Here the heat transfer is assumed to conductive, and Liu and Lienhard (1990) derive the expression for the Nusselt number as

$$Nu_d = 0.711\, Re_d^{1/2}\, Pr^{0.42} \qquad (1)$$

2. $\delta < h$ *region.* In this region the viscous boundary layer has not reached the surface. The flow outside the boundary layer is unaffected and approximately equal to the incoming jet velocity, uj. Using the radial integral energy equation

$$\frac{d}{dr}\int_0^{\delta} ru\,(T - T_f)\,dy = \frac{q}{\rho\, c_p}\ , \qquad (2)$$

and combining with the profiles

$$T - T_w = (T_f - T_w)\left[\frac{3\,y}{2\,\delta_t} - \frac{1}{2}\left(\frac{y}{\delta_t}\right)^3\right] \qquad (3)$$

and

$$u = u_{max}\left[\frac{3\,y}{2\,\delta} - \frac{1}{2}\left(\frac{y}{\delta}\right)^3\right] \quad , \qquad (4)$$

integrating, and using Sharan's (1984) expression for δ:

$$\delta = 2.679\left(\frac{r\,d}{Re_d}\right)^{1/2} \quad , \qquad (5)$$

Liu and Lienhard obtain an expression for the local Nusselt number

$$Nu_d = \frac{h\,d}{k} = 0.632\ Re_d^{1/2}\ Pr^{1/3}\left(\frac{d}{r}\right)^{1/2} \qquad (6)$$

This region ends at $r = r_0$, when the viscous boundary layer reaches the surface of the liquid. Liu and Lienhard use Sharan's expression for r_0,

$$r_0 = 0.1773\ Re_d^{1/3}\ d \qquad (7)$$

which defines the end of region 2.

3. $\delta = h$ *and* $\delta_t < h$. In this region the viscous boundary layer has reached the surface, so the entire flow is affected by the viscous forces of the wall. However, the thermal boundary layer, δ_t, is growing, but still has not reached the surface. Because the entire flow is affected by viscous retardation, u_{max} is no longer constant. Watson and Sharan show that

$$u_{max} = \frac{1}{5}\frac{u_f d^2}{h r} \tag{8}$$

and

$$h = 0.1713\left(\frac{d^2}{r}\right) + \frac{5.147}{Re_d}\left(\frac{r^2}{d}\right) \tag{9}$$

Integrating the energy equation with equations (2), (3), and (7), yields

$$Nu_d = \frac{0.407\, Re_d^{1/3}\, Pr^{1/3}\left(\frac{d}{r}\right)^{2/3}}{\left[0.1713\left(\frac{d}{r}\right)^2 + \frac{5.147}{Re_d}\frac{r}{d}\right]^{2/3}\left[\frac{1}{2}\left(\frac{r}{d}\right)^2 + C_3\right]^{1/3}} \tag{10}$$

The constant of integration, C_3, is obtained by combining equations (5) and (9), evaluating at $r = r_0$, and solving for C_3. This produces

$$C_3 = \frac{0.267\,(d/r_0)^{1/2}}{\left[0.1713\left(\frac{d}{r_0}\right)^2 + \frac{5.147}{Re_d}\frac{r_0}{d}\right]^2 Re_d^{1/2}} - \frac{1}{2}\left(\frac{d}{r_0}\right)^2 \tag{11}$$

This region ends at r_1, when the thermal boundary layer reaches the surface. For $Pr < 4.859$, Liu and Lienhard give r_1 to be

$$r_1 = \left\{-\frac{s}{2} + \left[\left(\frac{s}{2}\right)^2 + \left(\frac{p}{3}\right)^3\right]^{1/2}\right\}^{1/3} + \left\{-\frac{s}{2} + \left[\left(\frac{s}{2}\right)^2 + \left(\frac{p}{3}\right)^3\right]^{1/2}\right\}^{1/3} \tag{12}$$

where s and p are defined to be

$$p = \frac{-2C_3}{(0.2058\,Pr - 1)} \qquad s = \frac{0.00686\,Re_d\,Pr}{(0.2508\,Pr - 1)} \tag{13}$$

4. $\delta = h$ *and* $\delta_t = h$. Both the viscous boundary and the thermal boundary layer have reached the surface of the flow. Liu and Lienhard's analysis shows that this region only exists for $Pr < 4.859$. If Pr is greater than 4.859 the liquid sheet thickness, h, will grow faster than the thermal boundary layer, δ_t, and the thermal boundary layer will never reach the surface of the flow. If surface evaporation is small, the heat transfer from the liquid surface can be neglected, and the integral energy equation is written as

$$\frac{d}{dr}\int_0^h ruT\,dy = \frac{q}{\rho\,c_p}r \tag{14}$$

the temperature profile is given as

$$T - T_w = (T_{f4} - T_w)\left[\frac{3}{2}\frac{y}{h} - \frac{1}{2}\left(\frac{y}{h}\right)^3\right] \tag{15}$$

where T_{f4} is a function of r, given as

$$T_{f4} = T_w - \frac{2qh}{3k} \tag{16}$$

Substituting equations (3), (7) and (14) into equation (13), and integrating, Liu and Lienhard produce

$$Nu_d = \frac{0.25}{\frac{1}{Pr\,Re_d}\left(1-\frac{r_1^2}{r^2}\right)\left(\frac{r}{d}\right)^2 + 0.130\frac{h}{d} + 0.0371\frac{h_{r1}}{d}} \qquad (17)$$

where h_{r1} is the the film thickness at r_1 from equation (9).

5. *The boiling region region.* This region exists whenever $T_W > T_{sat}$ for the liquid. Boiling can occur in any region of the flow.

6. *The hydraulic jump.* In this region the liquid sheet thickness increases suddenly, and the velocity and heat transfer decrease greatly.

Neither regions 5 cr 6 are addressed in this study.

Stevens and Webb

Stevens and Webb investigated liquid jet heat transfer experimentally, using different jet diameters, nozzle-to-plate spacings (z), and Reynolds numbers. Their experimental jets were produced by long glass tubes giving turbulent pipe flows, in contrast to the laminar orifice jets of the present study. They fit their data for Nusselt number at the stagnation point, Nu_0, into an equation of the form

$$Nu_0 = ARe^q\left(\frac{z}{d}\right)^{s_2} Pr^{0.4} \qquad (18)$$

They used a multivariate least squares fit to determine values of A, q, and s_2 for each nozzle size. They also used the dimensional variable v/d as a correlating factor to account for the stagnation point velocity gradient to produce

$$Nu_0 = A\,Re^{0.57}\left(\frac{z}{d}\right)^{-1/30}\left(\frac{u_j}{d}\right)^{-1/4} Pr^{0.4} \qquad (19)$$

They normalized the Nusselt numbers from their heat transfer data with the expression for Nu_0 given above. Next, they chose a correlation equation in the form of

$$f(r/d) = ae^{b(r/d)} \tag{20}$$

to fit their Nusselt data between r/d = 0.75 and a transition zone, which may be associated with a turbulent boundary layer. The parameters a and b are dependent on the nozzle size. In their data, they found a region (r/d < 0.75) where Nu_d was approximately constant and another region (r/d > 0.75) where Nu_d behaved exponentially. Using a procedure suggested by Churchill and Usagi (1972), Stevens and Webb used an overall correlation equation of the form

$$\frac{Nu_d}{Nu_0} = \left[1 + (f(r/d))^{-9}\right]^{-1/9} \tag{21}$$

The function f (r/d) is the function shown above (equation 15). The parameters a and b, given by Stevens and Webb, depend on the nozzle size and as shown in Table 1. Stevens and Webb found that Equation (18) predicted 90% of their experimental data for Nu_0 within ±10% and 100% of their data to within ±15%. They also found that equation (21) to fit 87% of all their Nu_d/Nu_0 data to within ±15% and 96% of their data to within ±20%.

Table 1. Stevens and Webb's correlation coefficients for local Nud number for equation 20.

Nozzle size(mm)	2.2	4.1	5.8	8.9
a	1.15	1.34	1.48	1.57
b	-0.23	-0.41	-0.56	-0.70

Stevens and Webb's correlation only shows any accuracy for their data when r/d < 5.0. Beyond this point, the data are underpredicted. They attribute this rise in their experimental data to a possible transition to a turbulent boundary layer. In the present experiment, the turbulent transition was generally observed to occur at larger values of r/d (>10).

EXPERIMENTAL SETUP

The experimental apparatus is shown in Figures 2 and 3. The water is held in a 55-gallon drum, where it is sub-cooled by a Copeland refrigerating system with a 3,280 Btu/hour cooling capacity. The system consists of a 1.5 horsepower condensor, a 1.5 horsepower compressor, a thermal expansion valve and about 50 ft. of copper coil. The coil is placed in the 55-gallon drum and the working fluid, R-12, flows through the coil and cools the water. The pump is a 1.5 horsepower G.E. three-phase induction motor. All of the piping is 1 inch diameter PVC tubes. The flow rate can be controlled by two valves. One valve controls the amount of water going up the pipe, and the other allows liquid to be pumped back into the holding drum.

The fluid is pumped into an accumulator, a tank made of 6 inch diameter PVC tube 32 inches long sealed at both ends. On the top of the tank is the flow inlet, and at the bottom is the orifice plate. The tank damps turbulence and pump fluctuations to create a steady flow. Attached to the top of the tank is a release valve to remove air from the tank. Inside the tank, near the top, the fluid passes through 4 inches of honeycomb to help make the flow in the tank laminar. The bottom of the tank is a 1/2 inch thick piece of aluminum with a hole for the removable orifice plate. (See also Vassista, (1989).

Both the 55-gallon drum and the accumulator tank were wrapped with insulation to isolate them from the environment.

The liquid jets impinges upon a heater made of 0.004 inch thick, 6 inch wide stainless steel shim. The shim is stretched over a 6 inch by 7 inch Plexiglass insulation box and over 1 inch diameter copper rods that serve as electrodes. The insulation box isolates the heater from room air currents. Spring-loaded aluminum clamps are attached at an angle to the base of the heater in order to keep the shim taut under all conditions. Compressed air is blown into the insulation box to keep it dry. Clay is used for the seal between the box edge and the shim to keep the order the liquid out of the box. A 15kW generator, capable of producing up to 1000 amps at 15 Volts, heats the shim through

resistance heating. The leads from the generator are attached to the copper electrodes, creating a heater area of 10.5 inches by 6 inches.

The whole heater and tank is placed inside a Plexiglass box to confine the splattered liquid. Tubing from the bottom of the box leads back to the 55-gallon drum to make the system a closed loop

Measurement Systems

The pressure in the tank was measured by a pressure gage attached at the top of the tank and by a pressure transducer at the bottom. The pressure value at the top from the gage was converted to the pressure at the bottom by adding ρgh. Jet velocity is then calculated from Bernoulli's equation.

At first, the leads for the voltage measurement across the heater were attached to where the leads from the generator were joined to the copper electrodes. However, there was too much contact resistance between the leads and the electrodes and the electrodes and the shim to give an accurate voltage reading, so the voltage across the heater is measured from the ends of the shim to eliminate any contact resistance. The heater current is measured through a shunt located on the generator. The shunt gives a drop of 50 millivolts for 1200 amps. From the voltage and current values, power and the heat flux from the heater can be calculated.

The wall temperature distribution is measured by 0.003 inch J-type thermocouples attached to underside of the shim. Starting at the stagnation point of the jet, the thermocouples are placed at every 1/2 inch along arcs of circles, centered at the stagnation point, with radii equal to the distance of thermocouple to the stagnation point. The middle of each thermocouple is on a radial line that is perpendicular to the copper rods and passes through the stagnation point. Their placement is shown in Figure 4. Because the flow is radial, placing the thermocouples along arcs of a circle centered at the stagnation point an average temperature of the arc is found, instead of the temperature of just one point, which is subject to greater fluctuations.

The thermocouples are attached to the underside of the shim using high-temperature Kapton tape. Two thermocouples are placed at the stagnation point for greater accuracy. The thermocouple junctions are placed in a ice bath for a 0°C reference temperature, from the ice bath the leads are

connected to a junction box along with the leads from the pressure transducer and voltage. The junction box is then connected to a Fluke multimeter. The voltages from the thermocouples are converted to temperature using

$$T = -0.48868252 + 19873.14503x - 218{,}614.5353x^2 + 11{,}569199.78x^3 - 264{,}917531.4x^4 + 2{,}018{,}441{,}314x^5 \quad (22)$$

as given on page T-12 of the Omega Temperature Handbook where T is temperature and x is the thermocouple voltage in volts. With the calibrating procedure the thermocouples were determine to have an accuracy of $\pm 0.1^\circ$ C.

EXPERIMENTAL PROCEDURE

For the experiments the fluid used for the liquid jet was water. To increase the heat transfer and lower the experimental uncertainty, the water was cooled to near freezing temperatures. For most tests the temperature was between 35° and 40°F. The compressed air line was regulated to approximately 10 psi to keep the inside of insulation box dry.

Once the water became cold enough the pump was turned on, filling the accumulator tank and producing the liquid jet. Tests were run with the pressure in the tank, controlled by the two valves varying from 5 psi up to 27 psi producing jet velocities from 8 m/s up to 27 m/s. The actual value for the tank pressure was taken from the pressure transducer, while the pressure gauge was used only as a check. The orifices have small inner diameters and a countersunk larger diameters, which face out of the tank. The inner diameters were 1/8 inch, 1/4 inch, and 3/8 inch.

After the temperature became steady a calibration run for the thermocouples was performed. With the jet running, about ten voltage reading were taken for every thermocouple. Then the values for each thermocouple were averaged to eliminate random error and to give each thermocouple one value for the temperature of the incoming jet. Next, the mean for all of the thermocouple voltages was calculated. Finally, each thermocouple was calibrated by subtracting its average voltage from the mean giving a correction value for each thermocouple. This calibration is used to eliminate the systematic error that is present in the thermocouples.

Next the value of transition radius was recorded. When the flow starts to become turbulent an onset of waves occurs and a small distance afterwards the flow becomes a fully rippled turbulent flow. The transition radius that was recorded was when the flow became a fully turbulent flow. For the 3/8 inch orifice tests the transition radius was too large to be seen clearly on the heater, so it was not recorded. If a hydraulic jump occurred its radius was also recorded. For the experiments with hydraulic jumps, no data was taken beyond the point of the jump because the theories do not apply for this region.

Next, to heat the plate, the generator was turned on. It was usually set to a level so that the current would be between 200 and 250 amps; occasionally it was somewhat higher or lower. The current allowed enough heat flux so that the wall temperature rise would be significant compared to the uncertainty of the thermocouple. However, when higher currents were used, the stainless steel would react with the copper electrode and start to deteriorate. The heat fluxes generated ranged from a low of 15,600 W/m^2 up to 37,600 W/m^2, but were generally between 19,000W/m^2 and 24,000W/m^2. Even with the highest heat flux used, the greatest temperature change was less than 12° C; and since the water was sub-cooled to near freezing, the cooling due to evaporation was minimized. Liu and Lienhard estimate that if the surface temperature is kept below 30° C, the effects of evaporation are insignificant. In the present study the wall temperature never even reached 30° C, so the effects due evaporation are minimal.

After the heater and the water came to an equilibrium, a number of values were recorded and averaged for each thermocouple, to decrease the random error of the thermocouples, beginning with the thermocouple farthest away from the stagnation point but not past the hydraulic jump. The last thermocouple measurement taken was at the stagnation point. This procedure ensures lesser amount of error nearer to the stagnation point, and because there are smaller temperature changes nearer to the stagnation point, any error in temperature for this region to has a magnified effect on the results.

The inlet temperature was recorded after all the other voltages were taken. For the 1/8 inch orifice, the generator, the refrigerating system, and the pump were turned off. The water was allowed to drain out of the tank and onto the heater. After the heater reached an equilibrium (approximately 2 to 3 minutes), the voltage was recorded for the thermocouple at the stagnation point. The water in the tank was assumed to be isothermal and not warm up significantly. This is a good assumption because the tank was insulated and because there was a large amount of water in the tank to be warmed up in a short period. This value was used as the inlet temperature. For the 1/4 and the 3/8 inch orifices, the water drained out of the tank too quickly, before equilibrium could be reached. In these cases, the generator and the refrigerator were shut off and the pump left on. Then the temperature would come to an equilibrium and the thermocouple value of the stagnation point used as the inlet temperature.

For each thermocouple measurement, a number of values were taken to eliminate random error. These numbers were averaged and the correction value from the calibration tests was added to them to get the actual value used for the calculations.

CALCULATIONS AND RESULTS

Experimental values of Nusselt number were calculated and were compared to theoretical results from Liu and Lienhard's model and Stevens and Webb's correlation.

The experimental Nusselt numbers were calculated based on jet diameter instead of radial position. The formula for Nu_d is

$$Nu_d = \frac{q_w d_j}{k (T_w - T_{in})} \tag{23}$$

where T_{in} is the temperature of the incoming jet, T_w is the local wall temperature read from the thermocouples, k is the conductivity of the water, q_w is the heat flux, and d_j is the contracted jet diameter equal to

$$d_j = d \sqrt{c_c} \tag{24}$$

Here, d is the nozzle diameter and c_c is the contraction coefficient given as 0.611. For comparison to the theory of Liu and Lienhard, the Nusselt numbers were plotted versus r/d_j. Uncertainties of the experiment were calculated; the complete procedure is shown in Appendix A. Each thermocouple was given an uncertainty of ±0.1° C, so $(T_w - T_{in})$ has an uncertainty of ±0.2° C. An upper and lower bound on the Nusselt number was calculated and plotted. The uncertainties are not uniform, the upper bound is greater than the lower bound. The uncertainties near the stagnation point, where the difference in temperature is small, are very large, sometimes greater than ±20%. However, the uncertainty range rapidly decreases at larger r/d_j due to the larger temperature differences.

Liu and Lienhard's theoretical values for Nusselt number were calculated through a computer program written by Xin Liu, given in Appendix B. All of the diameters used in the program are jet diameters using the contraction coefficient. Values for thermocouples were calculated at the same

radial location as thermocouples were placed, for comparison. Along with the Nusselt number, the Prandtl number and Reynolds number were calculated and recorded by the computer program. Reynolds number changes with r/d because it is of function of its viscosity, v, which varies significantly with temperature. The temperature change is small enough at the stagnation point so that the stagnation Reynolds number is equal to the incoming jet Reynolds number. A hump was noticed in the experimental Nu_d plots, where the data began to rise above the predictions . To determine if this was due to turbulence in the boundary later, Re_r was calculated for the point where the hump began. These values are shown on the Nu_d graphs. The data for the 1/8 inch orifice are given in Figures 5 - 17 and the numerical values for the experimental Nu_d, theoretical Nu_d, Pr, Re_d,the hydraulic jump radius, and the turbulent transition radius are shown in Tables 2-14. For some of the 1/8 tests the is no viable data for the Nu_d at the stagnation point, usually because the uncertainty was too large to plot on the same graph as the other points. In these cases the graphs were plotted without the data at the stagnation point. The 1/4 inch orifice results are shown in Figures 18-32, and the numerical values in Tables 15-29. For the 3/8 inch orifice Figures 33-38 show the results, and Tables 30-35 show the numerical values.

For all cases, $Pr > 4.859$, so region 4 does not exist for any of the experiments. For the 1/8 inch orifice, r_0 was located around $r/d_j = 5$, for the 1/4 inch orifice r_0 was around $r/d_j = 6$, and for the 3/8 inch orifice r_0 was around $r/d_j = 7$. To show the difference between region 2 and 3, graphs were plotted showing $\log (Nu_d/(Re_d^{1/3}*Pr^{1/3}))$ for $r < r_0$ and $\log (Nu_d/(Re_d*Pr^{1/3}))$ for $r > r_0$ versus $\log (r/d_j)$. Region 2 should show a straight line for $\log (Nu_d/(Re_d^{1/3}*Pr^{1/3}))$ and region 3 should show a straight line for $\log (Nu_d/(Re_d*Pr^{1/3}))$. These results are shown in Figures 39-41.

For Nusselt numbers at the stagnation point, Nu_0, a graph was drawn comparing Liu and Lienhard's theoretical values and Stevens and Webb's correlated values for Nu_0 to experimental values. These data were plotted as a function of Re_d. However, the small experimental temperature difference causes the high uncertainty seen in the plot. These results are shown in Figures 42-44.

Some of the experiments used two thermocouples at the stagnation point. When the values of both thermocouples were similar, the Nu_d for both were calculated, but thermocouple 1, judged to be

more reliable was always used for the incoming temperature and the other thermocouple (2) was used just as a check. At times thermocouple 2 was unreliable and inconsistent, so for some tests thermocouple 2 was obviously incorrect, and in these cases the value was simply discarded.

Finally, the Stevens and Webb result for Nu_d/Nu_0 was calculated. Interpolated values for the parameters a and b were found by curve-fitting the values Stevens and Webb give, using a third-order quadratic equation. Graphs of the curve-fits are shown in Figures 45 and 46. The fitted equations are

$$a = 0.93425 + 8.8678E\text{-}2\ x + 6.3068E\text{-}3x^2 - 9.2635E\text{-}4x^3 \qquad (25)$$

and

$$b = -6.1257E\text{-}2 - 5.7374E\text{-}2\ x - 1.1139E\text{-}2\ x^2 + 1.0698\ x^3 \qquad (26)$$

where a and b are the parameters and x is nozzle size in millimeters. The present experimental results were divided by the theoretical expression for Nu_0 and plotted against the theoretical curves for Nu_d/Nu_0. These graphs are shown in Figures 47-49.

DISCUSSION

The experimental data gathered shows good agreement with the theory of Liu and Lienhard, for a wide variety of Reynolds numbers, heat fluxes, and jet diameters. Although the experimental uncertainty was, at times, very high, especially for small r/d, the plots of experimental Nu_d always follow the same shape as the theoretical curves calculated from Liu and Lienhard's theory. The correlation presented by Stevens and Webb does not agree as well with the data.

For the 1/8 orifice (Figures 5- 17), the number of points is limited because the hydraulic jump occurred before the end of the heater. For many of these graphs there is no viable value for Nu_d at the stagnation point, so no point is shown at $r/d = 0$ for some graphs. This is because either the theoretical Nu_d or the upper bound for the experimental uncertainty was too high to plot on the same graph. The uncertainty for the 1/8 inch orifice graphs is high for the first few points, but then drops off rapidly when the temperature difference increases. Liu and Lienhard's theory closely follows the data for the whole range of r/d, and for different Reynolds numbers and heat fluxes.

The largest amount of data was collected for the 1/4 inch orifice (Figures 18-32). The agreement for this data is excellent. After the stagnation point, the first few point usually fall well within the uncertainties and very close to Liu and Lienhard's theory. Towards the end of the flow ($r/d > 20$), however, the theory starts to underpredict the data by a small amount. Although the uncertainty is very low at these points, the data is always slightly higher than the theory. A reason for the rise could be that the flow becomes turbulent causes heat transfer to increase. The rise is usually after the observed value for the turbulent transition. This could mean that the flow does not become fully turbulent until well after r_{turb}.

Less data was collected for the 3/8 inch orifice (Figures 33-38), however, fairly good agreement still exists between Liu and Lienhard's theory and the data. Significant experimental uncertainty is present for the entire flow. This is because the high rate of cooling of the large jets provide keep the temperature changes small and consequently, the uncertainty high.

Tables 2-29 give the radius at which the flow changes from a laminar flow into a turbulent one. This radius is denoted as r_{turb}. For some graphs there is a apparent change in the data at this point. Most noticeably on the 1/8 inch graphs where a hump often occurred in the data right after r_{turb}. On the 1/4 inch graphs, the a hump in the the data also was noticed, but well after r_{turb}. For the 3/8 inch orifice, r_{turb} could not be recorded because the transition did not occur on the heater. For the 3/8 orifice, however, a hump is also observed. The Re_r for the point where the hump starts to develop shows the for the 1/8 inch orifice there is no correlation between Re_r and the hump. The hump seems to be solely caused by r_{turb}. For the 1/4 inch orifice, where the film thickness is greater, there the humps usually occurs around Re_r between 700,000 and 900,000. However, the range of Re_r where the hump occurs is great (from 600,000 to over 1,000,000). For the limited set of 3/8 inch orifice data, there appears to be a greater correlation between the hump and Re_r. Re_r is always in the range of 730,000 and 850,000. This suggests the turbulence could be occurring in the boundary layer, before the whole flow becomes turbulent for the flows where the film is thick.

Figure 39-41 attempt to show the differences between region 2 and region 3 in Liu and Lienhard's theory. Fairly straight lines can be drawn through the data for region 3 for the 1/8 inch and 1/4 inch orifices. However, only the 3/8 inch data gives enough points before r_0 to see region 2. For this set of data, a straight line can be drawn through the data at region 2; in region 3 a line can be drawn, but there is a slight hump in the middle of the data.

Stevens and Webb's correlation does not give very good agreement with the experimental data. The comparisons are shown in Figure 47-49. For all the different sized orifices, the first point after the stagnation point is usually close to the data, but after that the correlation quickly approaches zero while the experimental data has a much more gentle slope. The 1/8 inch orifice data is closer to the correlation than the 1/4 inch or 3/8 inch data, but it still does not agree very well.

A major problem in this study was obtaining values for Nu_d at the stagnation point. The experimental uncertainty was extremely high for this point because it had the smallest wall temperature difference and because it had to be located precisely. This can be seen in Figure 42-44. When the error was great enough, Liu and Lienhard's theory and Stevens and Webb's prediction would

sometimes fall within the uncertainty. However the theories are never really close to the data. Both always predict higher values than are obtained. Liu and Lienhard's predictions are higher than Stevens and Webb's, except for the 1/4 inch orifice where they are close, and the experimental data is always lower, usually by a significant amount.

CONCLUSIONS AND RECOMMENDATIONS

Liu and Lienhard's theory gives good results for predicting Nu_d for liquid jet impingement. Despite some large experimental uncertainties that were present, the data taken confirms the validity of their theory for different sized jets, and a range of heat fluxes and Reynolds numbers. A problem with their theory, however, is the difficulty and complexity of calculating predictions. This study used a computer program to calculate the theory. A simplified version of the theory for quick approximations would be very valuable.

Stevens and Webb's correlation fails to even come close to the data after small r/d. Examining their own set of data, it can be seen that they never collected any data past $r/d = 15$, and even their data rises above their correlation after $r/d \cong 5$. Their experimental set-up also used long glass tubes which produced turbulent jets, unlike the laminar jets used in this study. However, their technique of calculating Nu_d/Nu_0 is useful. This is a simple procedure for finding local Nu_d. For each size jet it gives a single curve because it is normalized to Nu_0. This is very convenient, unlike the different curves that need be calculated for Liu and Lienhard's theory for any change in parameters. It would be worthwhile to be developed a more accurate correlation that accounts for a wider range of r/d, in order to obtain quick and simple estimates of local Nu_d.

Further experiments need to be conducted to get more accurate data for Nu_d at the stagnation point. In this study the experimental uncertainty was too high at the stagnation point to get sufficiently accurate data. However, it appears that both Liu and Lienhard's and Stevens and Webb's predictions for Nu_0 are too high. Studies concentrating just on the stagnation point would provide more insight.

The behavior of turbulence in the flow and its effects on the heat transfer also warrant further study. For this study, there was a rise in the heat transfer immediately after the transition into turbulence for the 1/8 inch orifice. However, for the larger diameter jets a similar rise in the data occurred theat was not related to the observed turbulent transition. The similarity in the Re_r at the point where the rise occurs suggests that turbulence could occur in the wall boundary layer before the entire

flow becomes completely turbulent. Further investigation is needed to determine the entire role turbulence plays in liquid jet heat transfer.

Another worthwhile study would be to compare the results from the idealized liquid jets, like the set-up used in this study, to jets that are used in real systems. These jets would have more turbulence, be subject to more vibrations, and have more splattering of liquid. Because of the high heat transfer produced by liquid jets, practical knowledge of behavior in realistic engineering situations would be extremely useful.

ACKNOWLEDGEMENTS

This work was supported by the National Science Foundation under grant # CBT-8858288.

REFERENCES

Azuma T., and Hoshino, T., 1983,"LDV Measurements in Radial Flow of Thin Liquid Film", *Osaka Symposium on Flow Measuring Techniques.*

Liu, X., and Lienhard V, J. H., 1989, "Liquid jet impingement heat transfer on a uniform flux surface," *Heat Transfer Phenomena in Radiation, Combustion, and Fires*, ASME HTD-Vol. 106, pp. 523-530, 1989.

Liu, X. and Lienhard V, J.H., 1990, personal communication.

Omega Temperature Handbook, p. T-12.

Sharan, A., 1984, "Jet-disc boiling: burnout predictions and applications to solar receivers," Master's Thesis, University of Houston.

Stevens, J., and Webb, B.W., 1989, "Local heat transfer under an axisymmetric, single-phase liquid jet," *1989 National Heat Transfer Conference*, HTD-Vol 111, pp 113-119.

Vassista, V.K., 1989," Experimental Study of the Hydrodynamics of an Impinging Liquid Jet," Bachelor's Thesis, Massachusetts Institute of Technology.

Watson, E.J., 1964, "The radial spread of a liquid over a horizontal plane," *J. Fluid Mech.*, Vol. 20, pp.481-499.

APPENDIX A Calculation of Experimental Uncertainty for Nud

Experimental uncertainty was determined by calculating an upper and lower bound on the data could be based on the estimated uncertainties of the instruments. The greatest factor contributing to the uncertainty was the thermocouples. The different thermocouples would give different temperature readings even when they are at the same temperature. The thermocouples varied from each other; however, they varied consistently by the same amount. Therefore, by calibrating the thermocouples and calculating a correction value for each thermocouple, the experimental uncertainty is greatly reduced. For this study, the thermocouple's uncertainty was reduced to just ±0.1° C through the calibration procedure. Since Nu_d used $T_w - T_{in}$, the uncertainties are added and the uncertainty for ΔT is ±0.2°C.

An average conductivity, k, value of 0.575 W/m° K was used for all calculations of Nu_d. The variation in temperature was small and the effect on k minimal, only uncertainty employed for k was accounted using a value of 0.600 W/m°K for the lower bound. The value of 0.575 corresponds to a temperature of approximately 4°C and 0.600 corresponds to approximately 25° C. This range accounts for the entire range of temperatures in this study.

The heat flux was measured carefully; however, it still contributed some uncertainty. The measurements taken to get heat flux are the length and width of the heater, the voltage across the heater, and the current produced by the generator. All of these were carefully measured, and the uncertainty of the heat flux was estimated to be ± 10%.

The diameter of the orifice was precisely machined, so it does not contribute any significant amount of uncertainty to Nu_d. The jet diameter ($d_j = c_c^{1/2} d$) and the $c_c = 0.611$ were also assumed to be exact.

The experimental value for Nu_d was calculated as

$$Nu_d = \frac{q_w d_j}{0.575\ \Delta T} \qquad (27)$$

The lower bound was calculated as

$$Nu_{low} = \frac{(q_w - 0.1q_w)\, d_j}{0.6\,(\Delta T + 0.2^\circ C)} \tag{28}$$

and the upper bound was calculated as

$$Nu_{high} = \frac{(q_w + 0.1q_w)\, d_j}{0.575\,(\Delta T - 0.2^\circ C)} \tag{29}$$

This procedure gives uneven uncertainties. The upper uncertainty is larger than the lower uncertainty. The most significant factor in the uncertainty is the uncertainty in the temperature since ΔT is relatively small. This can be seen by examining Figure 5-38. The uncertainty decreases dramatically when the change in temperature increases.

APPENDIX B Computer code used to calculate Liu and Lienhard's theoretical values.

```
      PROGRAM JETCONVECT
      real*8 pp,qq,fqr
      COMMON uf,Q,RO,CP,COND,TF,TSAT,D,red,pr,c1,r1,aa,hr1
      REAL NUR
      WRITE (*,1)
  1   FORMAT (4X/,
     &    '*************************************************'/,
     &    '*                                               *'/,
     &    '*  FORTRAN PROGRAM: JET CONMVECTIVE HEAT XANSFER  *'/,
     &    '*                                               *'/,
     &    '*************************************************')
C     ------------------------
C     PARAMETERS PUTIN
C     ------------------------
      open (unit=4, file='dataj')
c     print *, 'input electrical heat voltage'
      read (4,FMT=*) flux, psi, d
      print *,'heat flux, press., d',flux,psi,d
      q=flux
      close (unit=4)
c     print *, 'input jet diameter'
c     read *, d
c     print *, 'input presure transduser voltage'
c     read *, prv
      ro=999.8
      uf=sqrt((psi*3.2*6894.8)*2./ro)
      print *, 'voltage of thermocouple of inlet water?'
      read *, viw
      call thcpl(viw, tem)
      tf=tem
  5   print *, '1 for continue and 0 for stop'
      read *, z
      if (z.eq.0) goto 60
      print *, 'R=?'
      read *, R
      call visc(tf,wtnu)
      vis=wtnu
      cp=4180.
      cond=0.575
      tsat=100.
      print*, 'd, uf, vis, ro, cp, cond,  q, tf,tsat'
      print*, d,uf,vis,ro,cp,cond,q,tf,tsat
  200 RED=UF*D/VIS
      print*, 'red=',red
      PR=VIS*RO*CP/COND
      print*,'pr=', pr
C     ----------------------
C     Nu CALCULATION
C     ----------------------
      a=0.00001
```

```
      b=5.125
      eps=1.e-6
      R0=0.1773*D*RED**(1./3.)
      fNUR=0.632*(RED*R0/D)**.5*PR**(1./3.)
      print*, 'r0=',r0,'Nur0=',fnur
      hr0=1.128*d/red**(1./3.)
      print *, 'hr0=',hr0
      c1=0.0675*red*pr*r0*r0*r0/(d*hr0**2.*fnur**3.)
&      -0.5*(r0/d)**2.
      print*, 'c1=',c1
      pp=-c1/(0.1029*pr-0.5)*d*d
      qq=0.00343*red*pr/(0.1029*pr-0.5)*d*d*d
      print*, 'p=',pp,'qq=',qq
      r1=fqr(pp,qq)
      if (r1.ge.0.0) go to 71
      print *, 'calculate r2 (1) or not (0)?'
      read *,z
      if (z.eq.0.) goto 72
      call fot(f3,a,b,eps,rt)
      rr2=rt
      print*, 'r2(in region3)=',rr2
      r2=rr2
      goto 72
 71   print*, 'r1',r1
      HR1=.1713*d*d/r1+5.147*r1*r1/(red*d)
      a=r1
      CALL FOT(f2,a,b,eps, RT)
      R2=rt
      print*, 'r2=',r2
 72   a=0.0
      print *, 'r=',R
      IF (R.LT.R0) GOTO 10
      if (r1.lt.0.) goto 20
      IF (R.LT.R1) GOTO 20
      IF (R.LT.R2) GOTO 30
      WRITE (*,*) ' NO RESULT '
 10   NUR=0.632*(RED*R/D)**.5*PR**(1./3.)
      GOTO 50
 20   hr=0.1713*(d*d/(r*r))+5.147*r/(red*d)
      nur=0.407*(red*pr*r/d)**(1./3.)/(hr**(2./3.)
&     *(0.5*r*r/(d*d)+c1)**(1./3.))
      GOTO 50
 30   hr=0.1713*d*d/r+5.147*r*r/(red*d)
      NUR=(0.25*r/d)/((1.-r1*r1/(r*r))*r*r/(d*d*red*pr)+0.13*hr/d
&      +0.0371*hr1/d)
 50   tem=q*r/(nur*cond)+tf
      print *, 'heat flux=',q
      tem=(tem+tf)/2.0
      call visc(tem, wtnu)
      red2=uf*d/wtnu
      error=(red2-red)/red
      if (abs(error).le.0.001) goto 54
      print *, 'tave. & tf', tem, tf
c     print *, 'input new tem.'
c     read *, tem
```

```
      call visc(tem, wtnu)
      vis=wtnu
      print *, 'water viscosity=', vis
      goto 200
 54   PRINT*, "Nur=", NUR
      dnur=nur*d/r
      print*, 'nur*d/r=',dnur
     Pr=ro*cp*wtnu/cond
      Print*, 'Pr=',Pr
     red=uf*d/wtnu
      Print*, 'Red=',red
      goto 5
C 99  FORMAT (F8.4)
 60   END
c
      function fqr(pp,qq)
      real*8 fqr,pp,qq
      print *, pp,qq
      tt=-qq/2.-sqrt((qq/2.)**2.+(pp/3.)**3.)
      if (tt.ge.0.0) goto 21
      tt=-tt
      fqr=(-qq/2.+sqrt((qq/2.)**2.+(pp/3.)**3.))**(1./3.)
&      -tt**(1./3.)
      goto 31
 21   fqr=(-qq/2.+sqrt((qq/2.)**2.+(pp/3.)**3.))**(1./3.)+
&      tt**(1./3.)
 31   print*, 'fqr=',fqr
      return
      end
c
      subroutine f1(x,result)
      common uf,q,ro,cp,cond,tf,tsat,d,red,pr,c1,r1,aa,hr1
      hrr=0.1713*(d*d/x)+5.147*x*x/(red*d)
      result=0.02*red*pr*hrr/d-x*x/(d*d*2.)-c1
c     print*, 'rnur=',rnur
      return
      end
c
      subroutine F2(x,result)
      COMMON uf,Q,RO,CP,COND,TF,TSAT,D,red,pr,c1,r1,aa,hr1
      result=tf-tsat+q*(0.518*h/cond+4.*(x*x-r1*r1)/(ro*cp*uf
&     *d*d)+0.149*hr1/cond)
      RETURN
      END
c
      subroutine f3(x,result)
      COMMON uf,Q,RO,CP,COND,TF,TSAT,D,red,pr,c1,r1,aa,hr1
     hr=0.1713*(d*d/(x*x))+5.147*x/(red*d)
      print *,'hr=',hr
      nurr=0.407*(red*pr*x/d)**(1./3.)/(hr**(2./3.)
&     *(0.5*x*x/(d*d)+c1)**(1./3.))
      print *,'nurr=',nurr
      result=tsat-tf-q*x/(nurr*cond)
      return
      end
```

```
c
      subroutine fot(f,a,b,eps,rt)
      external f
    logical fagtzr
      x1=a
      x2=b
      call f(a,result)
      fa=result
      fagtzr=fa.gt.0.0
 1    rt=(x1+x2)*0.5
      dif=x2-x1
      if (dif.ge.eps) go to 100
10    return
100   call f(rt,result)
      frt=result
      if (frt) 120,10,140
120   if (fagtzr) go to 150
130   x1=rt
      go to 1
140   if (fagtzr) go to 130
150   x2=rt
      go to 1
      end

      subroutine visc(tem, wtnu)
      dimension wnu(16), te(16)
      wnu(1)=1.792
      wnu(2)=1.519
      wnu(3)=1.308
      wnu(4)=1.141
      wnu(5)=1.007
      wnu(6)=0.897
      wnu(7)=0.804
      wnu(8)=0.727
      wnu(9)=0.661
      wnu(10)=0.605
      wnu(11)=0.556
      wnu(12)=0.477
      wnu(13)=0.415
      wnu(14)=0.367
      wnu(15)=0.328
      wnu(16)=0.296
      te(1)=0.0
      te(2)=5.0
      te(3)=10.0
      te(4)=15.0
      te(5)=20.0
      te(6)=25.0
      te(7)=30.0
      te(8)=35.0
      te(9)=40.0
      te(10)=45.0
      te(11)=50.0
      te(12)=60.0
      te(13)=70.0
```

```
      te(14)=80.0
      te(15)=90.0
      te(16)=100.0
      do 4 i=1,16
      if (tem.gt.te(i)) goto 4
      wtnu=wnu(i-1)+(tem-te(i-1))*(wnu(i)-wnu(i-1))/(te(i)-te(i-1))
      wtnu=wtnu*1.0e-6
      goto 6
4     continue
6     return
      end

      subroutine thcpl(v,tem)
      dimension t(30)
      t(1)=0.507
      t(2)=1.019
      t(3)=1.536
      t(4)=2.058
      t(5)=2.585
      t(6)=3.115
      t(7)=3.649
      t(8)=4.186
      t(9)=4.725
      t(10)=5.268
      t(11)=5.812
      t(12)=6.359
      t(13)=6.907
      t(14)=7.457
      t(15)=8.008
      t(16)=8.560
      t(17)=9.113
      t(18)=9.667
      t(19)=10.222
      t(20)=10.777
      t(21)=11.332
      t(22)=11.887
      t(23)=12.442
      t(24)=12.998
      t(25)=13.553
      t(26)=14.108
      t(27)=14.663
      t(28)=15.217
      t(29)=15.771
      t(30)=16.325
      do 1 i=1,30
      if (v.ge.t(i)) goto 1
      tem=float(i-1)*10.+10.*(v-t(i-1))/(t(i)-t(i-1))
      goto 3
1     CONTINUE
3     return
      end
```

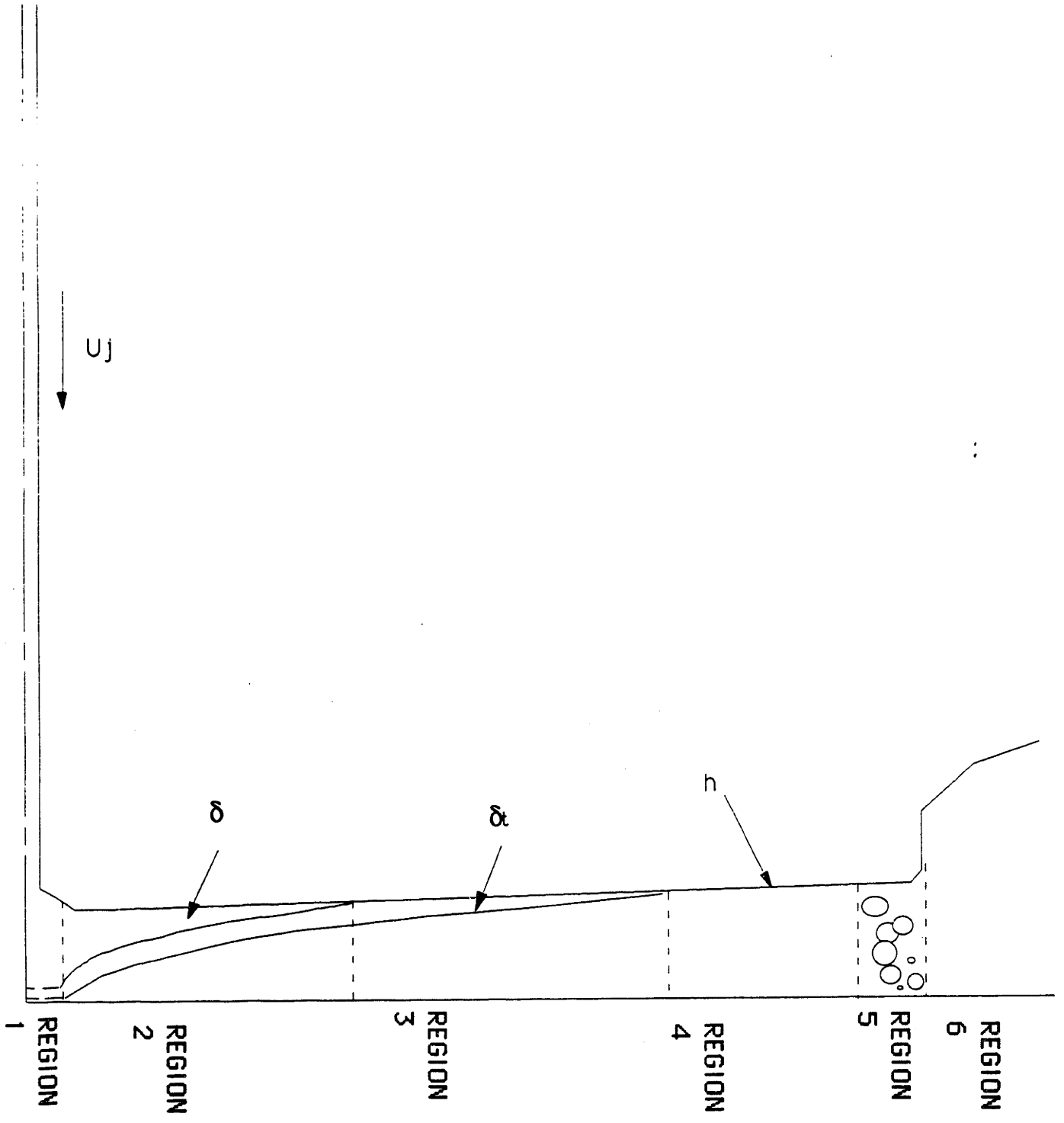

Figure 1. Profile of the flow showing the various heat transfer regions. For Pr > 4.859 region 4 does not exist.

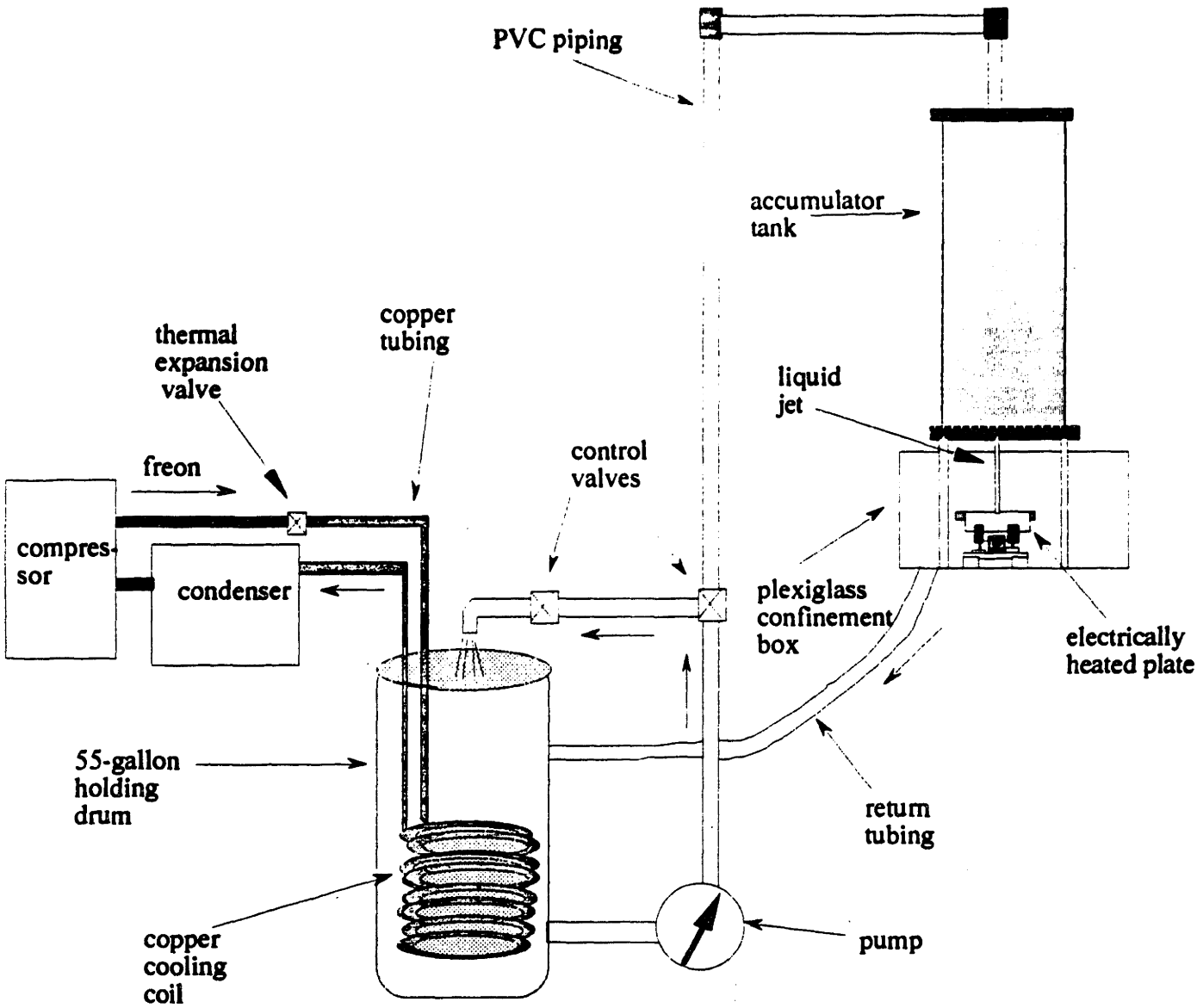

Figure 2. Experimental apparatus used to conduct heat transfer experiments

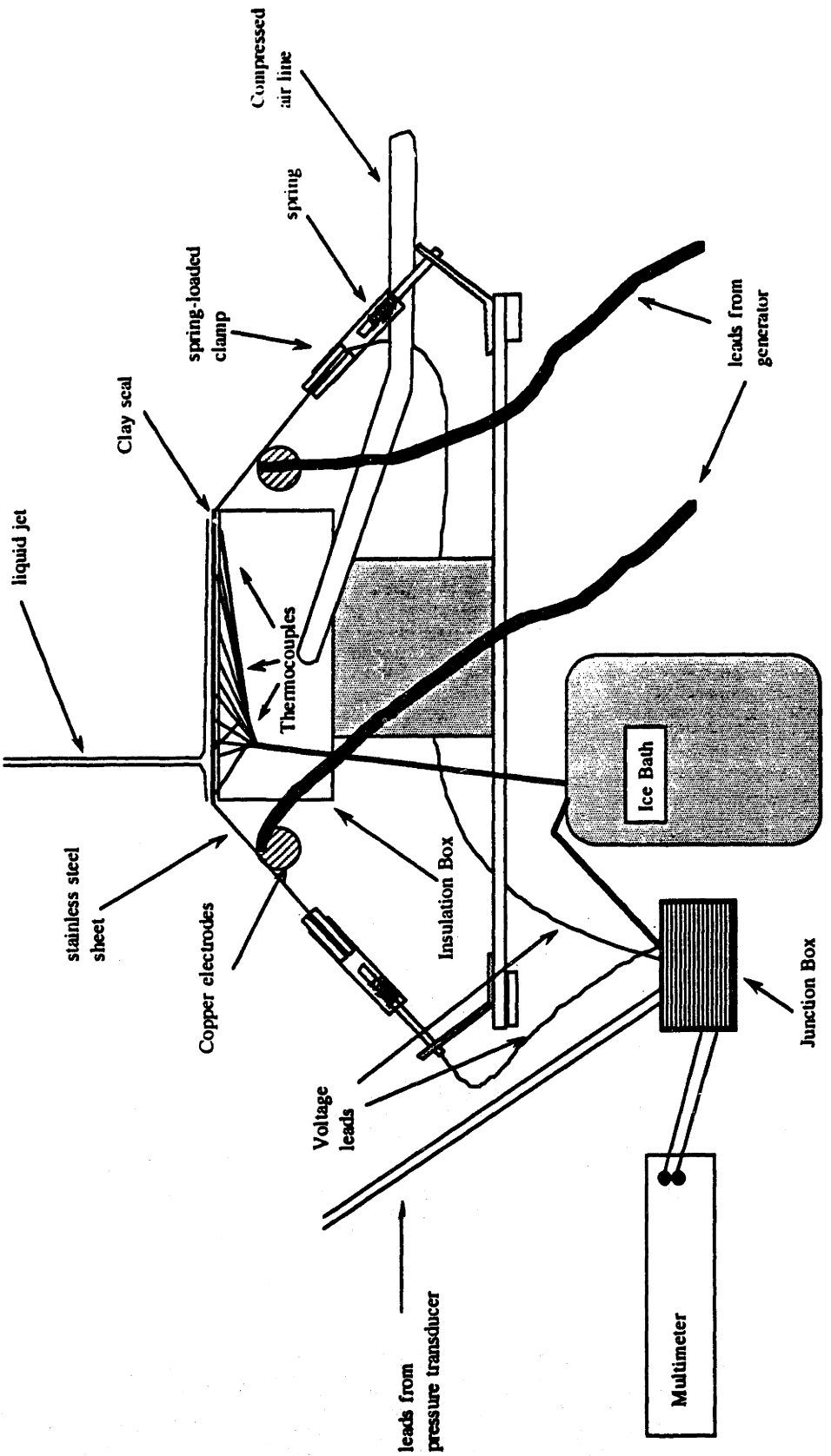

Figure 3. Detail of the heater apparatus and some of the measurement systems.

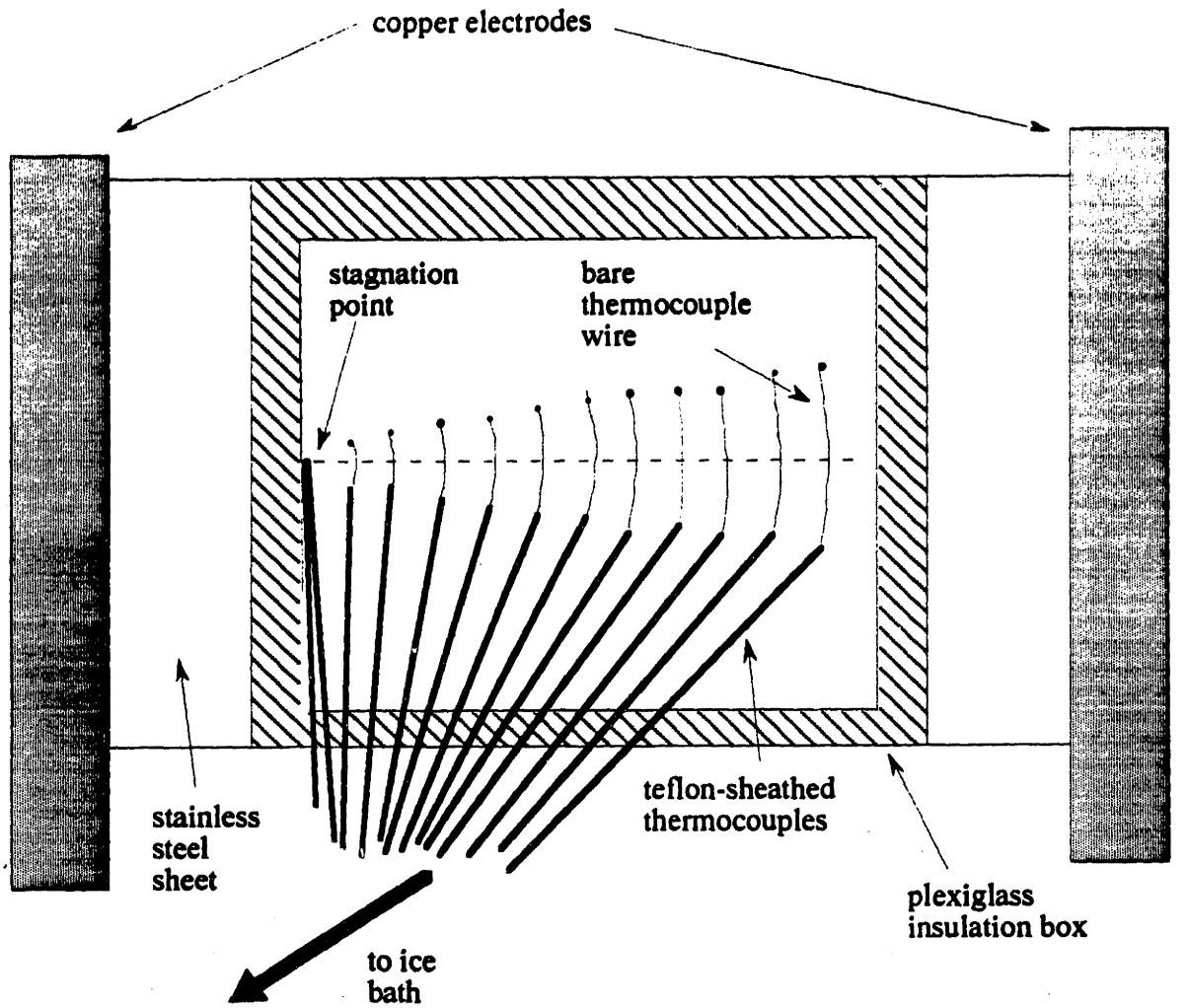

Figure 4. Bottom view of the heater showing thermocouple placement

Table 2. Values for Figure 5.

Nu_d	Theory	RE_d	Pr	r (m)
204.87	329.5	32760	9.38	0
123.48				0
92.93	107	33120	9.28	0.0127
70.42	71.4	33300	9.23	0.0254
45.76	42.9	33670	9.13	0.0381
40.6	26.9	34240	8.98	0.0508
22.65	18.1	35610	8.78	0.0635
15.38	13	35970	8.54	0.0762
11.71	9.87	37130	8.28	0.0889
T_{in} (°C)	q_w (W/m^2)	U_j (m/s)	r_{turb} (r/d)	d_j (m)
10.48	20900	17.1	15.4	0.00248

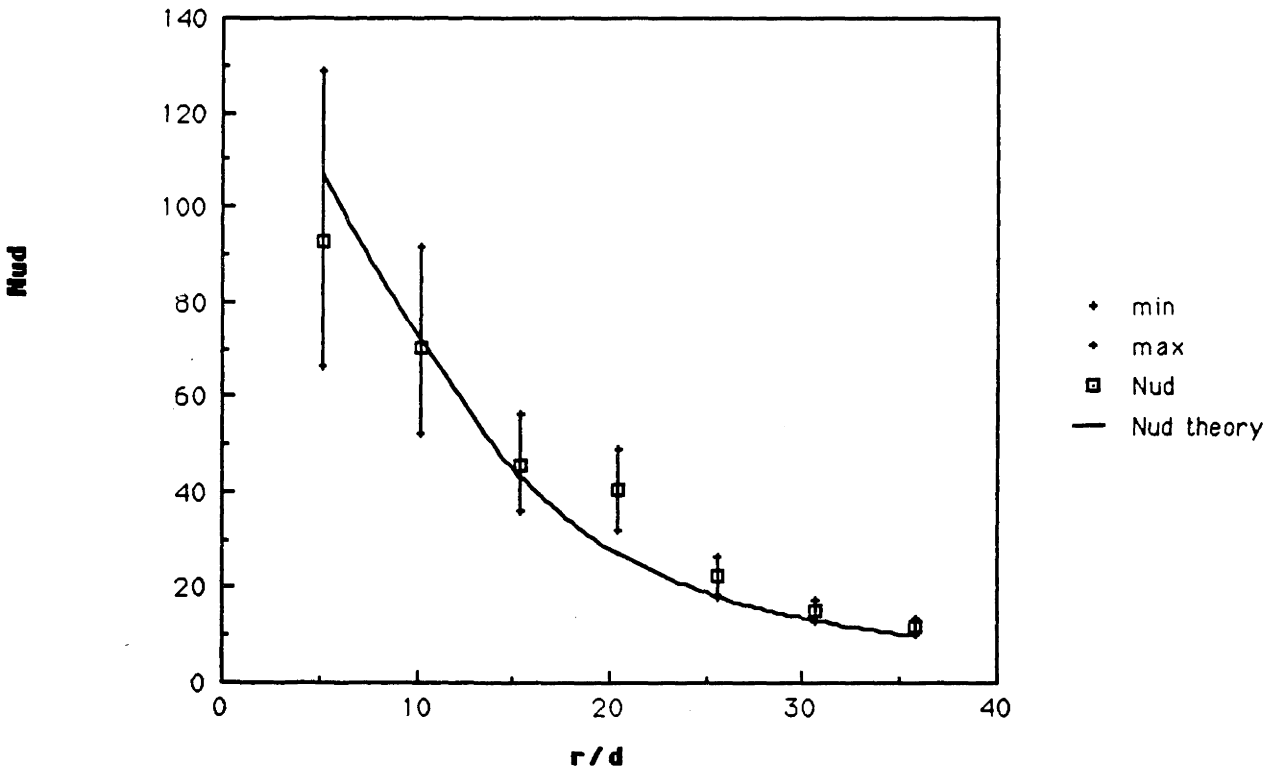

Figure 5. 1/8 inch orifice, q_w = 20,900 = W/m^2, U_j = 17.1 m/s, r_{jump} = 35.8 r/d, $Re_{r\ hump}$ = 517,000.

Table 3. Values for Figure 6.

Nu_d	Theory	Re_d	Pr	r (m)
269 13	349.8	37450	9.22	0
129 39				
96.12	114	37770	9.15	0.0127
73.94	77.4	37910	9.12	0.0254
48.06	47.5	38190	9.05	0.0381
46.72	30	38610	8.95	0.0508
25.29	20.2	39190	8.82	0.0635
17.03	14.5	39910	8.66	0.0762
13.14	10.9	40780	8.48	0.0889
10.73	8.54	41780	8.28	0.1016
T_{in} (°C)	q_w (W/m^2)	U_j (m/s)	rturb (r/d)	d_j (m)
11.14	15600	19.2	15.4	0.00248

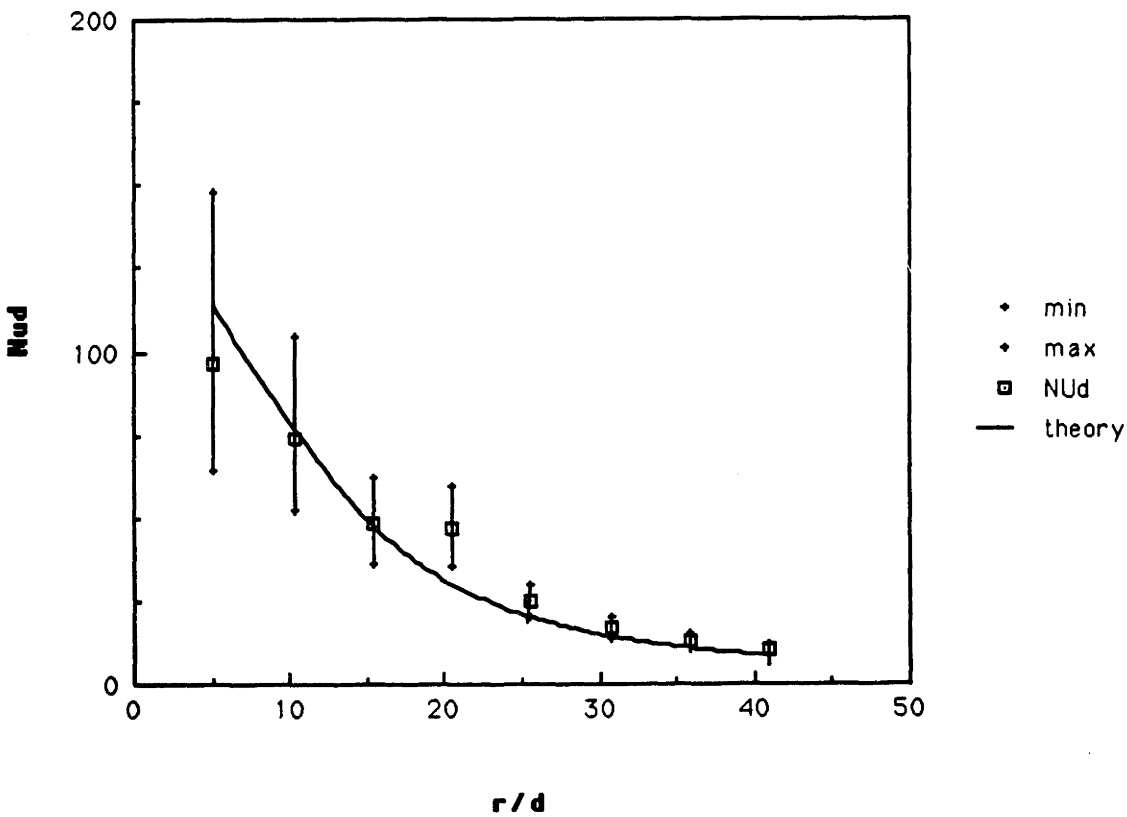

Figure 6. 1/8 inch orifice, q_w = 15,600 W/m^2, U_j = 19.2 m/s, r_{jump} = 41.0 r/d, Re_r hump = 790,900.

Table 4. Values for figure 7.

Nu_d	Theory	Re_d	Pr	r (m)
310.54	305.3	28580	9.2	0
141.15				
99.53	99	28380	9.1	0.0127
70.58	64.7	29040	9.05	0.0254
48.83	37.9	29370	8.95	0.0381
34.97	23.5	29880	8.8	0.0508
26.77	15.8	30560	8.6	0.0635
18.1	11.3	31420	8.37	0.0762
T_{in} (°C)	q_w (W/m2)	U_j (m/s)	r_{turb} (r/d)	d_j (m)
11.25	18000	14.6	12.3	0.00248

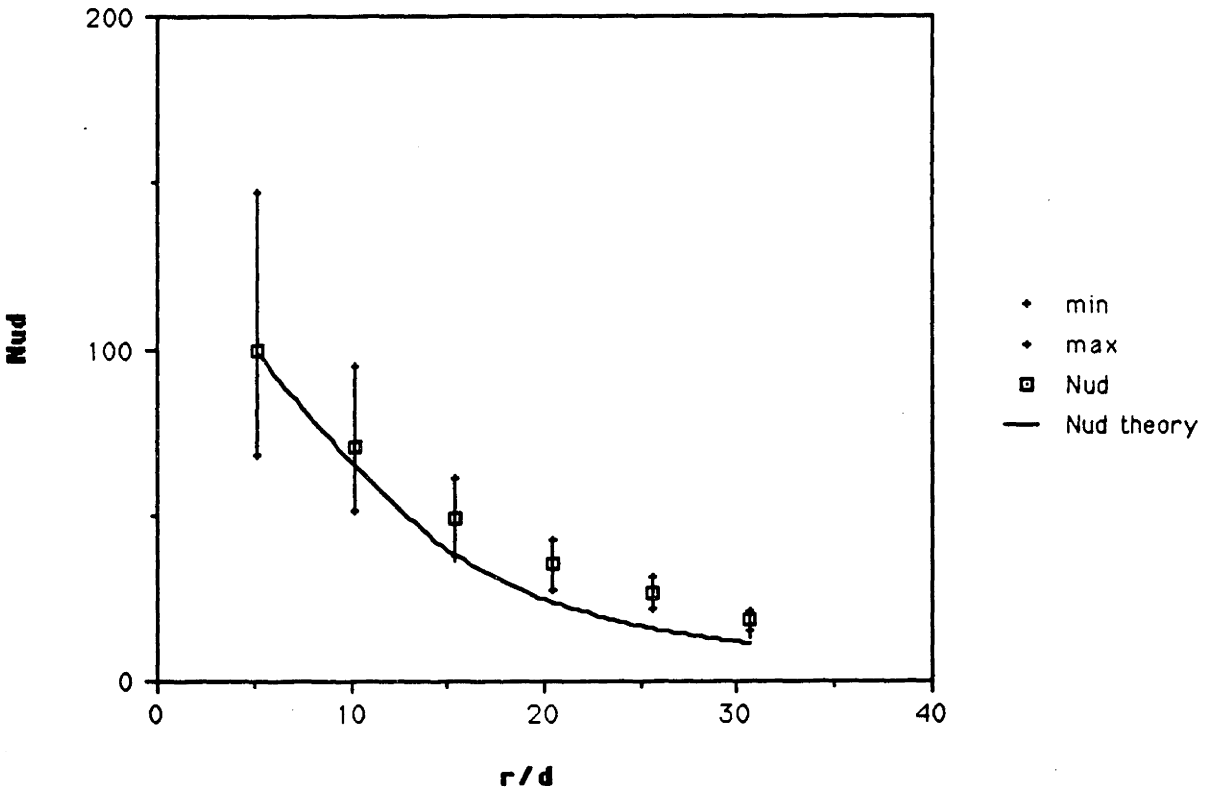

Figure 7. 1/8 inch orifice, q_w = 18,000 W/m2, U_j= 14.6 m/s, r_{jump} = 30.7 r/d, $Re_{r\ hump}$ = 451,200.

Table 5. Values for Figure 8.

Nu_d	Theory	Re_d	Pr	r (m)
251.59	317.2	31400	9.01	0
135.18				
106.56	103	31770	8.91	0.0127
73.04	68.5	31960	8.85	0.0254
47.42	40.9	32360	8.74	0.0381
40.8	25.5	32970	8.58	0.0508
23.22	17.2	33780	8.38	0.0635
17.25	12.4	34680	8.16	0.0762
T_{in} (°C)	q_w (W/m2)	U_j (m/s)	r_{turb} (r/d)	d_j (m)
12.01	21000	15.7	13.3	0.00248

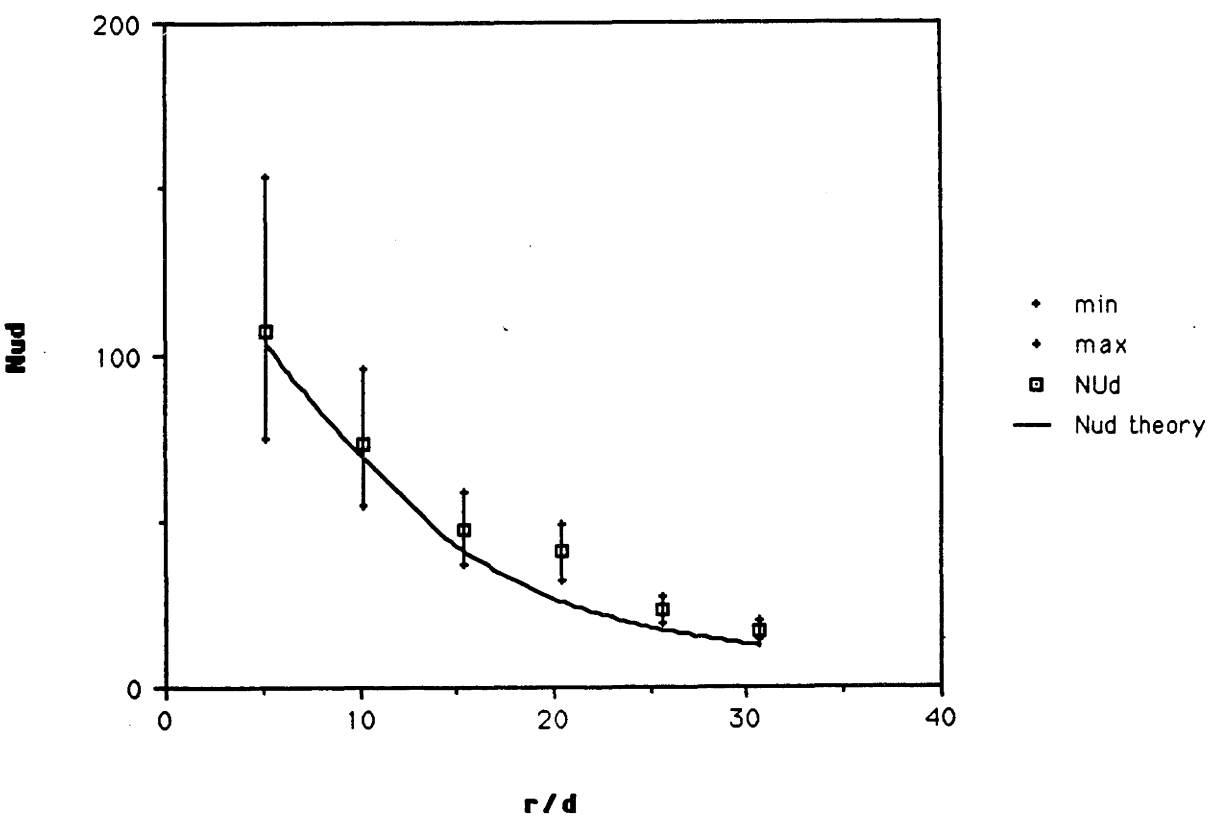

Figure 8. 1/8 inch orifice, q_w = 21,000 W/m2, U_j = 15.7 m/s, r_{jump} = 497100 r/d, $Re_{r\ hump}$ = 497,100.

Table 6. Values for Figure 9.

Nu_d	Theory	Re_d	Pr	r (m)
205.13	336.1	35960	8.8	0
110.66				
100.12	109.5	36340	8.71	0.0127
69.51	74.3	36530	8.67	0.0254
46.21	45.3	36900	8.58	0.0381
42.26	28.6	37480	8.45	0.0508
22.07	19.3	38240	8.28	0.0635
13.72	13.9	39020	8.11	0.0762
10.41	10.5	39970	7.92	0.0889
T_{in} (°C)	q_w (W/m^2)	U_j (m/s)	r_{turb} (r/d)	d_j (m)
12.88	19500	17.6	10.2	0.00248

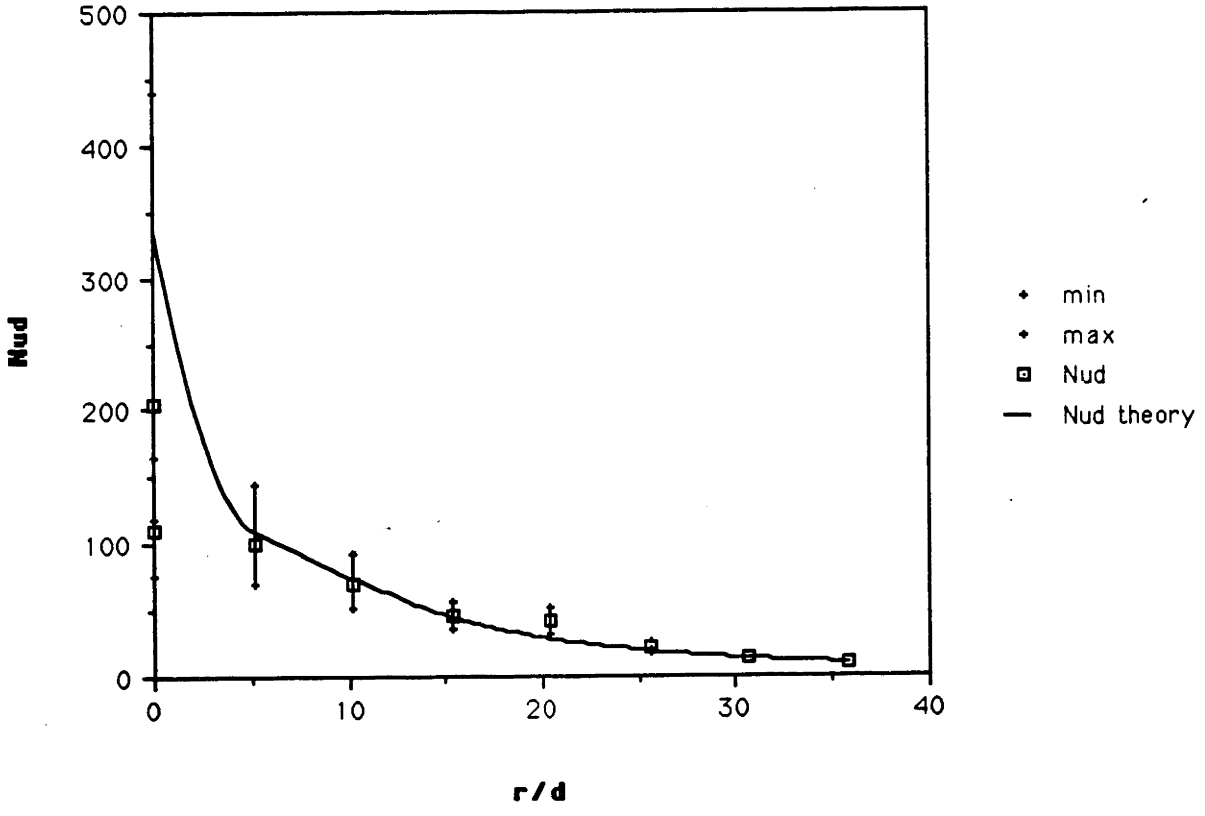

Figure 9. 1/8 inch orifice, q_w = 19,500 W/m^2, U_j = 17.6 m/s, r_{jump} = 35.8 r/d, $Re_{r\ hump}$ = 767,700.

Table 7. Values for Figure 10.

Nu_d	Theory	Re_d	Pr	r (m)
92.42	250.9	17010	10.7	0
74.65	82	17300	10.6	0.0127
51.08	47	17520	10.4	0.0254
31.1	25.6	17980	10.2	0.0381
20.52	15.6	18660	9.78	0.0508
14.21	10.5	19510	9.36	0.0635
T_{in} (°C)	q_w (W/m^2)	U_j (m/s)	r_{turb} (r/d)	d_j (m)
5.97	22500	10.1	14.1	0.00248

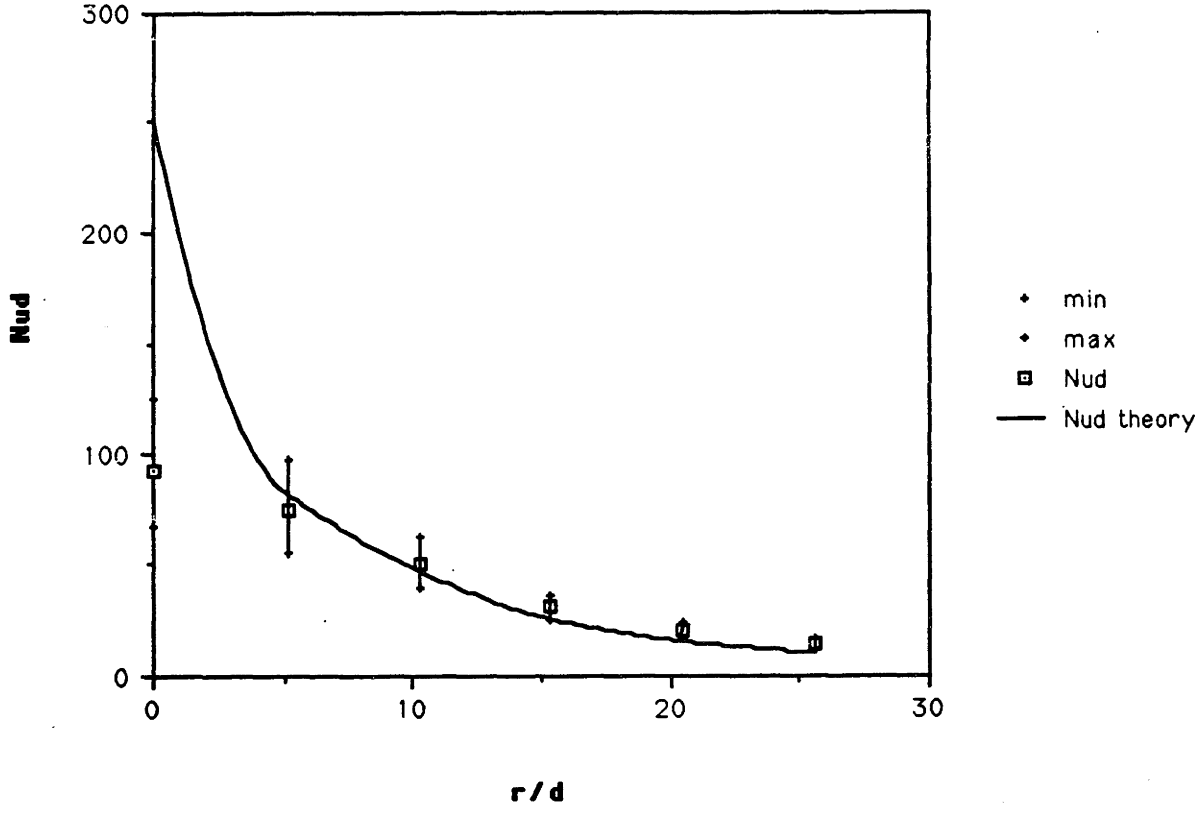

Figure 10. 1/8 inch orifice, q_w = 22,500 W/m^2, U_j = 10.1 m/s, r_{jump} = 29.7 r/d, $Re_{r\ hump}$ = 276,200.

Table 8. Values for Figure 11.

Nu_d	Theory	Re_d	Pr	r (m)
96.93	294.7	23370	10.75	0
77.04	94.5	23690	10.6	0.0127
58.53	59.3	23880	10.5	0.0254
40.42	33.8	24290	10.3	0.0381
28.17	20.8	24910	10.1	0.0508
19.9	14	25730	9.77	0.0635
15.9	10.1	26710	9.41	0.0762
T_{in} (°C)	q_w (W/m^2)	U_j (m/s)	rturb (r/d)	d_j (m)
5.89	20900	13.9	15.4	0.00248

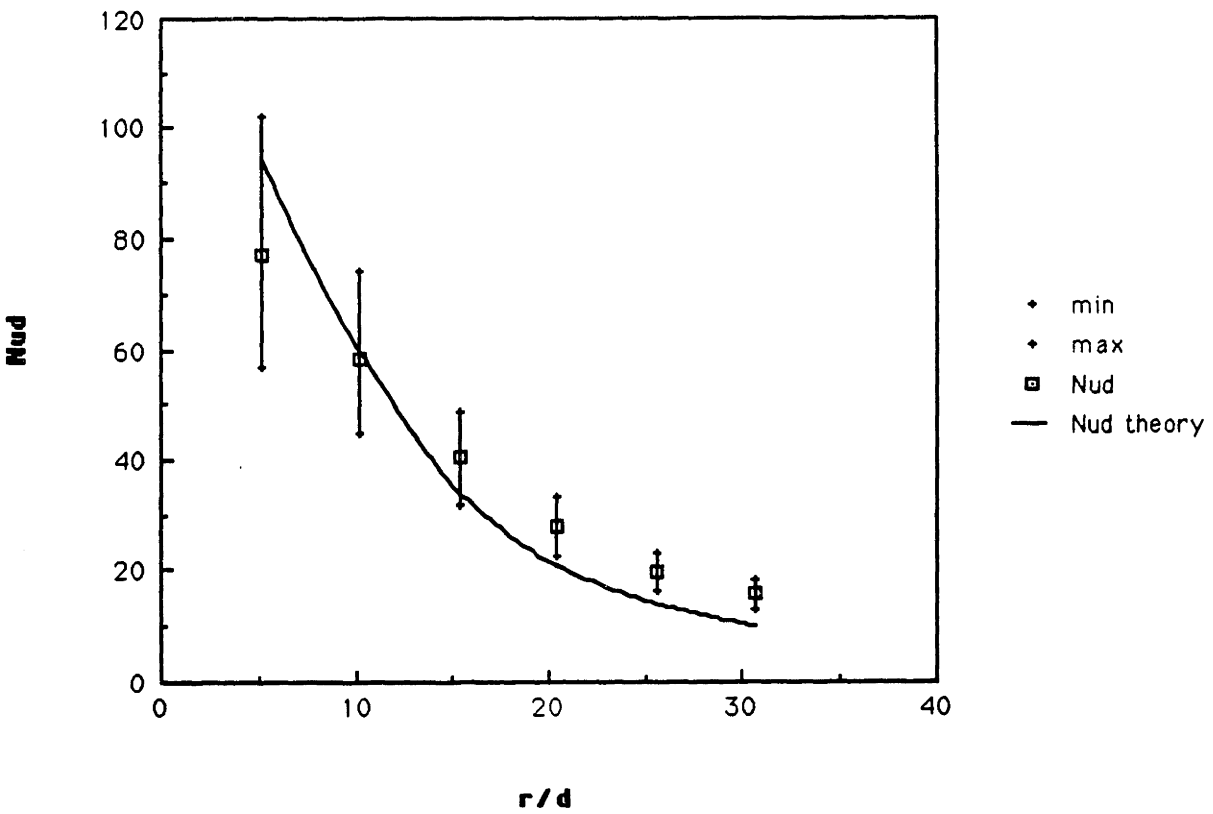

Figure 11. 1/8 inch orifice, q_w = 20,900 W/m^2, U_j = 13.9 m/s, r_{jump} = 32.0 r/d, $Re_{r\ hump}$ = 373,200.

Table 9. Values for Figure 12.

Nu_d	Theory	Re_d	Pr	r (m)
119.94	321.2	27230	11	0
92.16	103	27560	10.9	0.0127
64.86	66.5	27740	10.8	0.0254
40.91	38.7	28110	10.7	0.0381
29.18	24	28690	10.5	0.0508
22.28	16.1	29460	10.2	0.0635
18.13	11.6	30420	9.86	0.0762
13.79	8.82	31590	9.49	0.0889
T_{in} (°C)	q_w (W/m2)	U_j (m/s)	r_{turb} (r/d)	d_j (m)
5.06	20300	16.6	12.8	0.00248

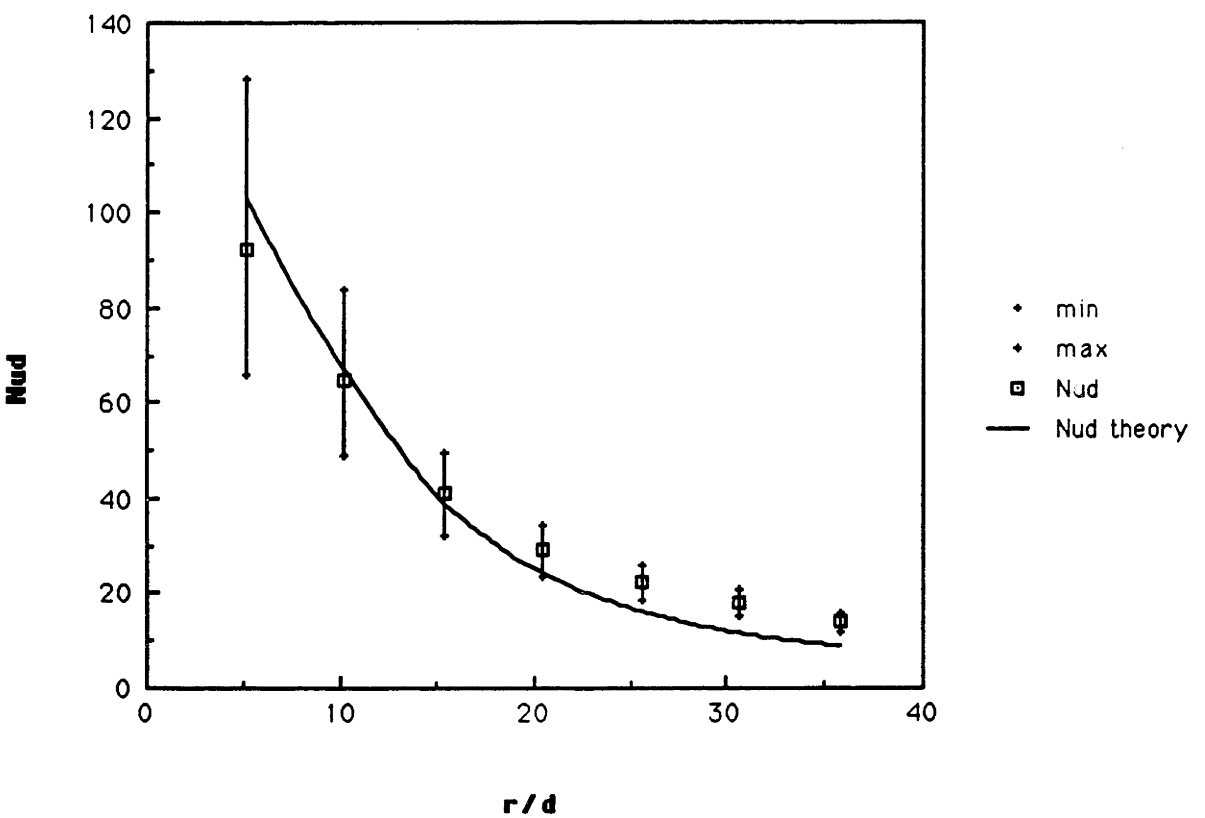

Figure 12. 1/8 inch orifice, q_w = 20,300 W/m^2, U_j = 16.6 m/s, r_{jump} = 38.4 r/d, $Re_{r\ hump}$ = 587,700.

Table 10. Values for Figure 13.

Nu_d	Theory	Re_d	Pr	r (m)
109.13	346.4	32160	10.8	0
87.09	111	32540	10.7	0.0127
62.9	74	32730	10.6	0.0254
44.62	44.3	33120	10.5	0.0381
39.38	27.7	33720	10.3	0.0508
30.29	18.7	34530	10.1	0.0635
19.03	13.5	35550	9.79	0.0762
13.16	10.2	36740	9.47	0.0889
10.22	8.04	37910	9.18	0.1016
7.04	6.52	39270	8.86	0.1143
T_{in} (°C)	q_w (W/m^2)	U_j (m/s)	r_{turb} (r/d)	d_j (m)
5.7	21000	19.3	12.3	0.00248

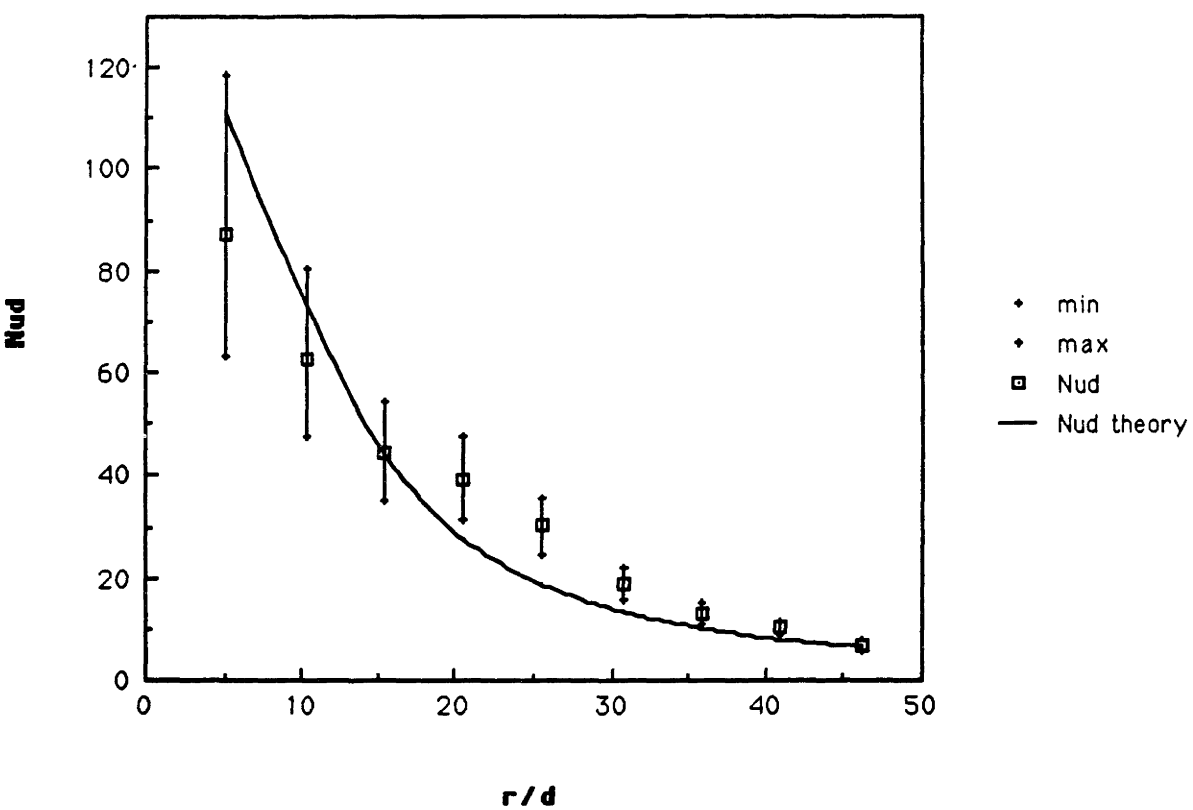

Figure 13. 1/8 inch orifice, q_w = 21,000 W/m^2, U_j = 19.3 m/s, r_{jump} = 46.1 r/d, $Re_{r\ hump}$ = 690,700.

Table 11. Values for Figure 14.

Nu_d	Theory	Re_d	Pr	r (m)
117.31	299.8	24480	10.6	0
104.75	96.1	24810	10.4	0.0127
68.74	61	25000	10.4	0.0254
45.12	34.9	25410	10.2	0.0381
31.31	21.5	26020	9.96	0.0508
20.7	14.5	26840	9.65	0.0635
16.51	10.4	27760	9.33	0.0762
13.99	7.9	28760	9.01	0.0889
9.34	6.24	29960	8.65	0.1016
T_{in} (°C)	q_w (W/m^2)	U_j (m/s)	r_{turb} (r/d)	d_j (m)
6.47	20400	14.4	15.4	0.00248

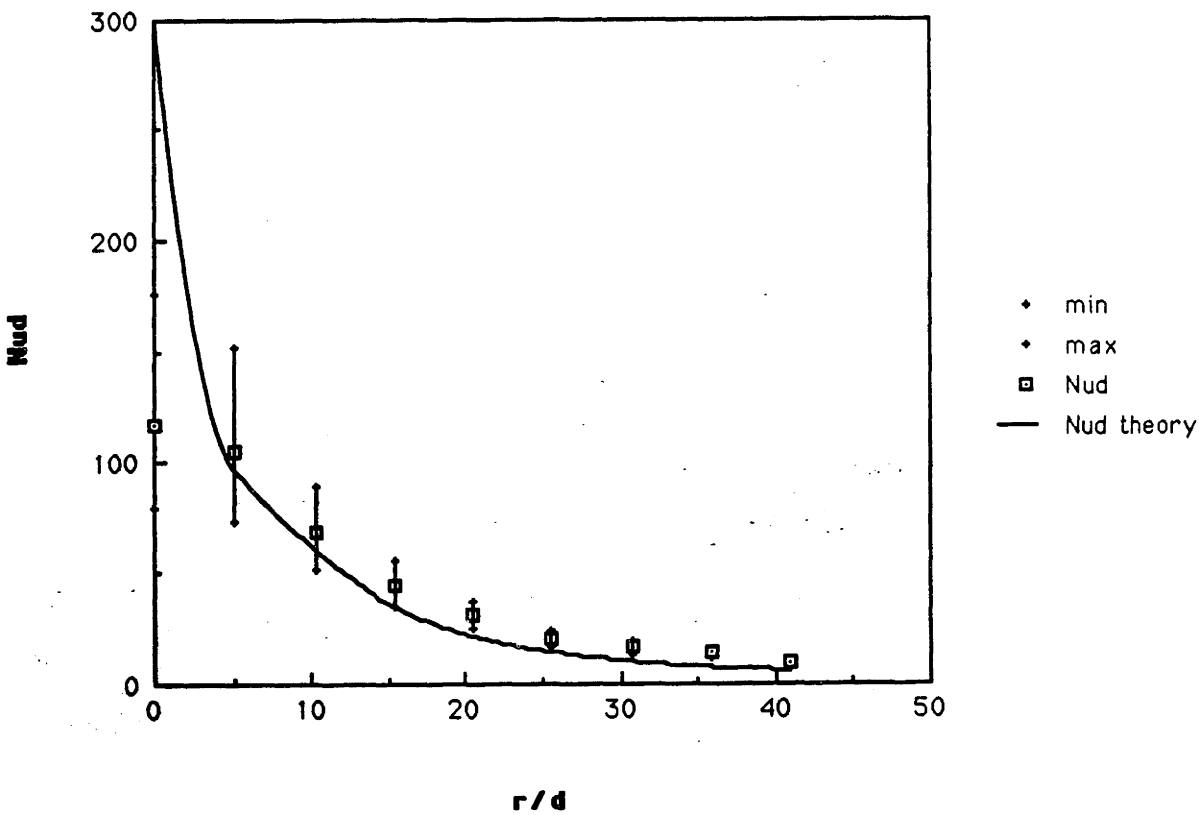

Figure 14. 1/8 inch orifice, q_w = 20,400 W/m^2, U_j = 14.4 m/s, r_{jump} = 38.4 r/d, $Re_{r\ hump}$ = 390,400.

Table 12. Values for Figure 15.

Nu_d	Theory	Re_d	Pr	r (m)
126.03	376.2	38540	10.6	0
111.54	104	38930	10.5	0.0127
77.02	68	39140	10.4	0.0254
43.91	39.9	39570	10.3	0.0381
32.9	24.8	30240	10	0.0508
26.23	16.8	31130	9.76	0.0635
20.47	12.1	32200	9.43	0.0762
15.96	9.17	33300	9.12	0.0889
11.46	7.24	34600	8.78	0.1016
T_{in} (°C)	q_w (W/m^2)	U_j (m/s)	r_{turb} (r/d)	d_j (m)
6.27	22500	16.9	12.8	0.00248

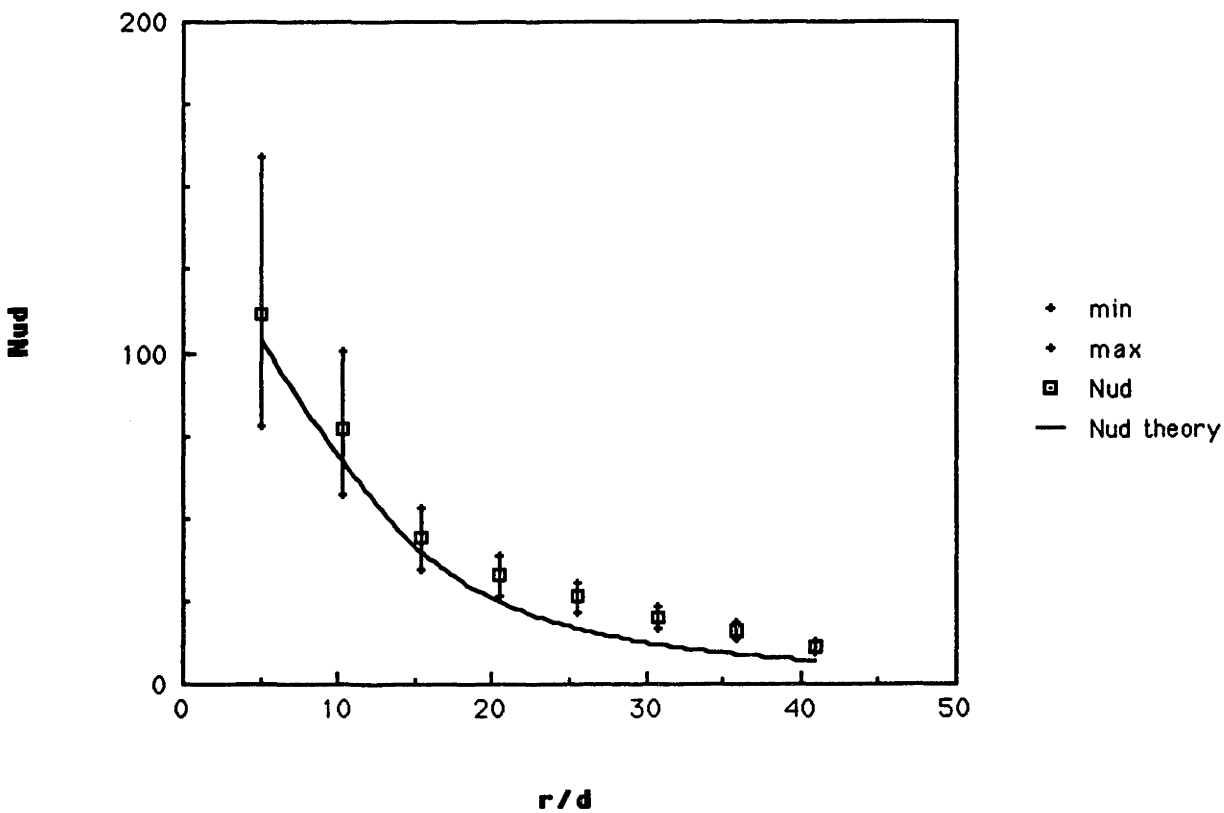

Figure 15. 1/8 inch orifice, q_w = 22,500 W/m^2, U_j = 16.9 m/s, r_{jump} = 41.0 r/d, $Re_{r\ hump}$ = 607,900.

Table 13. Values for Figure 16.

Nu_d	Theory	Re_d	Pr	r (m)
135.47	349.1	33440	10.5	0
97.15	112	33860	10.4	0.0127
82.21	75.3	34070	10.3	0.0254
57.94	45.4	34500	10.2	0.0381
48.33	28.5	35160	10	0.0508
30.83	19.3	36050	9.78	0.0635
19.16	13.9	37150	9.49	0.0762
15.46	10.5	38240	9.22	0.0889
11.7	8.3	39520	8.92	0.1016
T_{in} (°C)	q_w (W/m2)	U_j (m/s)	r_{turb} (r/d)	d_j (m)
6.6	22300	19.6	10.2	0.00248

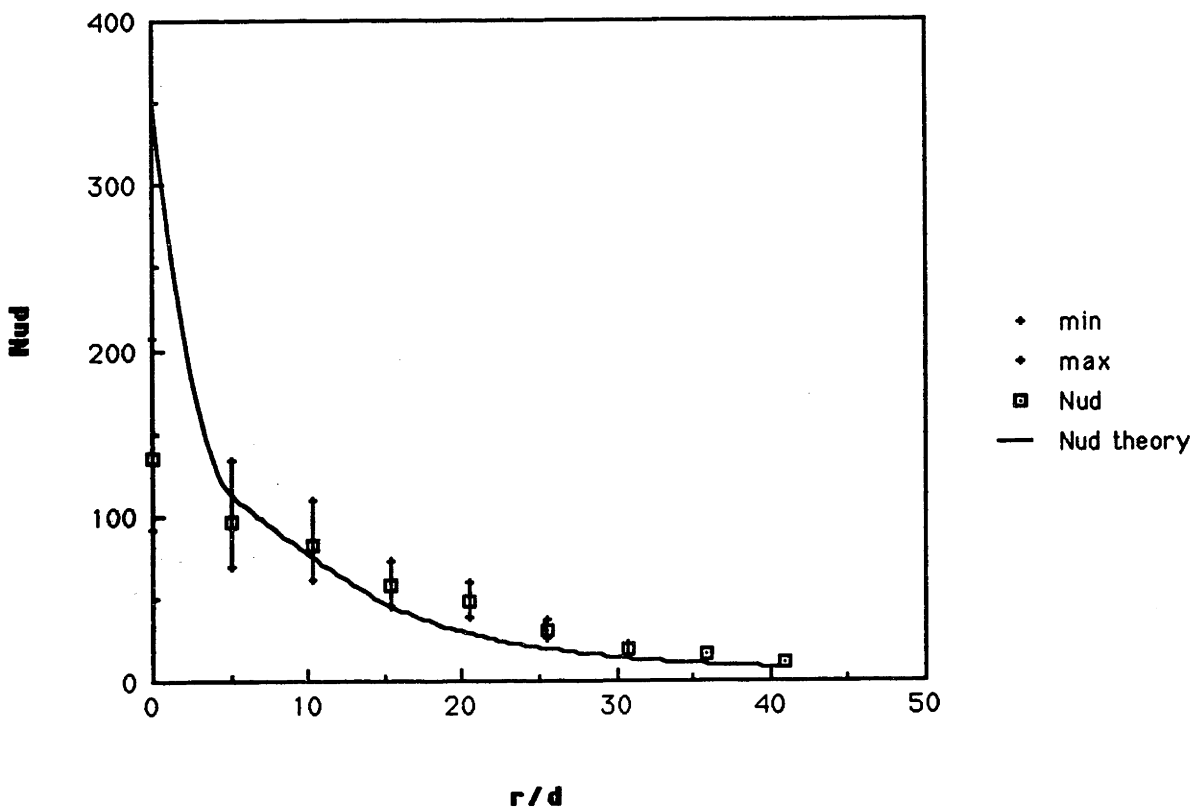

Figure16. 1/8 inch orifice, q_w = 22,300 W/m^2, U_j = 19.6 m/s, r_{jump} = 41.0 r/d, $Re_{r\ hump}$ = 348,900.

Table 14. Values for Figure 17.

Nu_d	Theory	Re_d	Pr	r (m)
87.02	249.6	16960	10.6	0
70.86	81.6	17270	10.4	0.0127
46.36	46.7	17500	10.3	0.0254
29.18	25.5	17980	9.99	0.0381
21.29	15.5	18690	9.61	0.0508
15.62	10.5	19500	9.21	0.0635
12.95	7.6	20470	8.77	0.0762
T_{in} (°C)	q_w (W/m2)	U_j (m/s)	r_{turb} (r/d)	d_j (m)
6.45	23000	10	12.8	0.00248

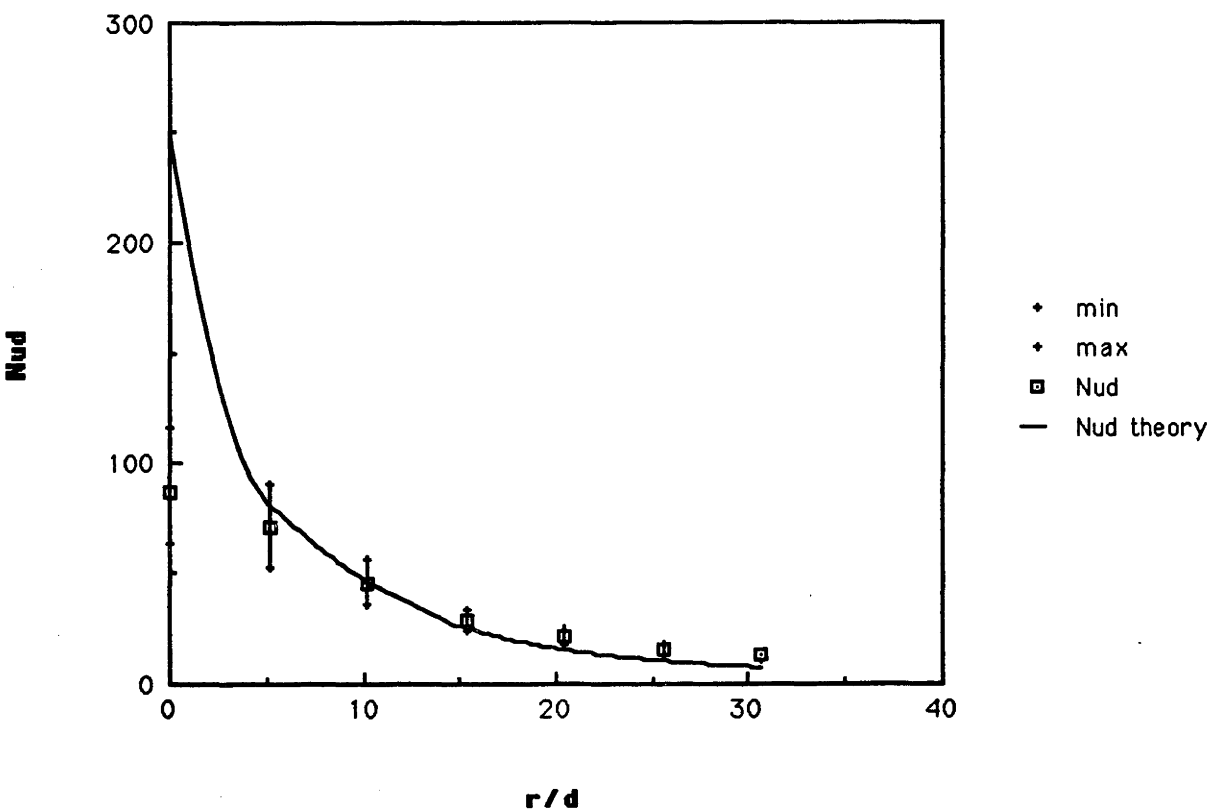

Figure 17. 1/8 inch orifice, q_w = 23,000 W/m^2, U_j = 10.0 m/s, r_{jump} = 30.7 r/d, $Re_{r\,hump}$ = 276,200.

Table 15. Values for Figure 18.

Nu_d	Theory	Re_d	Pr	r (m)
192.53806	330.88	28250	11.3	0
153.635219	150	28960	11.1	0.0127
123.808608	106	29150	11	0.0254
94.2852792	88.2	29300	10.9	0.0381
73.5809233	69.6	29550	10.8	0.0508
57.1907854	53.4	29900	10.7	0.0635
44.3585116	41.2	30390	10.5	0.0762
38.7124959	32.4	30980	10.3	0.0889
36.0313762	26	31690	10.1	0.1016
31.54671	21.3	32510	9.8	0.1143
26.9092515	17.9	33450	9.6	0.127
24.0308344	15.1	34340	9.31	0.1397
T_{in} (°C)	q_w (W/m^2)	U_j (m/s)	r_{turb} (r/d)	d_j (m)
4.27	22900	8.9	11.5	0.004964

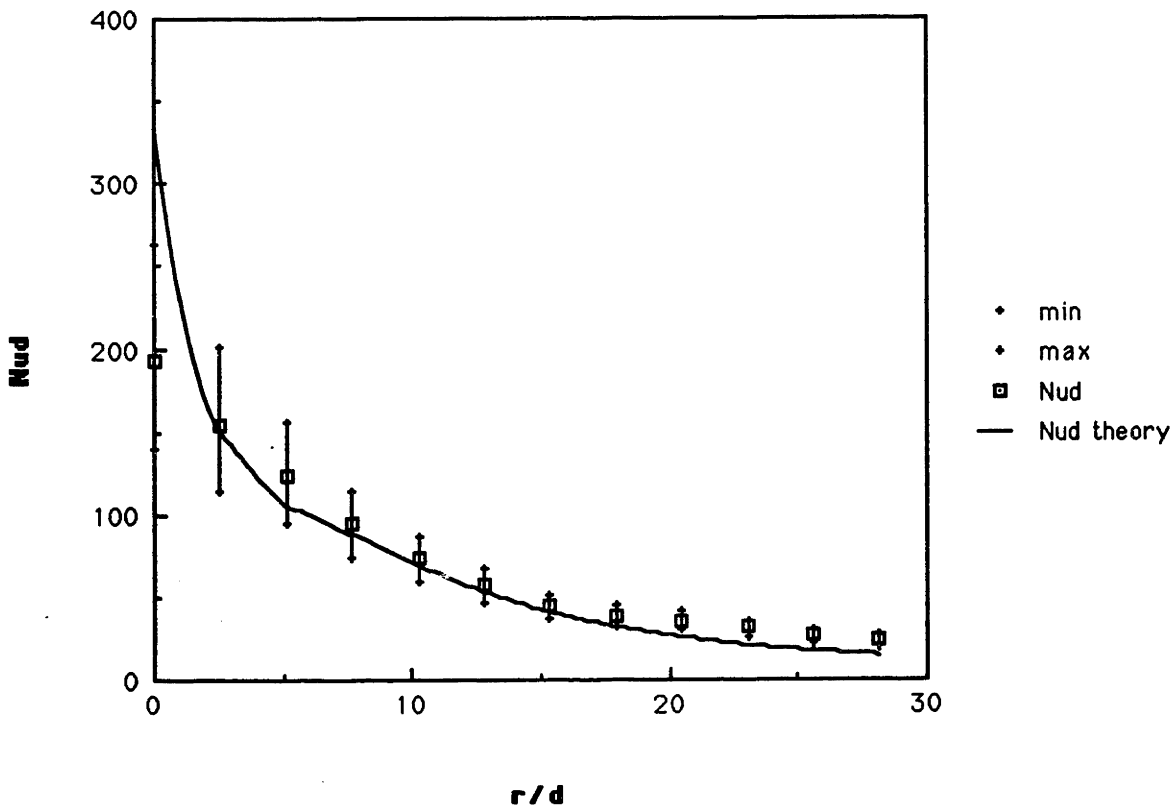

Figure 18. 1/4 inch orifice, q_w = 22,900W/m^2, U_j = 8.9 m/s, $Re_{r\ hump}$ = 554,800.

Table 16. Values for Figure 19.

Nu_d	Theory	Re_d	Pr	r (m)
246.66	397.08	41300	11.1	0
186.2	179	41920	10.9	0.0127
146.1	127	42180	10.8	0.0254
117.24	106	42360	10.8	0.0381
93.56	88	42580	10.7	0.0508
80.48	70.2	42920	10.6	0.0635
65.49	55.5	43370	10.5	0.0762
58.08	44.2	43930	10.4	0.0889
53.5	35.7	44590	10.2	0.1016
56.69	29.4	45370	10.1	0.1143
48.2	24.6	46270	9.87	0.127
38.45	20.9	47270	9.66	0.1397
T_{in} (°C)	q_w (W/m2)	U_j (m/s)	r_{turb} (r/d)	d_j (m)
4.93	22000	12.7	11.5	0.004964

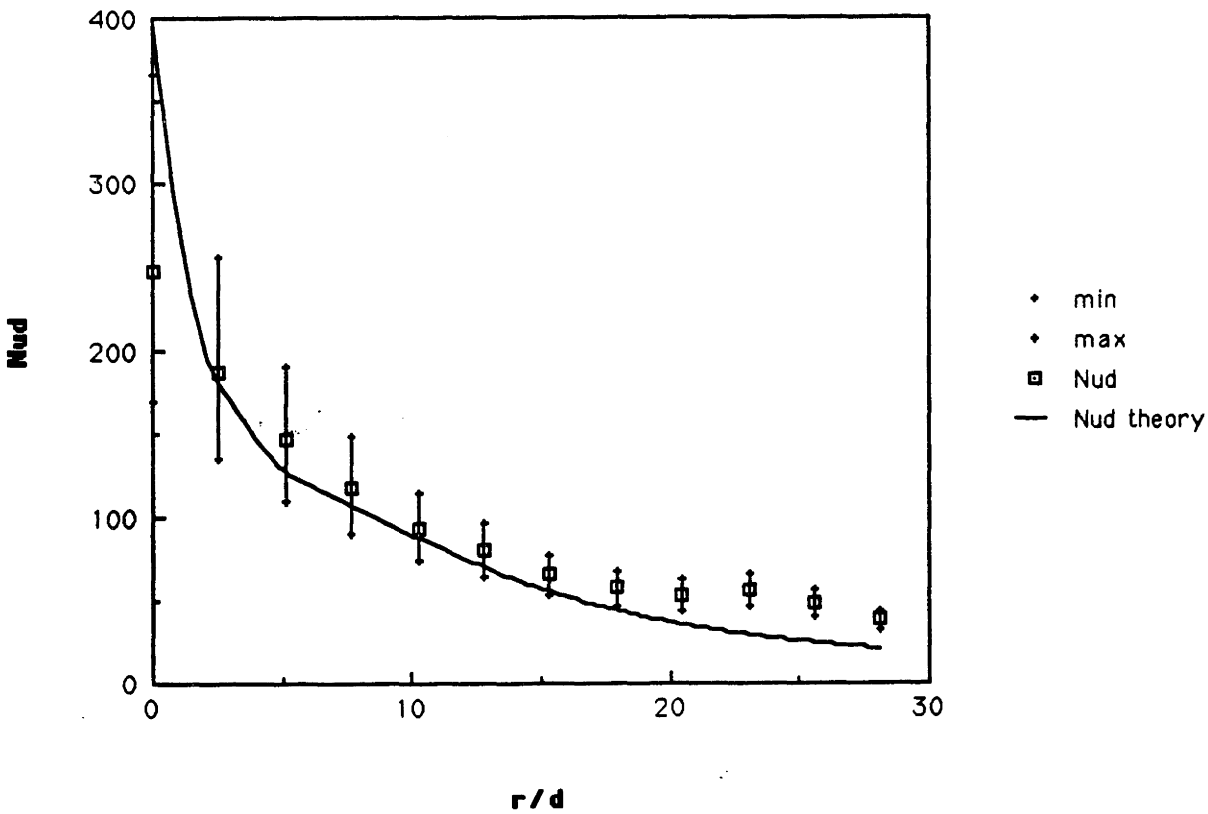

Figure 19. 1/4 inch orifice, q_w = 22,000 W/m^2, U_j = 12.7 m/s, $Re_{r\ hump}$ = 786,700.

Table 17. Values for Figure 20.

Nu_d	Theory	Re_d	Pr	r (m)
382.56	421.39	45480	11.4	0
229.54	190	46300	11.2	0.0127
168.2	135	46650	11.1	0.0254
133.63	113	46890	11.1	0.0381
110.23	94.5	47140	11	0.0508
97.07	76.2	47470	10.9	0.0635
76.81	60.7	47910	10.8	0.0762
65.04	48.6	48460	10.7	0.0889
52.59	39.4	49120	10.6	0.1016
60.97	32.5	49900	10.4	0.1143
55.9	27.2	50780	10.2	0.127
43.94	23.1	51770	10	0.1397
T_{in} (°C)	q_w (W/m2)	U_j (m/s)	r_{turb} (r/d)	d_j (m)
4.02	22600	14.4	12.8	0.004964

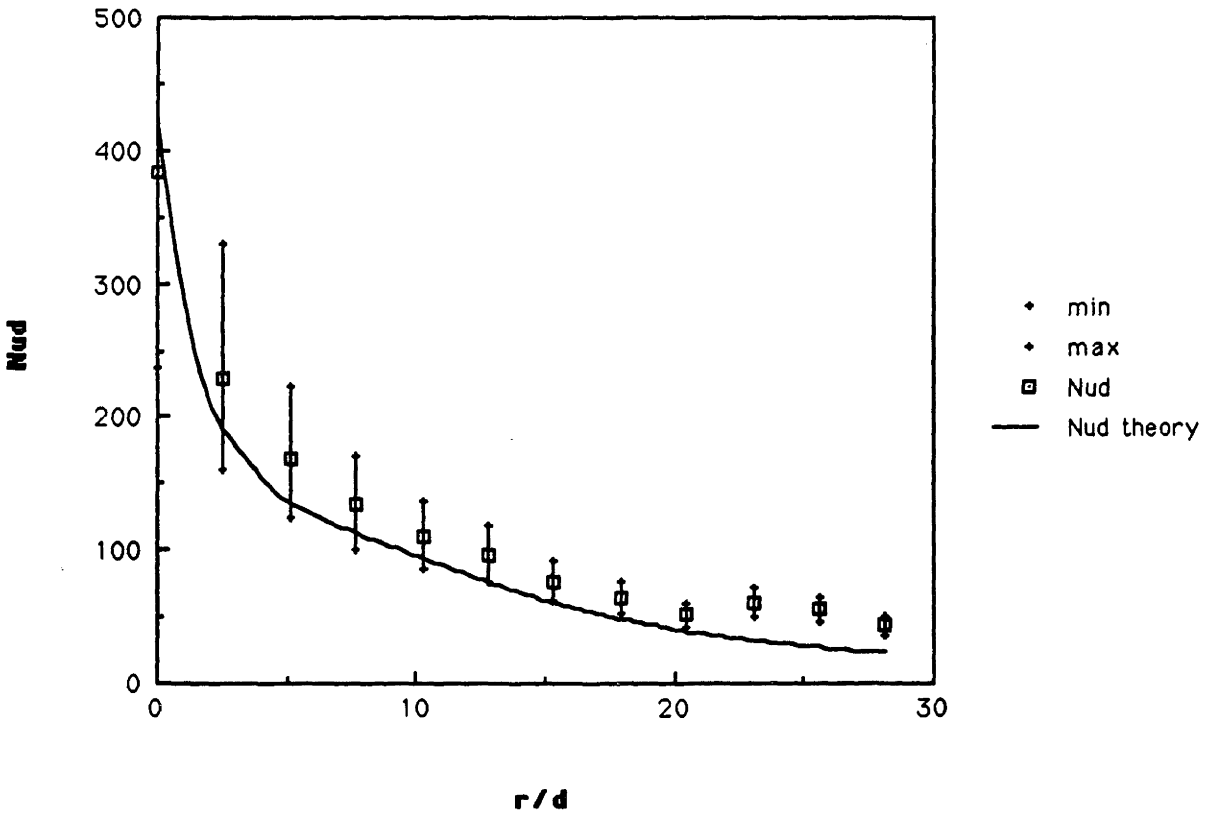

Figure 20. 1/4 inch orifice, q_w = 22,600 W/m^2, U_j = 14.4 m/s, $Re_{r\ hump}$=1,005,000.

Table 18. Values for Figure 21.

Nu_d	Theory	Re_d	Pr	r (m)
361.02	383	36770	11.7	0
181.89	173	37650	11.4	0.0127
148	122	38020	11.3	0.0254
117.96	103	38270	11.2	0.0381
97.65	83.8	38630	11.1	0.0508
77.61	66.2	39100	11	0.0635
61.1	52.1	39650	10.8	0.0762
54.52	41.4	40320	10.7	0.0889
53.54	33.4	41130	10.5	0.1016
44.21	27.5	42070	10.2	0.1143
34.99	23.1	43150	9.96	0.127
31.77	19.7	44370	9.69	0.1397
q_w (W/m^2)	T_{in} (°C)	U_j (m/s)	r_{turb} (r/d)	d_j (m)
27600	3.32	11.9	11.5	0.004964

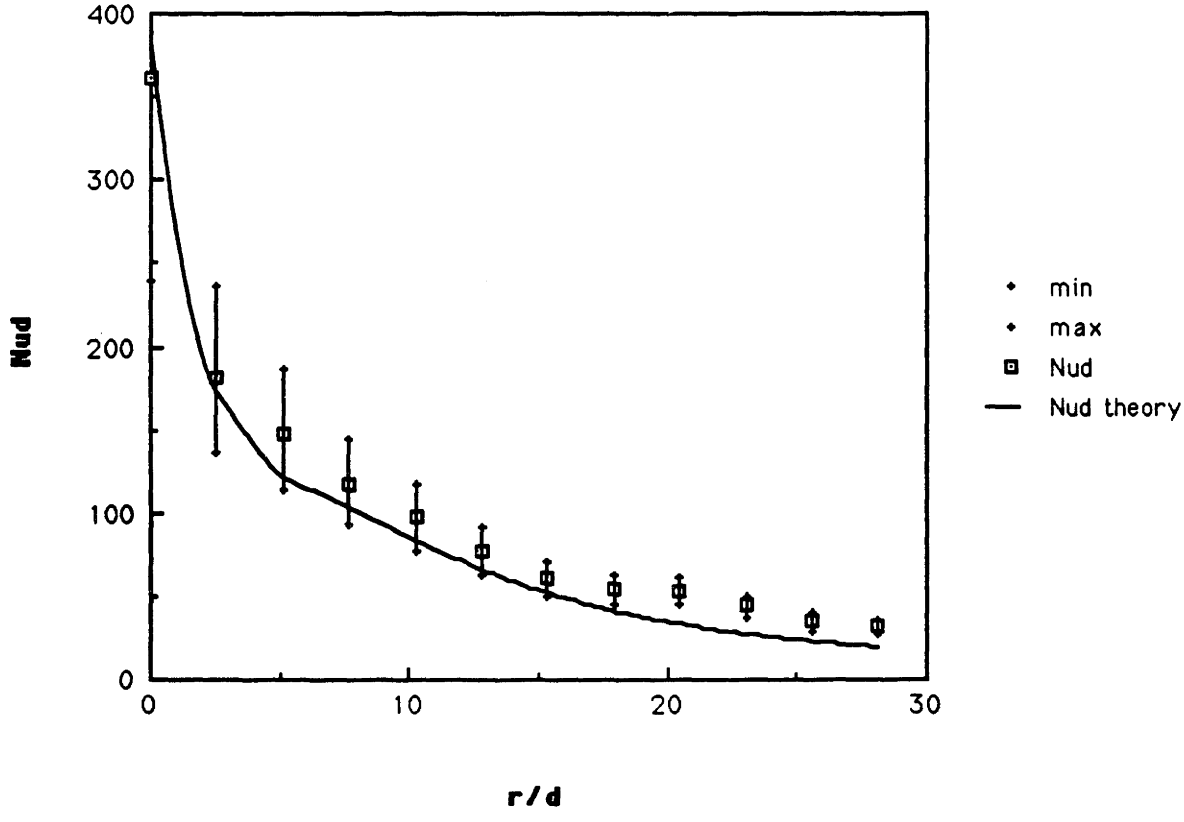

Figure 21. 1/4 inch orifice, q_w = 27,600 W/m^2, U_j = 11.9 m/s, $Re_{r\ hump}$ = 722,100.

Table 19. Values for Figure 22.

Nu_d	Theory	Re_d	Pr	r (m)
308.383635	422.2	44670	11.7	0
293.928152				0
198.014755	190	45420	11.5	0.0127
146.964076	134	45750	11.4	0.0254
120.585909	113	45960	11.3	0.0381
104.507787	94	46230	11.3	0.0508
89.1535627	75.7	46630	11.2	0.0635
72.9124098	60.3	47160	11.1	0.0762
63.7674635	48.2	47690	10.9	0.0889
60.8783228	39.1	48310	10.8	0.1016
61.676727	32.2	49030	10.6	0.1143
48.8607837	26.9	49850	10.5	0.127
37.3242098	22.8	50780	10.3	0.1397
q_w (W/m^2)	T_{in} (°C)	U_j (m/s)	r_{turb} (r/d)	d_j (m)
21790	0.31	14.5	12.8	0.004964

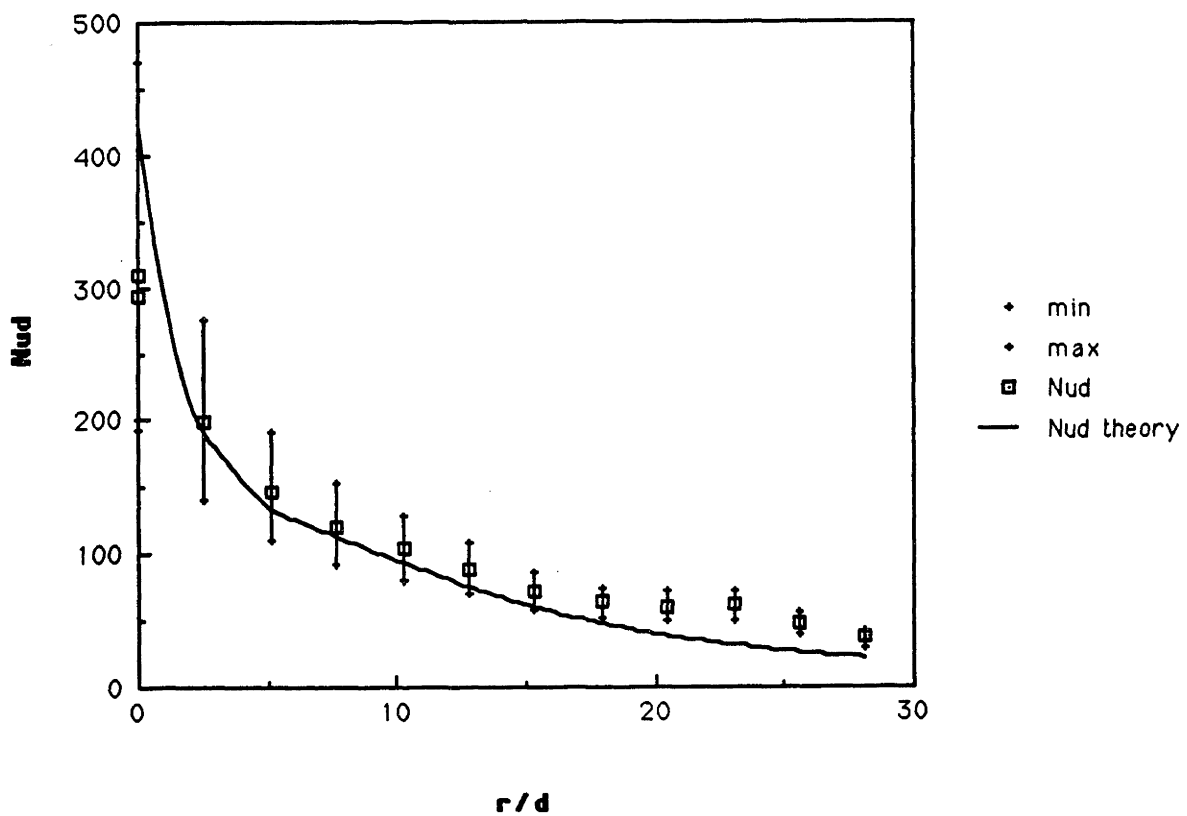

Figure 22. 1/4 inch orifice, q_w = 21,790 W/m^2, U_j = 14.5 m/s, $Re_{r\ hump}$ = 854,100.

Table 20. Values for Figure 23.

Nu_d	Theory	Re_d	Pr	r (m)
277.9	384.31	37280	11.6	0
273.56				0
175.08	173	37930	11.4	0.0127
131.64	123	38210	11.3	0.0254
110.81	103	38390	11.3	0.0381
92.15	84	38650	11.2	0.0508
75.79	66.3	39040	11.1	0.0635
59.96	52	39460	11	0.0762
49.18	41.3	39950	10.8	0.0889
43.99	33.2	40540	10.7	0.1016
47.97	27.3	41230	10.5	0.1143
40.81	22.8	42010	10.3	0.127
31.66	19.3	42880	10.1	0.1397
q_w (W/m^2)	T_{in} (°C)	U_j (m/s)	r_{turb} (r/d)	d_j (m)
20280	3.56	11.98	12.8	0.004964

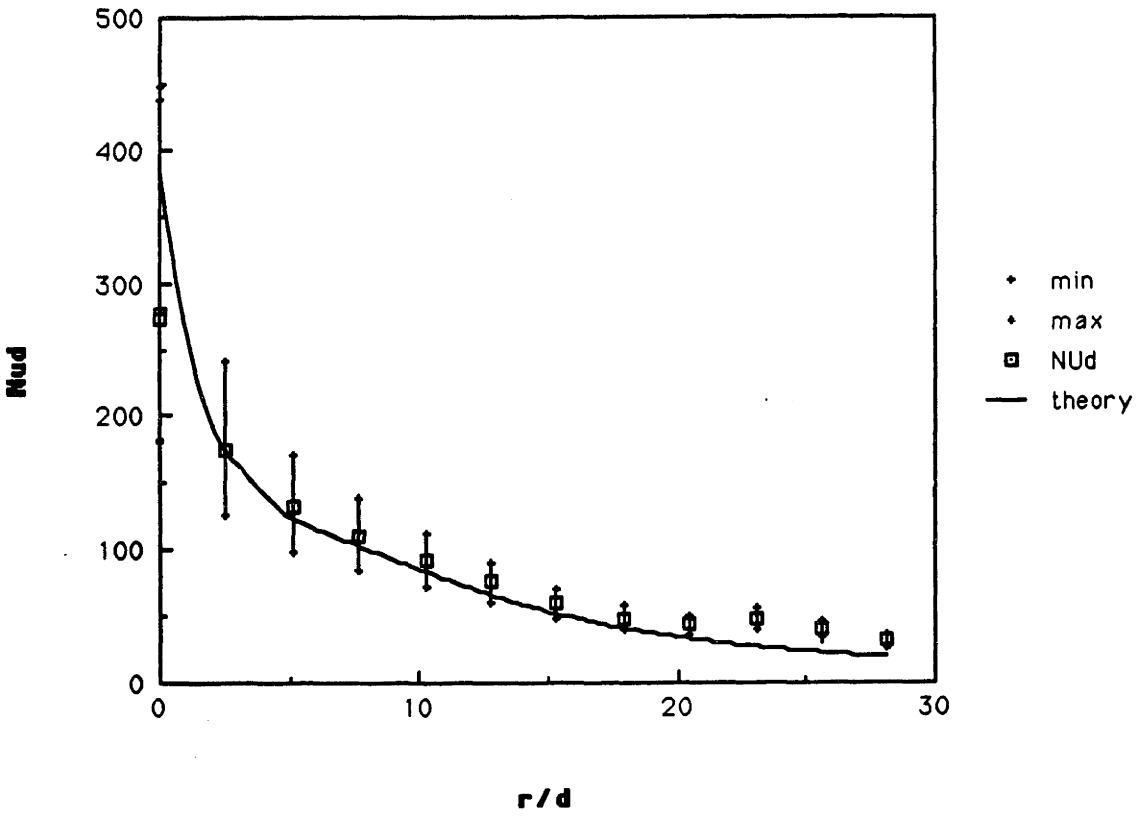

Figure 23. 1/4 inch orifice, q_w = 20,280 W/m^2, U_j = 11.98 m/s, $Re_{r\ hump}$= 829,700.

Table 21. Values for Figure 24.

Nu_d	Theory	Re_d	Pr	r (m)
187.57583	331.22	30600	10.3	0
193.759648				0
138.835654	151	31130	10.2	0.0127
108.840296	107	31360	10.1	0.0254
86.8577734	89.4	31520	10.1	0.0381
67.0423118	71.2	31760	10	0.0508
52.4765714	55.1	32120	9.9	0.0635
43.6438812	42.7	32590	9.76	0.0762
35.4058795	33.6	33170	9.59	0.0889
33.5850057	27	33780	9.41	0.1016
33.3310548	22.1	34420	9.24	0.1143
27.3790807	18.4	35160	9.04	0.127
22.1787774	15.6	35990	8.83	0.1397
q_w (W/m^2)	T_{in} (°C)	U_j (m/s)	r_{turb} (r/d)	d_j (m)
20424	7.09	8.807	11.5	0.004964

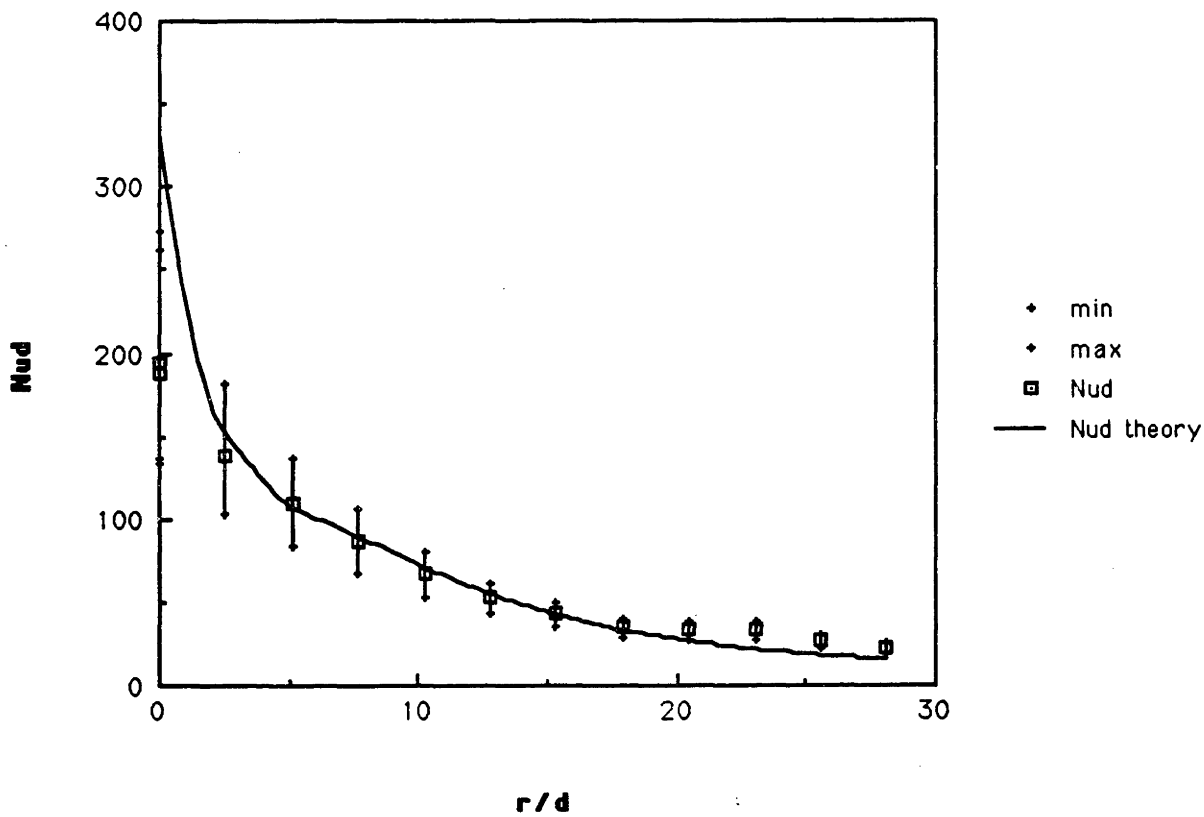

Figure 24. 1/4 inch orifice, q_w = 20,424 W/m^2, U_j = 8.8 m/s, $Re_{r\ hump}$ = 691,400.

Table 22. Values for Figure 25.

Nu_d	Theory	Re_d	Pr	r (m)
169.963043	332.34	29240	10.96	0
177.905242				0
120.480132	151	29770	10.8	0.0127
98.1229942	107	29990	10.7	0.0254
81.0036633	88.8	30140	10.6	0.0381
64.7478261	70.3	30390	10.5	0.0508
51.0344795	54.1	30750	10.4	0.0635
39.8239767	41.9	31230	10.3	0.0762
34.9281851	32.9	31810	10.1	0.0889
31.2575712	26.4	32510	9.85	0.1016
31.6210313	21.7	33330	9.61	0.1143
26.512341	18.1	34160	9.38	0.127
20.7815075	15.4	35010	9.15	0.1397
q_w (W/m^2)	T_{in} (°C)	U_j (m/s)	r_{turb} (r/d)	d_j (m)
22050	5.25	8.9	11.5	0.004964

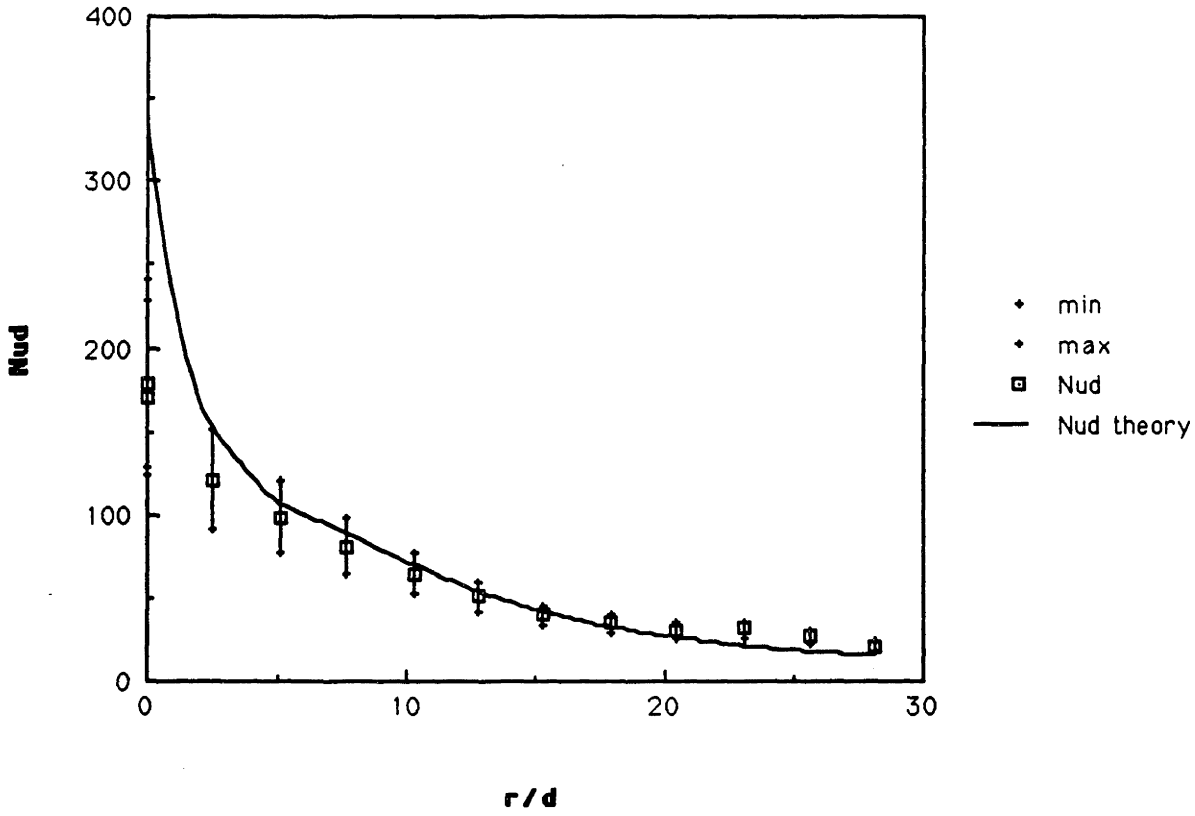

Figure 25. 1/4 inch orifice, q_w = 22,050 W/m^2, U_j = 8.9 m/s, $Re_{r\ hump}$ = 665,400.

Table 23. Values for Figure 26.

Nu_d	Theory	Re_d	Pr	r (m)
287.768116	393.03	38164	11.9	0
287.768116				0
194.939691	174	38870	11.6	0.0127
139.456856	123	39170	11.6	0.0254
114.742983	103	39370	11.5	0.0381
92.027367	84.8	39600	11.4	0.0508
79.1676476	67.1	40070	11.3	0.0635
62.0869565	52.7	40460	11.2	0.0762
53.7964134	41.9	40780	11	0.0889
58.8616601	33.8	41600	10.9	0.1016
49.1311417	27.7	42320	10.7	0.1143
39.8448161	23.1	43140	10.5	0.127
32.8431002	19.7	44110	10.26	0.1397
q_w (W/m^2)	T_{in} (°C)	U_j (m/s)	r_{turb} (r/d)	d_j (m)
21000	4.77	12.25	11.5	0.004964

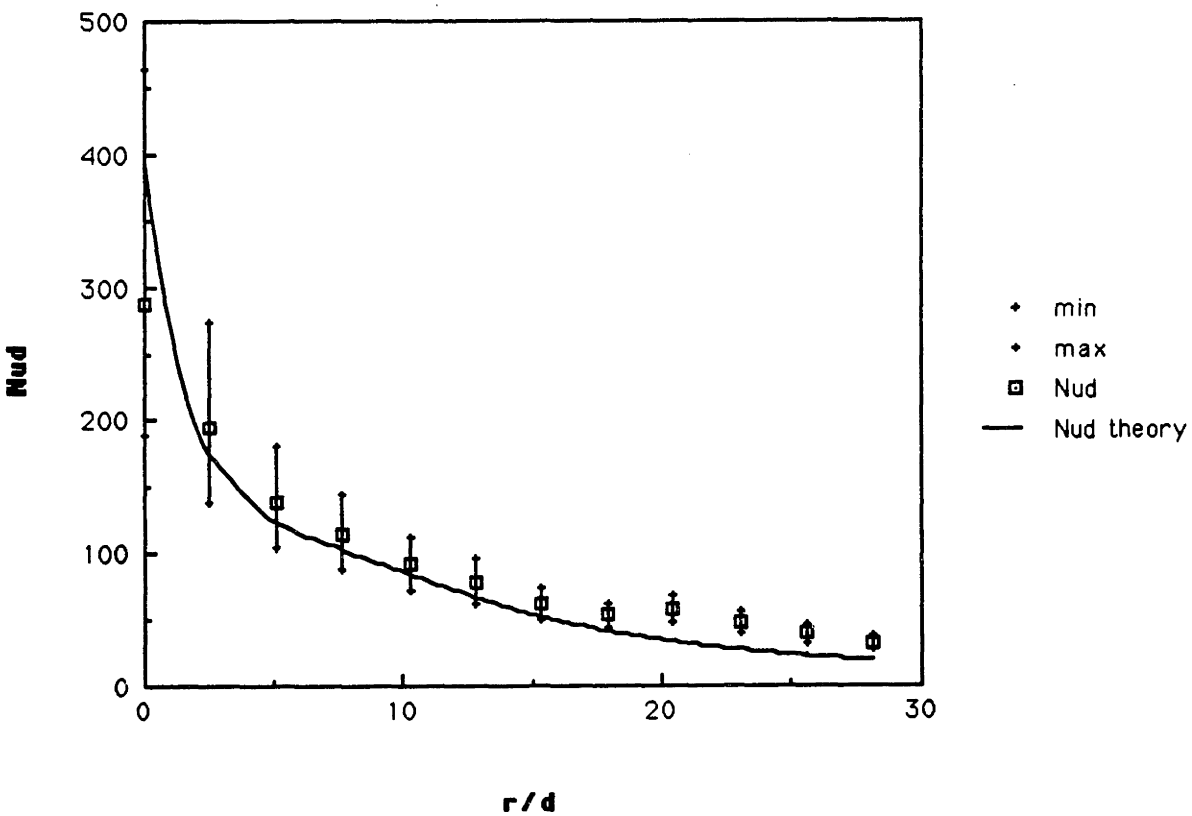

Figure 26. 1/4 inch orifice, q_w = 21,000 W/m^2, U_j = 12.25 m/s, $Re_{r\ hump}$=730,300.

Table 24. Values for Figure 27.

Nu_d	Theory	Re_d	Pr	r (m)
319.285576	434.72	48440	11.39	0
319.3				0
216.290229	193.7	49230	11.2	0.0127
154.730702	137.1	49530	11.1	0.0254
127.310072	114.7	49730	11.1	0.0381
102.106555	96.6	49970	11.1	0.0508
87.83839	78.4	50330	11	0.0635
68.8869565	62.7	50770	11.9	0.0762
59.6884015	50.4	51350	11.8	0.0889
65.3084133	41	52050	10.6	0.1016
54.5121716	33.8	52860	10.4	0.1143
44.2087721	30.2	53780	10.3	0.127
36.4402016	24.1	54810	10.1	0.1397
q_w (W/m^2)	T_{in} (°C)	U_j (m/s)	r_{turb} (r/d)	d_j (m)
23300	4.77	14.95	12.8	0.004964

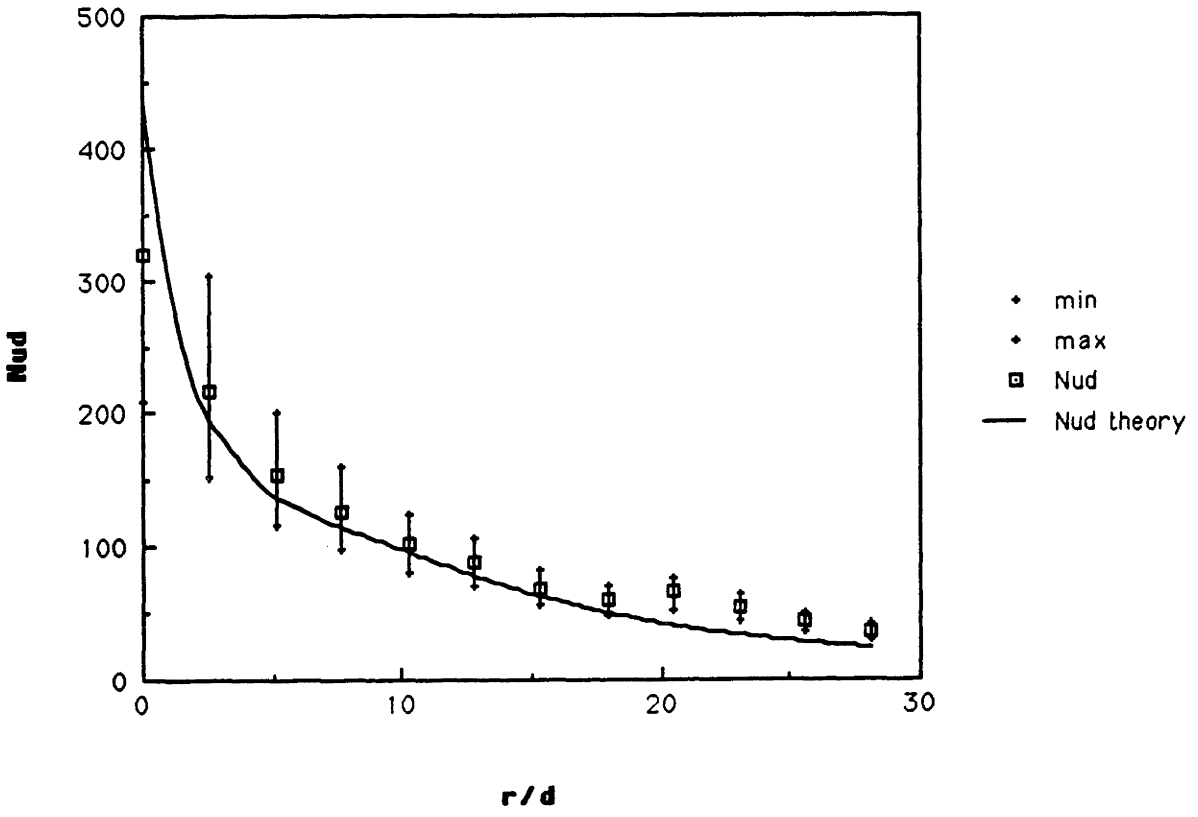

Figure 27. 1/4 inch orifice, q_w = 23,300 W/m^2, U_j = 14.95 m/s, $Re_{r\ hump}$=919,600.

Table 25. Values for Figure 28.

Nu_d	Theory	Re_d	Pr	r (m)
214.276566	427.06	49540	10.63	0
219.915423				0
159.176878	194	50170	10.5	0.0127
126.617971	137	50440	10.4	0.0254
107.829498	115	50620	10.4	0.0381
92.8531787	96.8	50820	10.4	0.0508
78.8376046	78.7	55130	10.3	0.0635
62.1322386	63.1	51530	10.2	0.0762
53.9147489	50.7	52050	10.1	0.0889
49.3025728	41.2	52660	10	0.1016
50.0406353	33.9	53380	9.87	0.1143
41.9938999	28.4	54200	9.72	0.127
35.6366144	24.1	55130	9.56	0.1397
q_w (W/m^2)	T_{in} (°C)	U_j (m/s)	r_{turb} (r/d)	d_j (m)
19360	6.29	14.6	12.8	0.004964

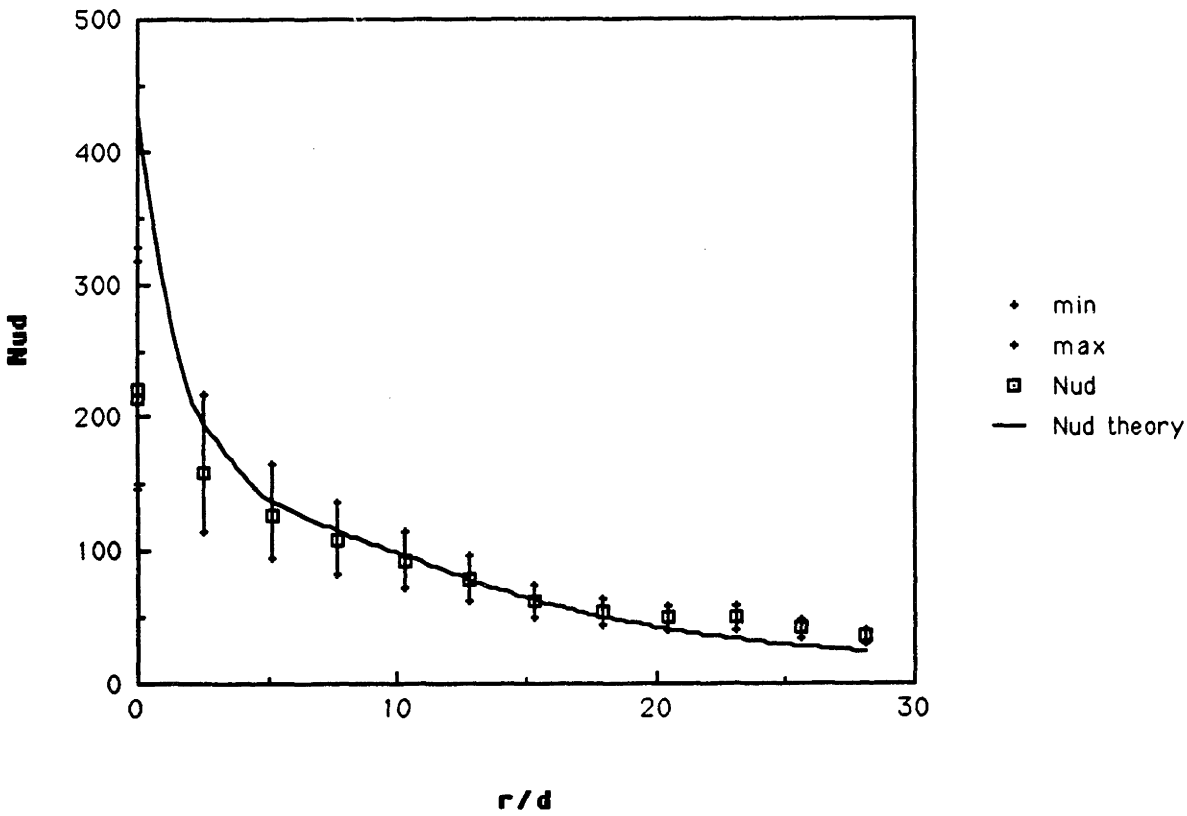

Figure 28. 1/4 inch orifice, q_w = 19,360 W/m^2, U_j = 14.6 m/s, $Re_{r\ hump}$ = 932,200.

Table 26. Values for Figure 29.

Nu_d	Theory	Re_d	Pr	r (m)
298.304856	458.39	56100	10.85	0
302.96587				0
217.863097	208	56840	10.7	0.0127
149.152428	147	57160	10.6	0.0254
121.948526	122	57380	10.6	0.0381
108.931549	105	57600	10.6	0.0508
91.4613946	86.3	57930	10.5	0.0635
74.8641531	69.9	58380	10.4	0.0762
63.3654106	56.6	58950	10.3	0.0889
56.2023642	46.2	59630	10.2	0.1016
60.5931739	38.2	60420	10.1	0.1143
47.9945932	32.1	61330	9.92	0.127
42.708845	27.3	62360	9.76	0.1397
q_w (W/m^2)	T_{in} (°C)	U_j (m/s)	r_{turb} (r/d)	d_j (m)
22460	5.64	16.9	13.8	0.004964

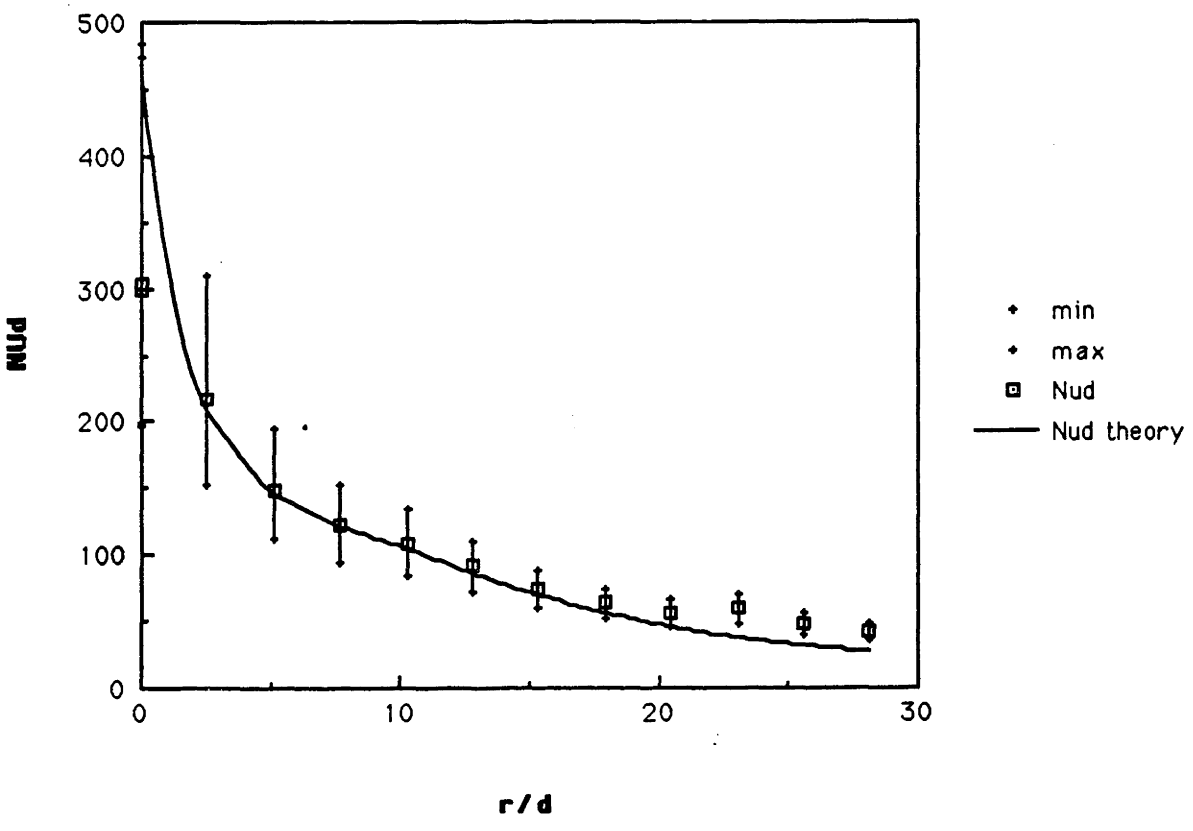

Figure 29. 1/4 inch orifice, q_w = 22,460 W/m^2, U_j = 16.9 m/s, $Re_{r\ hump}$=1,055,700.

Table 27. Values for Figure 30.

Nu_d	Theory	Re_d	Pr	r (m)
292.311823	498.8	64288	11.28	0
292.311823				0
196.02087	222.2	64960	11.16	0.0127
137.700611	157.2	65242	11.11	0.0254
111.823986	130.1	65444	11.08	0.0381
100.372132	113	65626	11.05	0.0508
93.0825358	94.3	65904	11	0.0635
94.66917	77.16	66284	10.94	0.0762
80.1046823	62.9	66767	10.86	0.0889
70.6007369	51.56	67278	10.78	0.1016
60.3687461	42.73	67930	10.67	0.1143
49.0052174	35.85	68673	10.56	0.127
45.1538588	30.46	69509	10.43	0.1397
q_w (W/m^2)	T_{in} (°C)	U_j (m/s)	r_{turb} (r/d)	d_j (m)
19300	5.08	19.63	16.2	0.004964

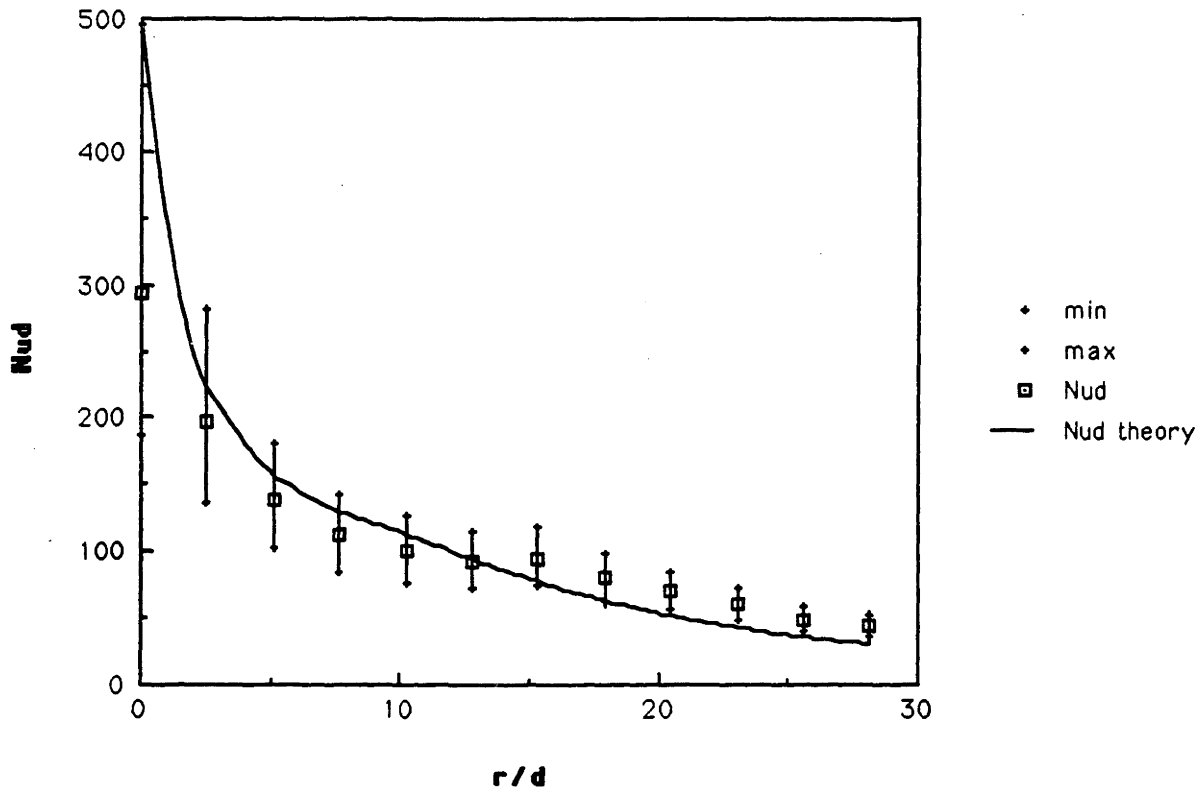

Figure 30. 1/4 inch orifice, q_w = 19,300 W/m^2, U_j = 19.63 m/s, $Re_{r\ hump}$=843,100.

Table 28. Values for Figure 31.

Nu_d	Theory	Re_d	Pr	r (m)
347.564088	404.9	42748	11.16	0
347.564088				0
252.4758	221.3	43489	10.97	0.0127
182.057379	156.7	43804	10.89	0.0254
151.200197	128.1	44048	10.83	0.0381
130.548462	112.7	44231	10.78	0.0508
109.234428	101.6	44405	10.74	0.0635
91.9671298	89.3	44652	10.68	0.0762
76.2462529	77.3	44977	10.61	0.0889
67.4116745	66.4	45315	10.53	0.1016
60.0054592	56.96	45766	10.42	0.1143
54.9536649	49.06	46290	10.3	0.127
53.8479573	42.51	46884	10.17	0.1397
q_w (W/m^2)	T_{in} (°C)	U_j (m/s)	r_{turb} (r/d)	d_j (m)
31000	5.46	19.63	16.2	0.004964

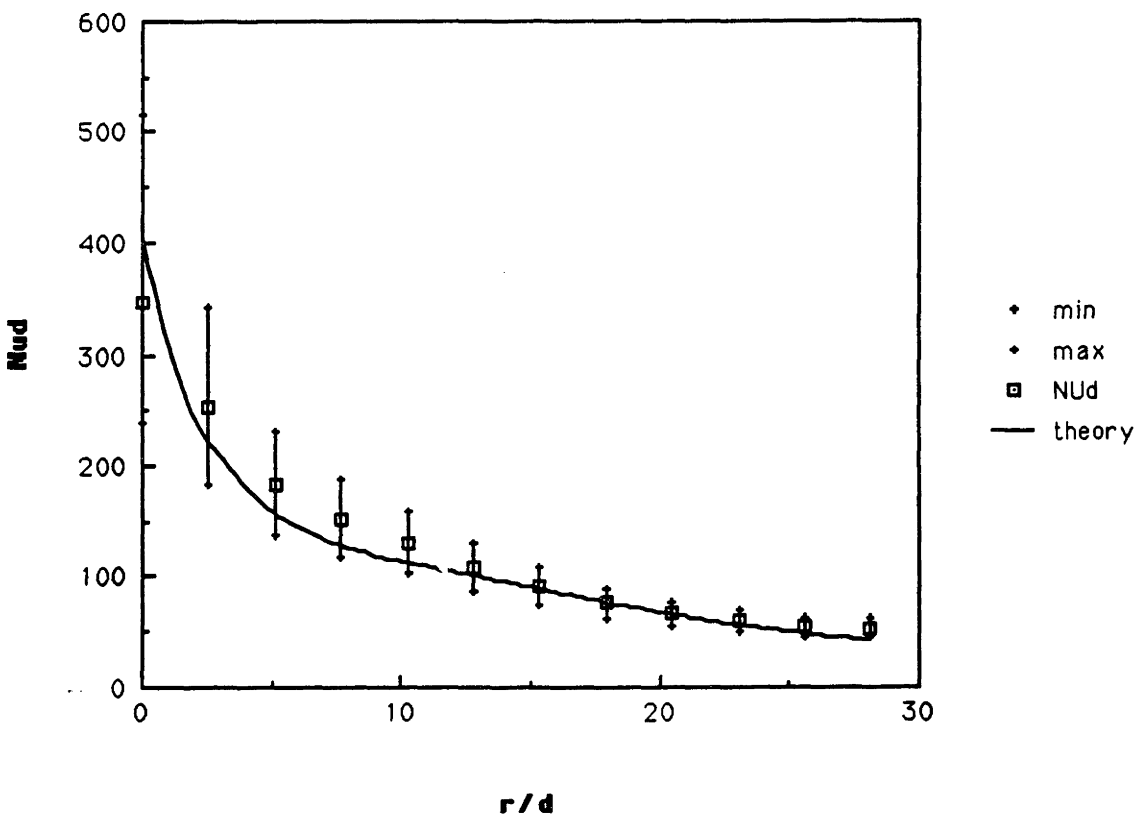

Figure 31. 1/4 inch orifice, q_w = 31,000 W/m^2, U_j = 19.63 m/s. No hump.

Table 29. Values for Figure 32.

Nu_d	Theory	Re_d	Pr	r (m)
377.444692	403.1	40696	11.71	0
377.444692				0
210.780802	219.85	41764	11.41	0.0127
162.301217	155.7	42206	11.29	0.0254
130.888079	127.3	42483	11.22	0.0381
116.344959	112.16	42687	11.16	0.0508
99.8776722	100.8	42892	11.11	0.0635
84.3123207	88.43	43184	11.04	0.0762
77.286294	76.34	43500	10.96	0.0889
73.6059943	65.49	43940	10.85	0.1016
70.4126757	56.18	44462	10.72	0.1143
59.5600798	48.39	45062	10.58	0.127
51.6882858	41.94	45753	10.42	0.1397
q_w (W/m^2)	T_{in} (°C)	U_j (m/s)	r_{turb} (r/d)	d_j (m)
37600	3.98	8.61	11.5	0.004964

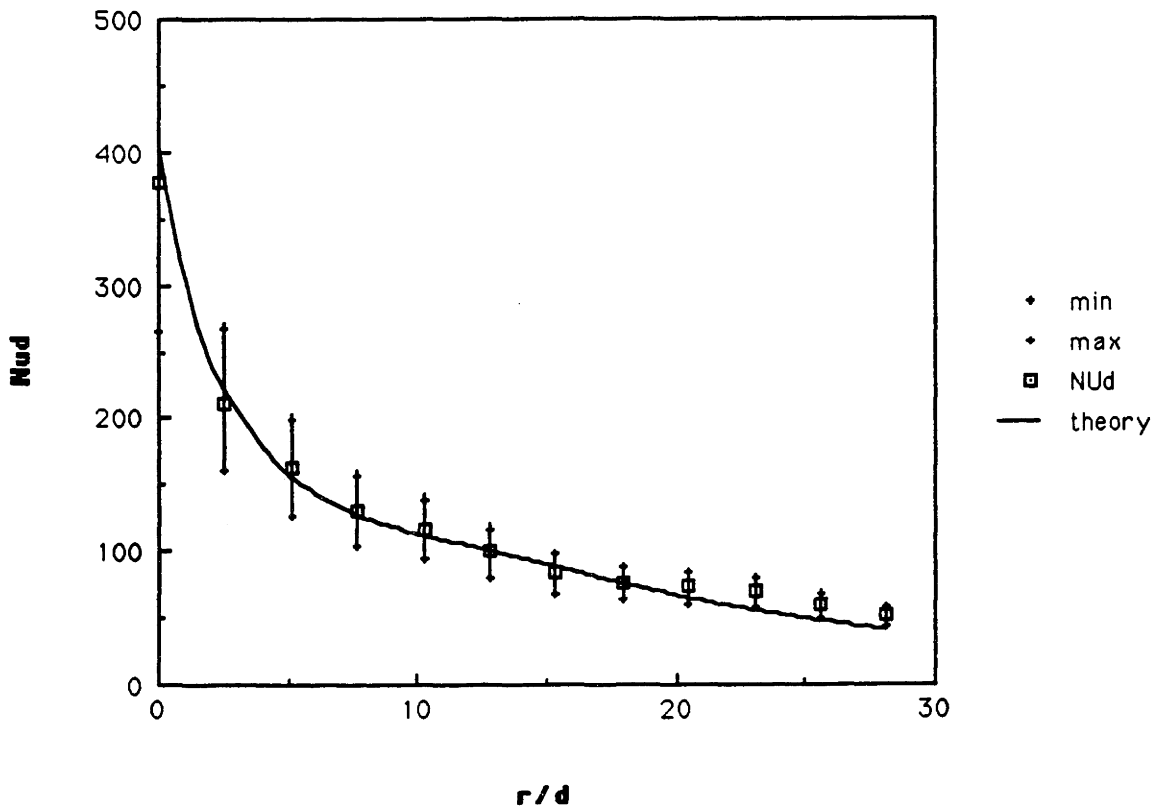

Figure 32. 1/4 inch orifice, q_w = 37,600 W/m^2, U_j = 8.61 m/s, $Re_{r\ hump}$ = 779,00.

Table 30. Values for Figure 33.

Nu_d	Theory	Re_d	Pr	r (m)
388.77	522.97	71100	11.2	0
374.19				0
255.86	290	72370	11	0.0127
194.39	205	72800	11	0.0254
163.58	168	73140	10.9	0.0381
143.23	145	73420	10.9	0.0508
134.84	133	73620	10.8	0.0635
125.25	121	73850	10.8	0.0762
126.31	109	74150	10.8	0.0889
112.54	96.4	74520	10.7	0.1016
103.94	84.8	74980	10.6	0.1143
98.47	74.5	75510	10.6	0.127
93.55	65.5	76120	10.5	0.1397
q_w (W/m^2)	T_{in} (°C)	U_j (m/s)		d_j (m)
23120	4.53	14.7		0.07445

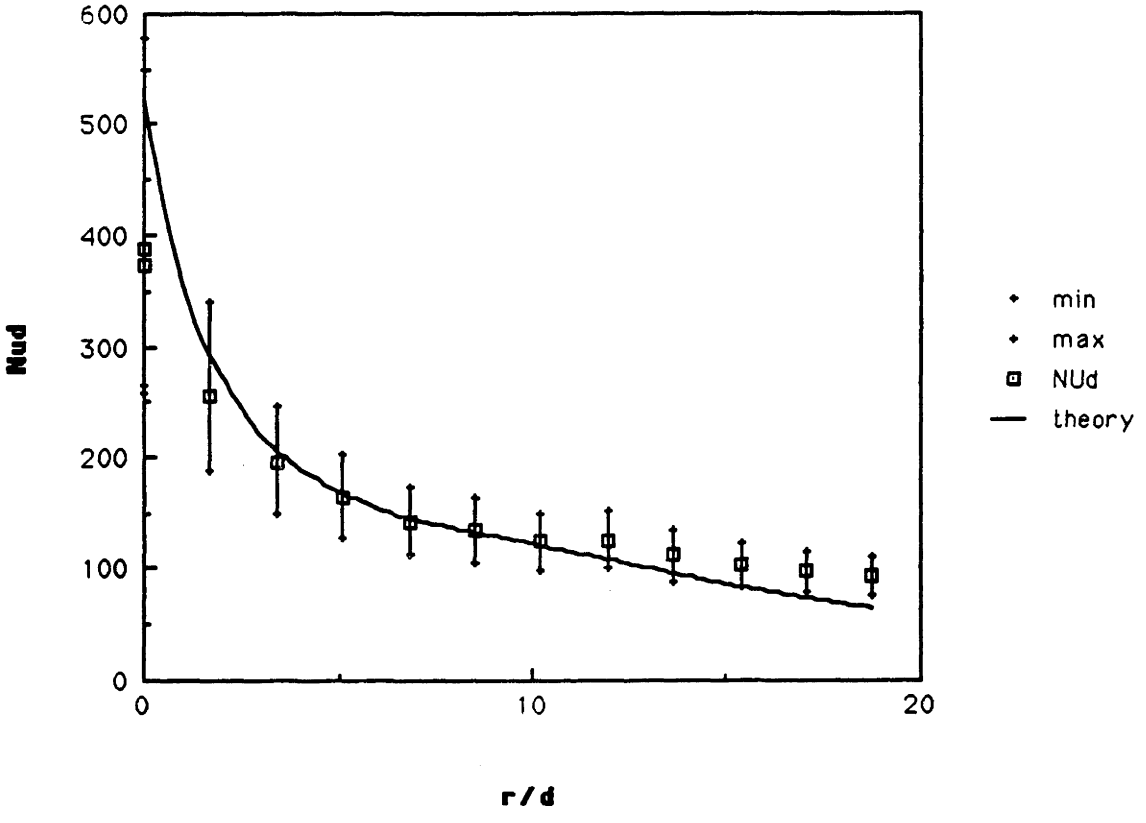

Figure 33. 3/8 inch orifice, q_w = 23,120 W/m^2, U_j = 14.7 m/s, $Re_{r\ hump}$ = 755,900.

Table 31. Values for Figure 34.

Nu_d	Theory	Re_d	Pr	r (m)
375.93	518.69	68910	11.4	0
352.06				0
217.45	287	69840	11.3	0.0127
189.57	203	70230	11.2	0.0254
156.19	166	70540	11.2	0.0381
121.87	144	70800	11.1	0.0508
125.31	131	70980	11.1	0.0635
96.43	120	71190	11.1	0.0762
114.33	107	71430	11	0.0889
117.35	94.7	71700	11	0.1016
113.16	83.1	72030	10.9	0.1143
92.42	72.9	72410	10.9	0.127
83.7	63.9	72850	10.8	0.1397
q_w (W/m^2)	T_{in} (°C)	U_j (m/s)		d_j (m)
17130	3.99	14.5		0.007445

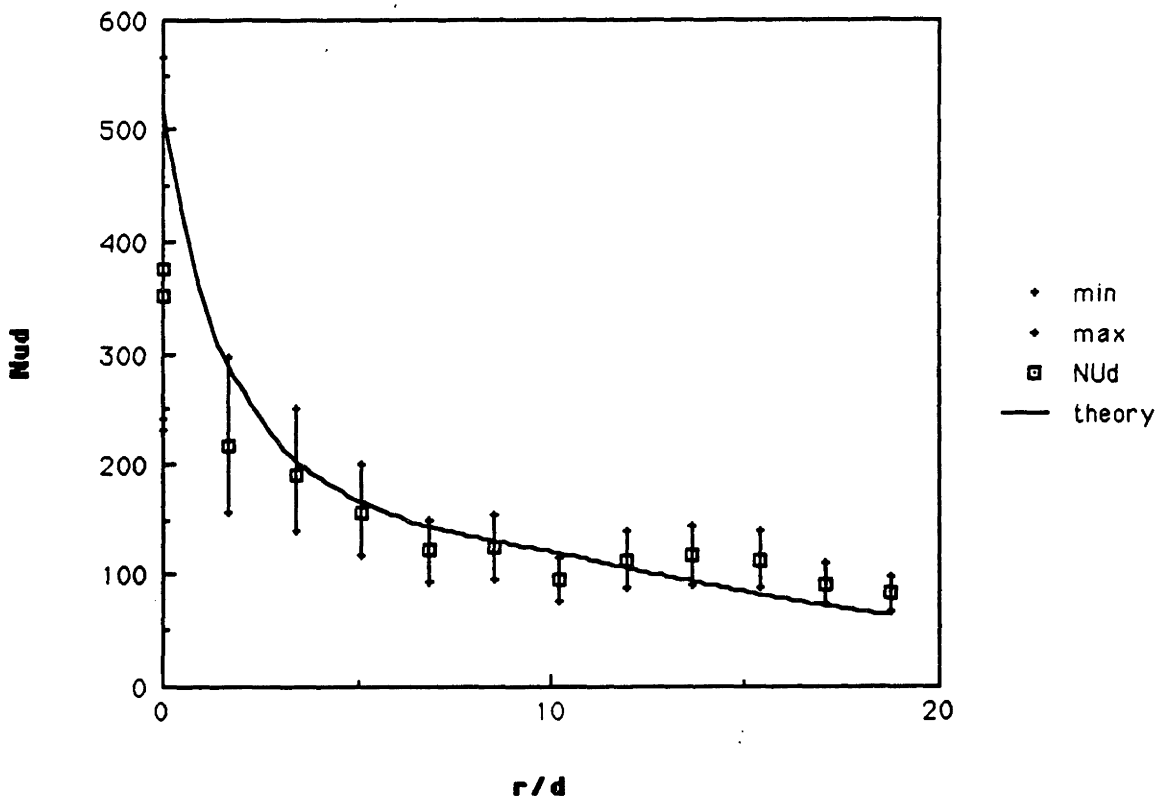

Figure 34. 3/8 inch orifice, q_w = 17,130 W/m^2, U_j = 14.5 m/s, $Re_{r\ hump}$ = 852,900.

Table 32. Values used for Figure 35.

Nu_d	Theory	Re_d	Pr	r (m)
448.71	580.06	85550	11.5	0
426.64				0
299.14	320	86760	11.3	0.0127
211.59	226	87270	11.2	0.0254
173.5	185	87670	11.2	0.0381
168.99	160	88010	11.1	0.0508
168.99	145	88270	11.1	0.0635
180.73	134	88500	11.1	0.0762
209.88	122	88810	11	0.0889
195.68	109	89110	11	0.1016
153.09	97.2	89480	11	0.1143
145.39	86.1	89920	10.9	0.127
118.3	76.1	90420	10.8	0.1397
q_w (W/m^2)	T_{in} (°C)	U_j (m/s)		d_j (m)
20100	3.93	18.1		0.007445

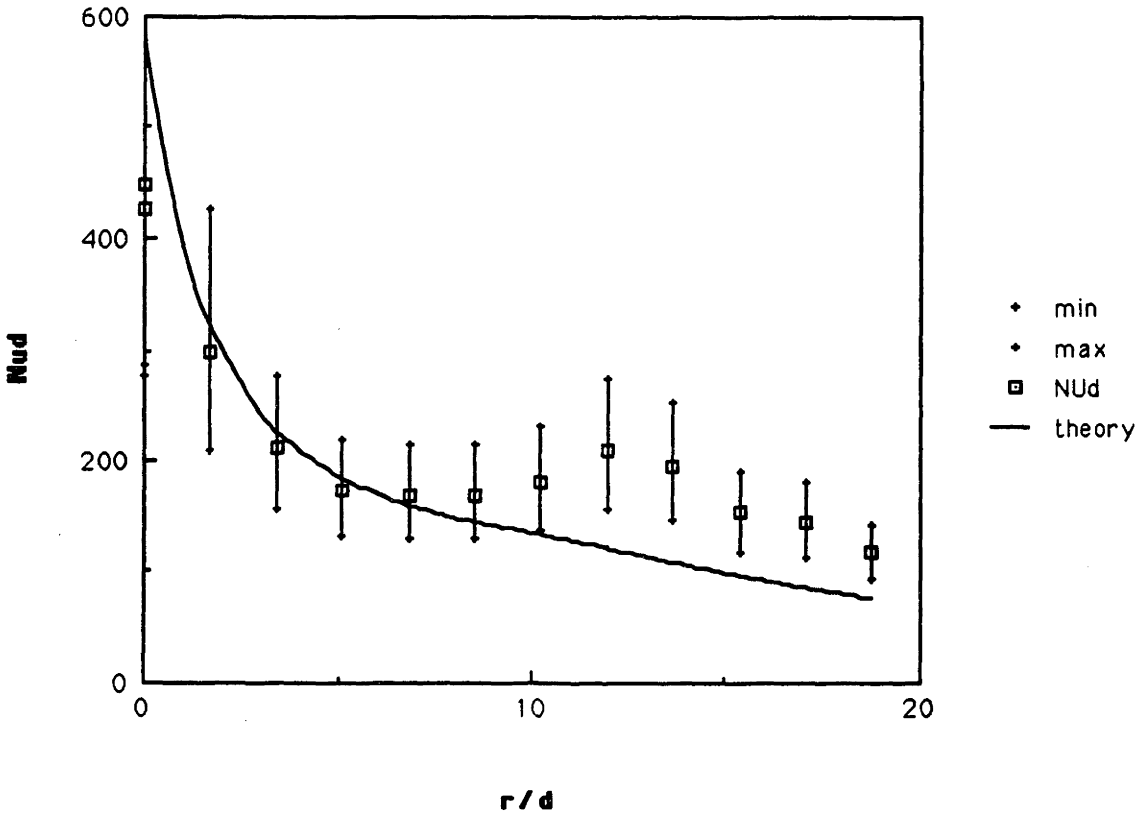

Figure 35. 3/8 inch orifice, q_w = 20,100 W/m^2, U_j = 18.1 m/s, $Re_{r\ hump}$ = 753,000.

Table 33. Values for Figure 36.

Nu_d	Theory	Re_d	Pr	r (m)
392.23	496.72	66650	10.7	0
				0
249.99	276	67430	10.6	0.0127
239.47	195	67770	10.6	0.0254
183.46	160	68020	10.5	0.0381
166.05	138	68240	10.5	0.0508
138.72	127	68390	10.5	0.0635
137.04	115	68570	10.4	0.0762
127.81	103	68820	10.4	0.0889
121.65	90.6	69120	10.4	0.1016
110.97	79.4	69480	10.3	0.1143
107.82	69.5	69910	10.2	0.127
85.85	60.9	70390	10.2	0.1397
q_w (W/m^2)	T_{in} (°C)	U_j (m/s)		d_j (m)
17570	5.93	13.2		0.007445

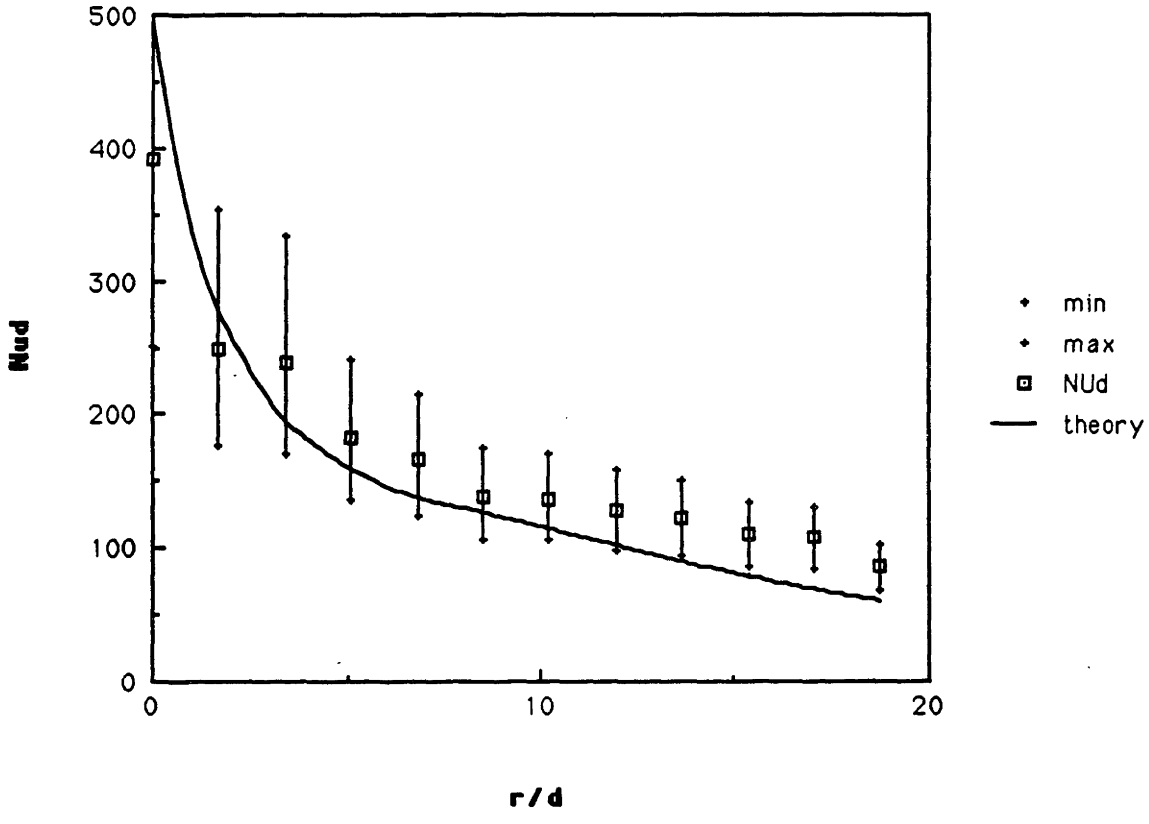

Figure 36. 3/8 inch orifice, q_w = 17,570 W/m^2, U_j = 13.2 m/s. No hump.

Table 34. Values for Figure 37.

Nu_d	Theory	Re_d	Pr	r (m)
458.66	499.82	68020	10.6	0
451.02				0
330.01	278	68940	10.5	0.0127
237.38	197	69330	10.4	0.0254
194.68	161	69640	10.4	0.0381
178.03	139	69890	10.3	0.0508
157.33	128	70070	10.3	0.0635
143.94	116	70280	10.3	0.0762
136.67	104	70560	10.2	0.0889
127.65	91.7	70910	10.2	0.1016
119.74	80.5	71330	10.1	0.1143
111.36	70.6	71830	10.1	0.127
97.34	61.9	72400	9.99	0.1397
q_w (W/m^2)	T_{in} (°C)	U_j (m/s)		d_j (m)
20900	6.32	13.4		0.007445

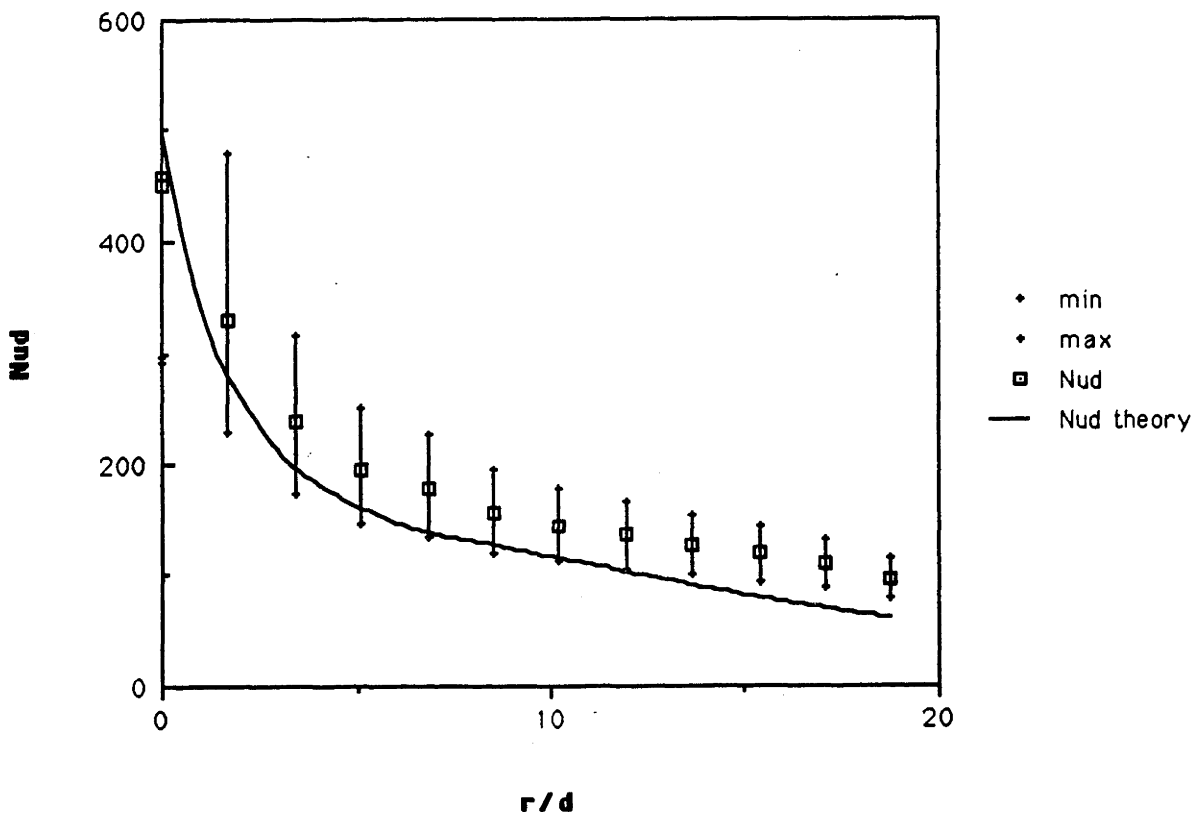

Figure 37. 3/8 inch orifice, q_w = 20,900 W/m^2, U_j = 13.4 m/s. No hump.

Table 35. Values for Figure 38.

Nu_d	Theory	Re_d	Pr	r (m)
439.3	558.05	83470	10.8	0
323.7				0
267.4	310	84390	10.7	0.0127
193.71	219	84790	10.6	0.0254
151.86	179	85100	10.6	0.0381
132.26	155	85360	10.6	0.0508
136.67	141	85560	10.5	0.0635
150.01	130	85750	10.5	0.0762
150.01	118	85990	10.5	0.0889
130.86	105	86300	10.5	0.1016
123	93.5	86680	10.4	0.1143
103.36	82.7	87120	10.4	0.127
89.46	73	87630	10.3	0.1397
q_w (W/m^2)	T_{in} (°C)	U_j (m/s)		d_j (m)
19000	5.72	16.7		0.007445

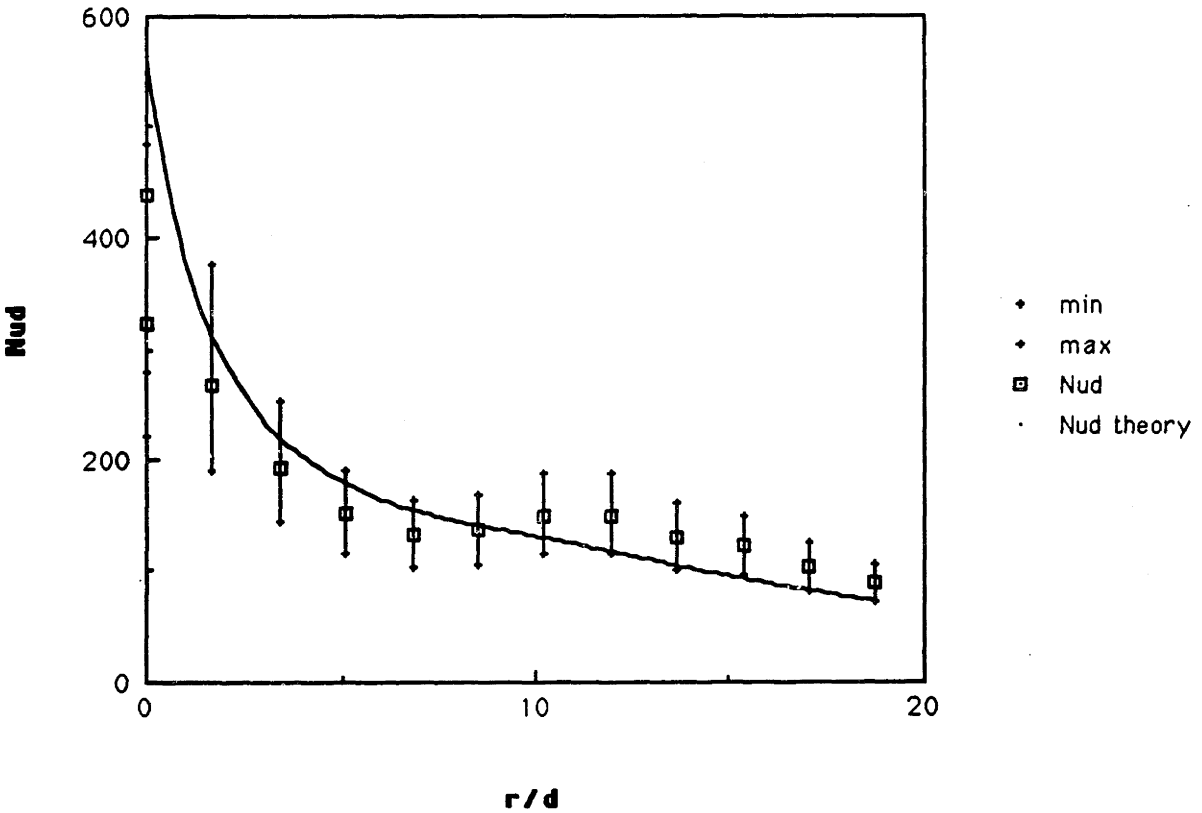

Figure 38. 3/8 inch orifice, q_w = 19,000 W/m^2, U_j = 16.7 m/s, $Re_{r\ hump}$ = 729,800.

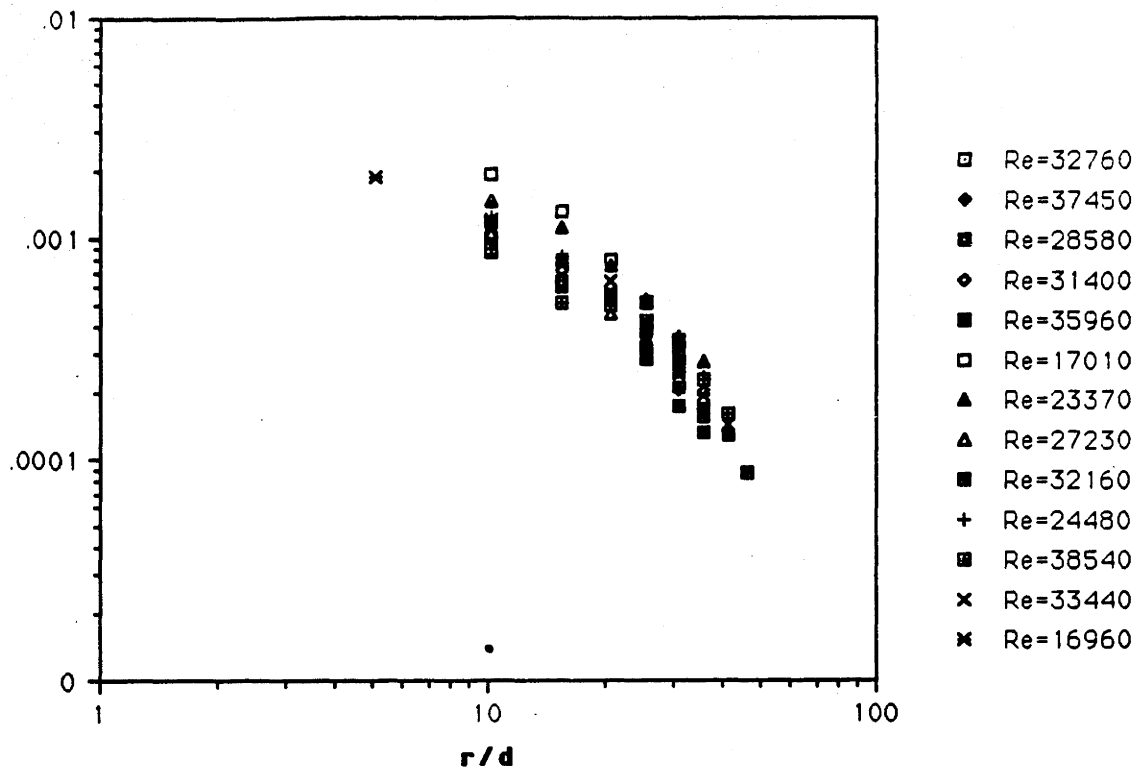

Figure 39. Plot of (Nu/(Re*Pr^1/3)) for region 2; 1/8 inch orifice.

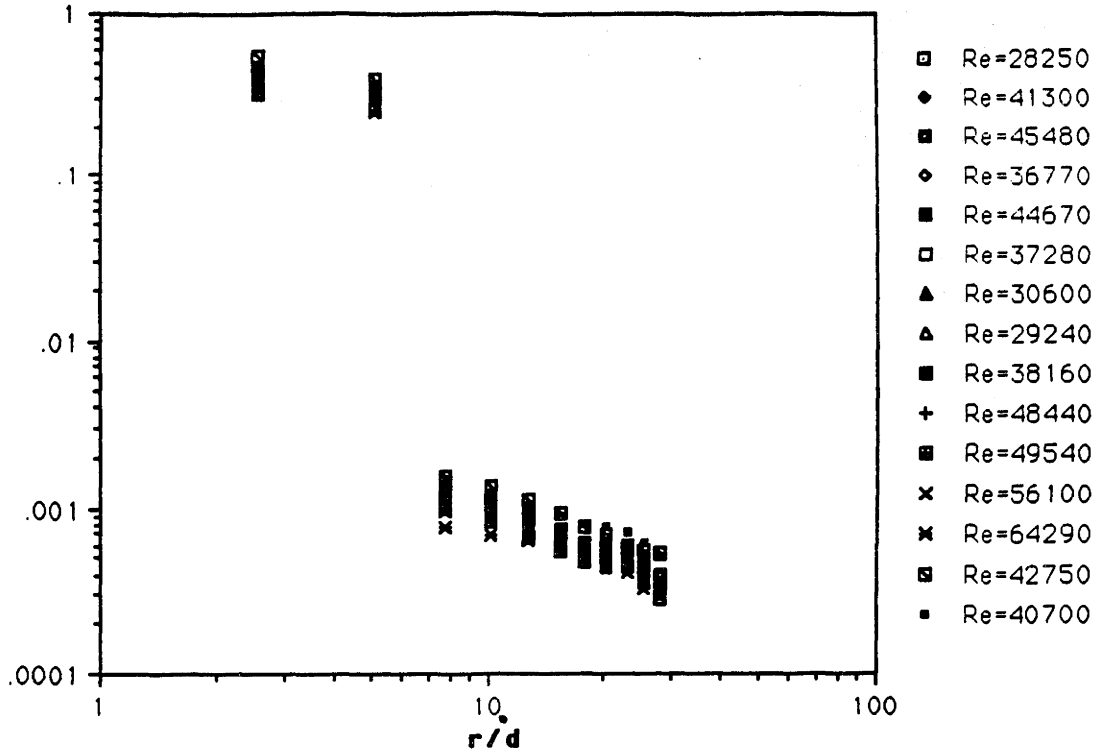

Figure 40. Plot of (Nu/(Re^1/2*Pr^1/3)) for region 2, and (Nu/(Re*Pr^1/3)) for region 3; 1/4 inch orifice.

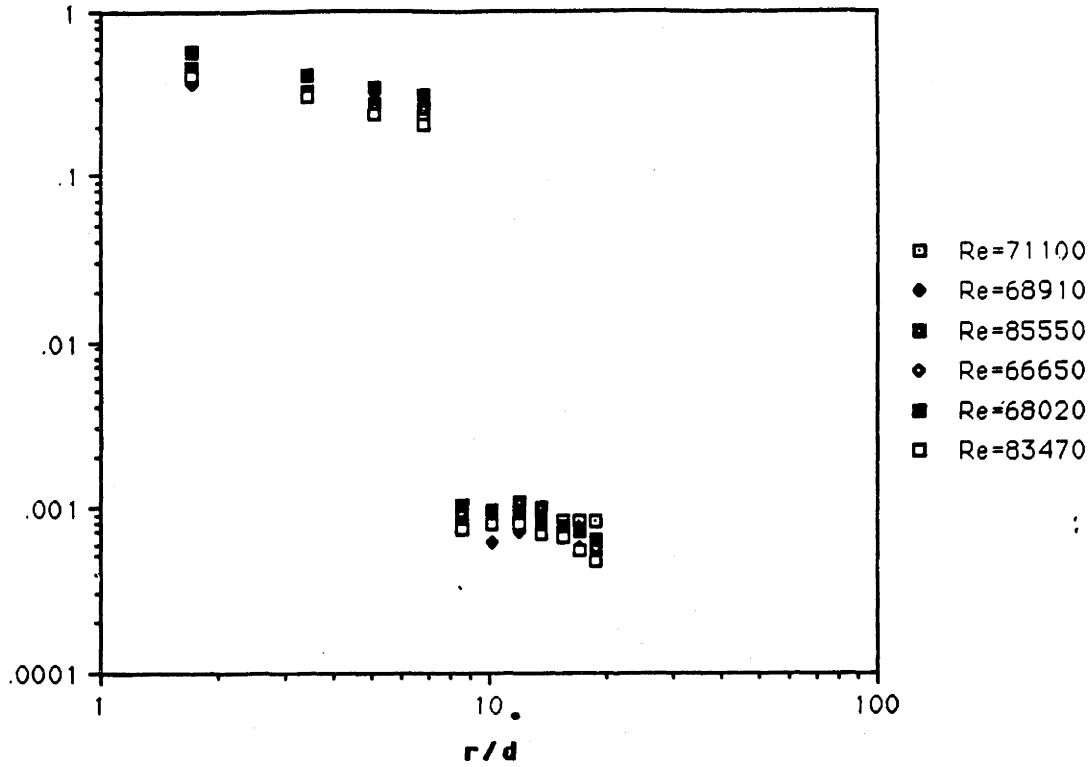

Figure 41. Plot of (nu/(Re^1/2*Pr^1/3)) for region 2, and (Nu/Re*Pr^1/3)) for region 3; 3/8 inch orifice.

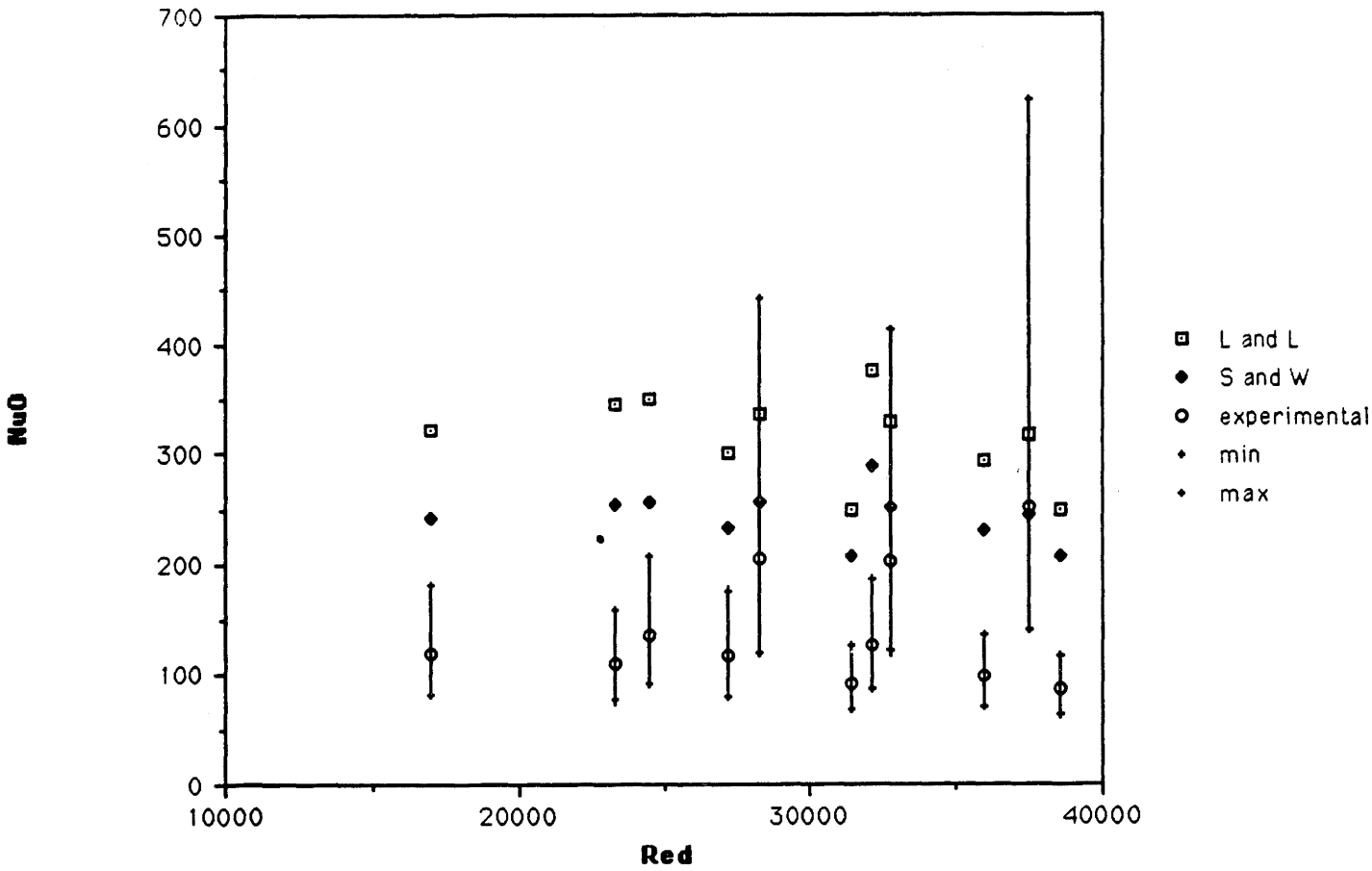

Figure 42. Comparison of theory with experimental data from stagnation point Nud, for 1/8 inch orifice

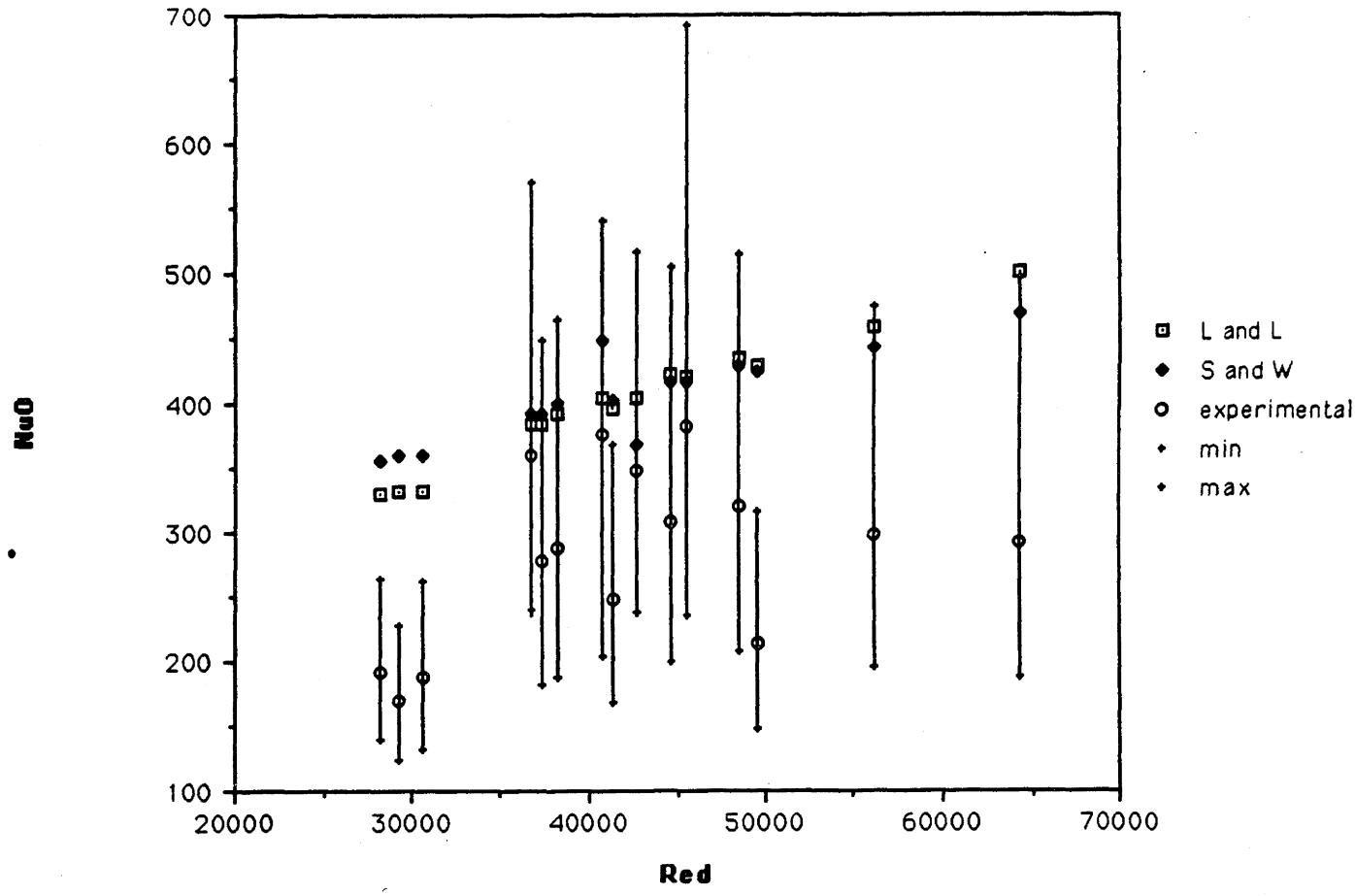

Figure 43. Comparison of theory and experimental data for stagnation point Nud, for 1/4 orifice.

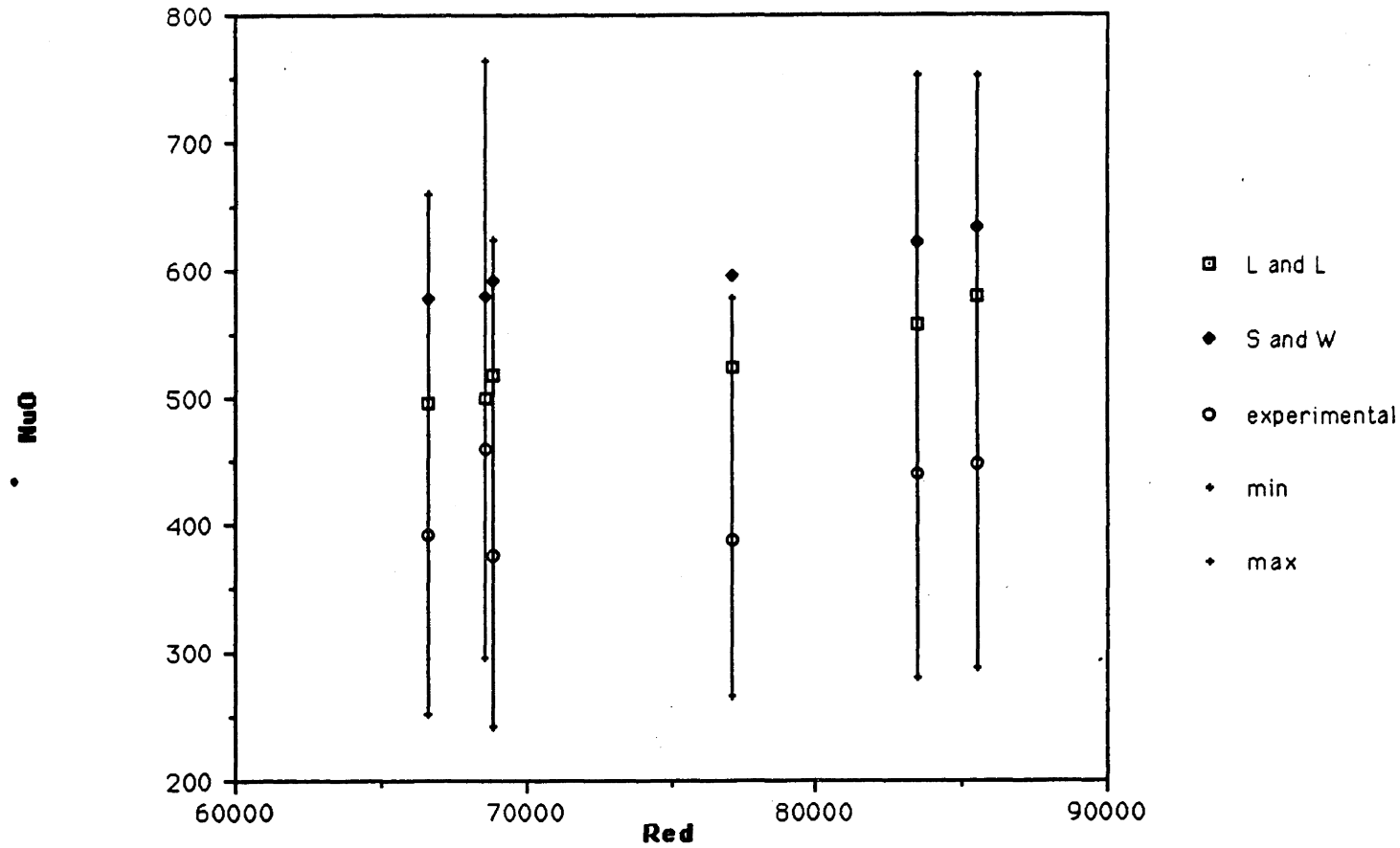

Figure 44. Comparison of theory and experimental data for stagnation point Nud, for 3/8 inch orifice.

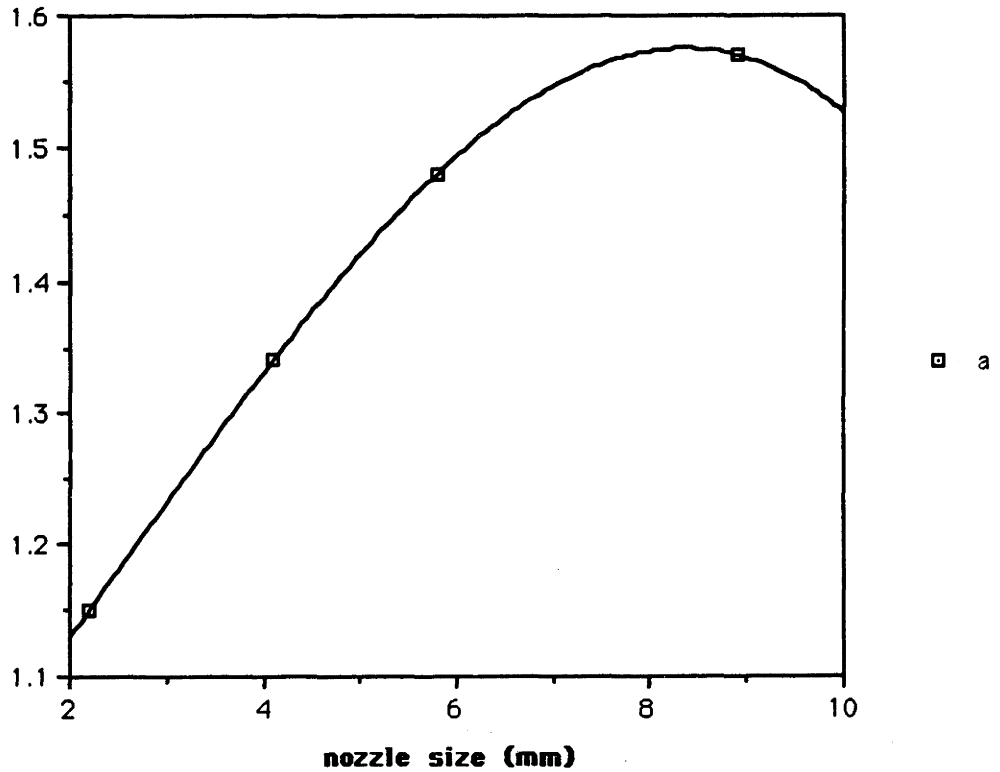

Figure 45. Curve-fit for the parameter a.

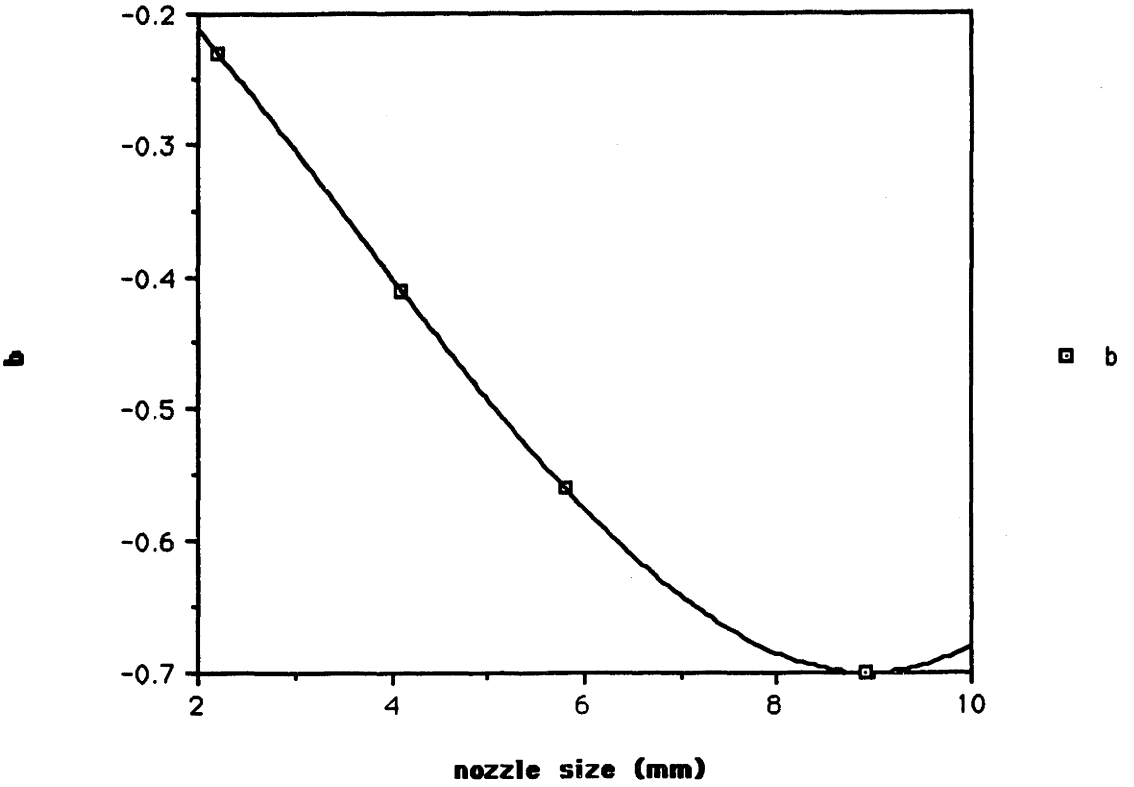

Figure 46. Curve-fit for the parameter b

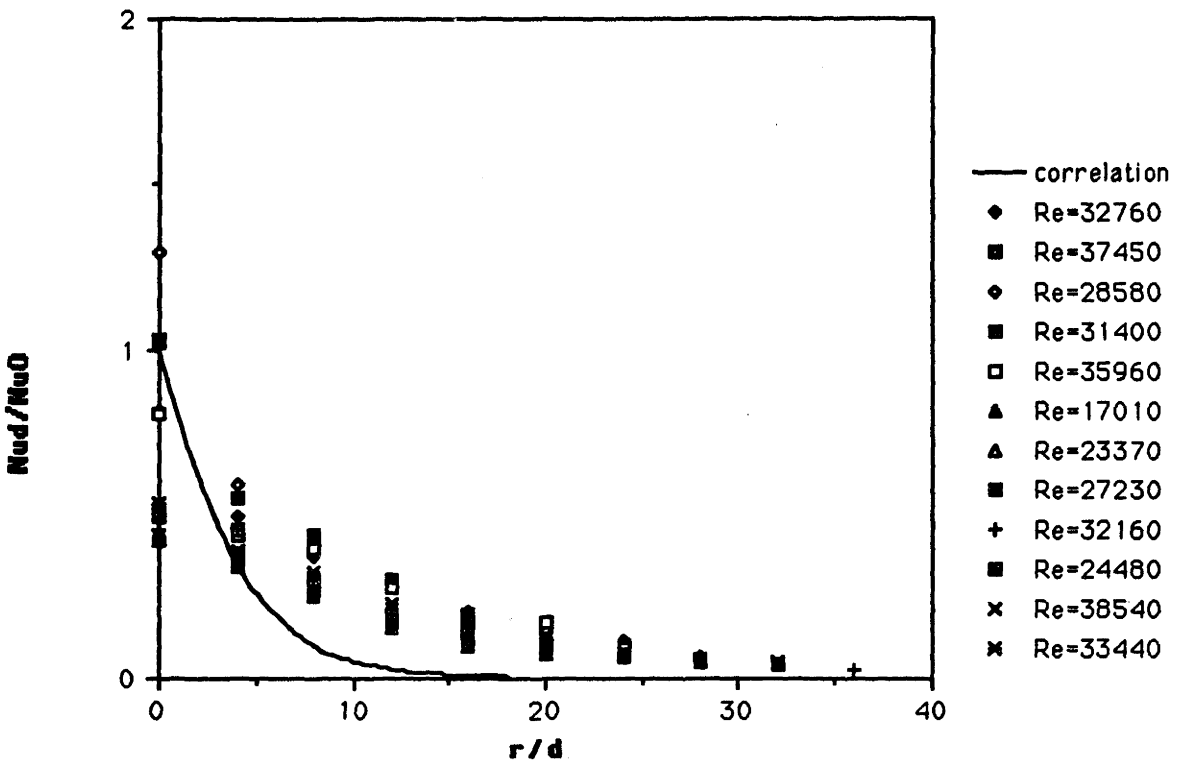

Figure 47. Comparison of experimental data and Stevens and Webb's correlation for 1/8 inch orifice

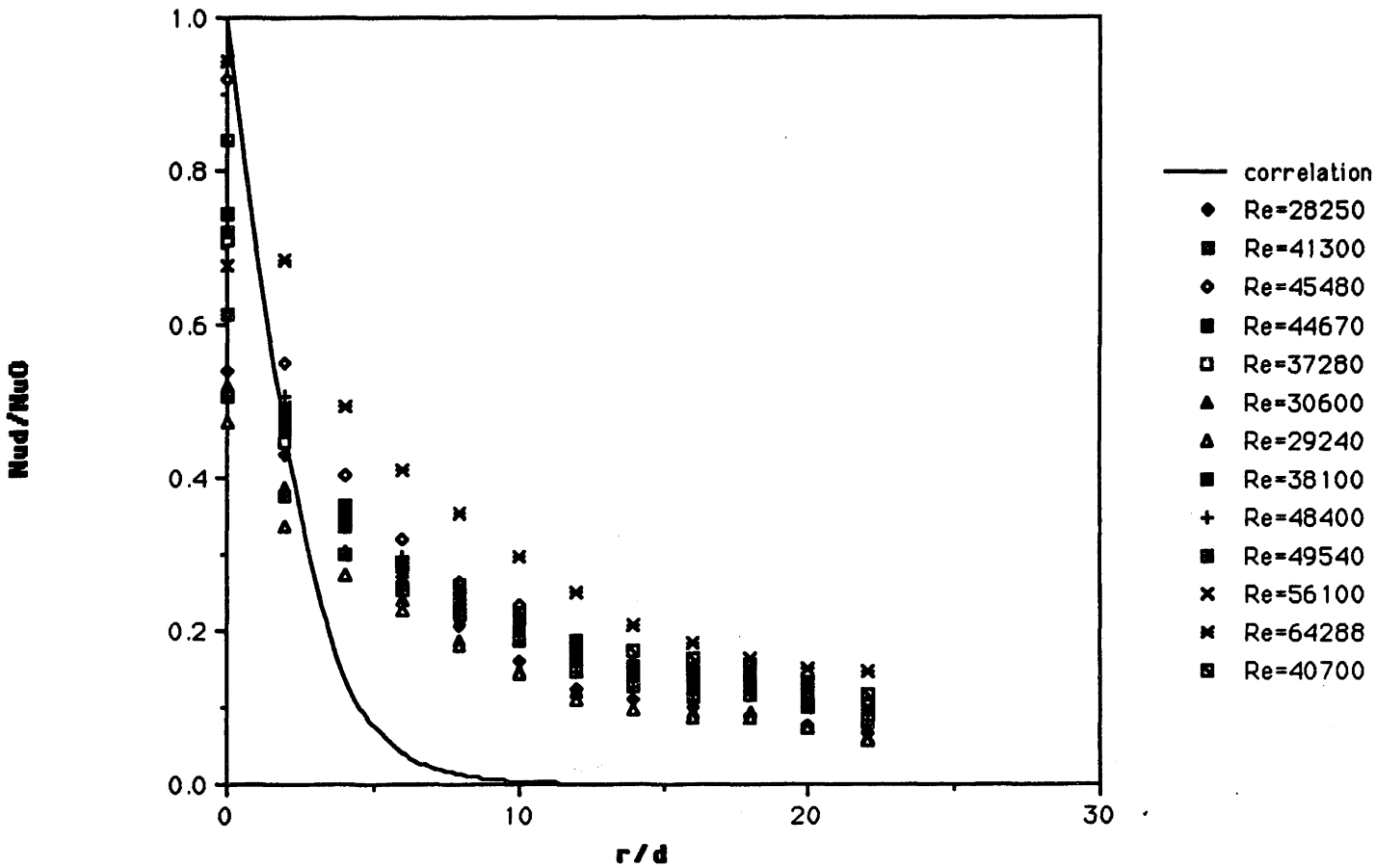

Figure 48. Comparison of experimental data and Stevens and Webb correlation for 1/4 inch orifice.

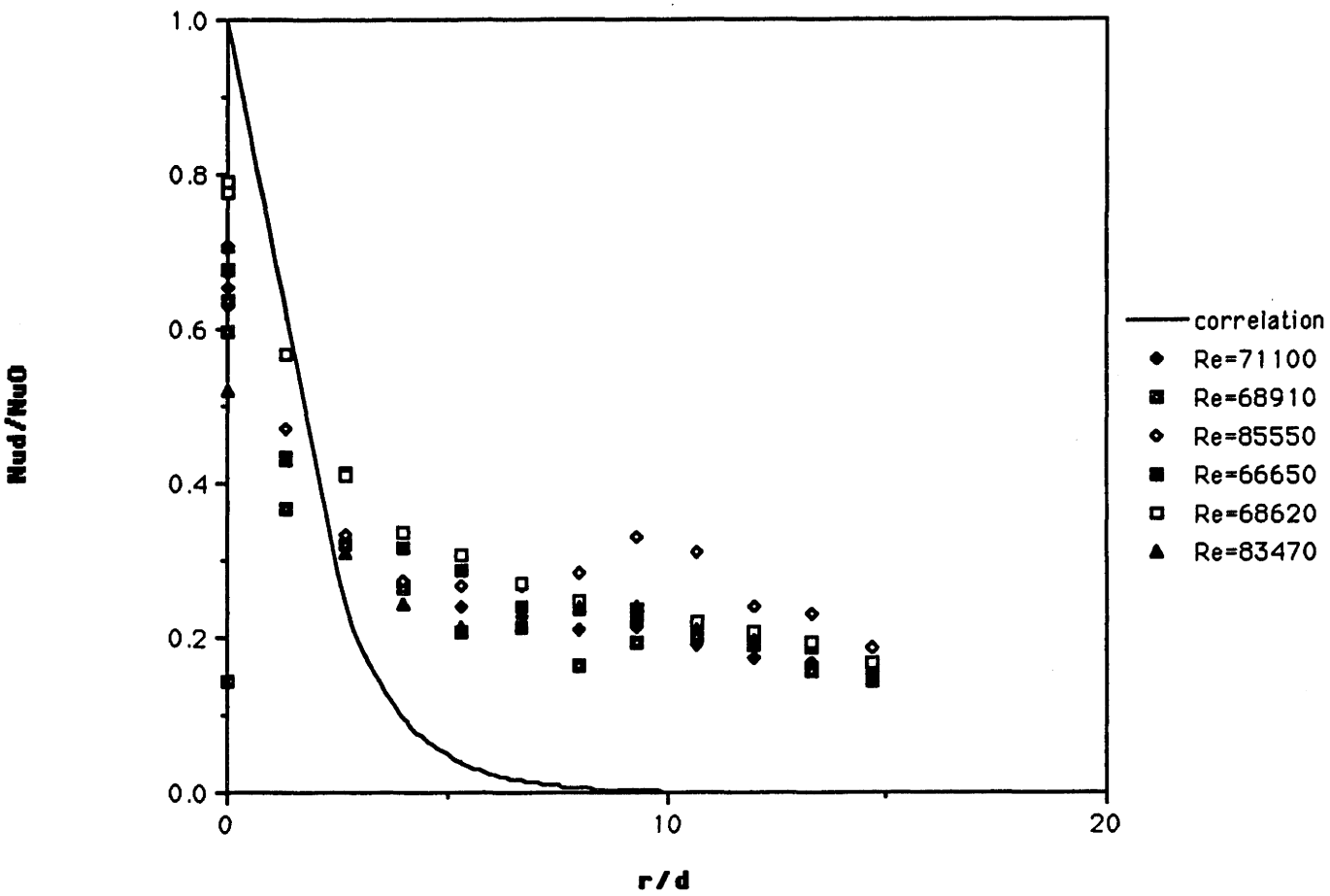

Figure 49. Comparison of experimental data and Stevens and Webb's correlation for 3/8 inch orifice